Numerical Evaluation of Criticality in Debris Beds formed during Severe Accidents in Light Water Reactors

María Freiría López

IKE

University of Stuttgart
Institute of Nuclear Technology
and Energy Systems

Numerical Evaluation of Criticality in Debris Beds formed during Severe Accidents in Light Water Reactors

von der Fakultät Energie-, Verfahrens- und Biotechnik der Universität Stuttgart zur Erlangung der Würde eines Doktor-Ingenieurs (Dr.-Ing.) genehmigte Abhandlung

vorgelegt von
M. Sc. María Freiría López
geboren in Madrid, Spanien

Hauptberichter : Prof. Dr.-Ing. Jörg Starflinger
Mitberichter   : Prof. Dr. Rafael Macián-Juan

Tag der Einreichung   : 16.12.2020
Tag der mündlichen Prüfung : 17.05.2021

IKE

Eidesstattliche Erklärung zu meiner Dissertation mit dem Titel:
Numerical Evaluation of Criticality in Debris Beds formed during
Severe Accidents in Light Water Reactors

Hiermit erkläre ich, dass ich die beigefügte Dissertation selbstständig verfasst und keine anderen als die angegebenen Hilfsmittel genutzt habe. Alle wörtlich oder inhaltlich übernommenen Stellen habe ich als solche gekennzeichnet.

Ich versichere außerdem, dass ich die beigefügte Dissertation nur in diesem und keinem anderen Promotionsverfahren eingereicht habe und, dass diesem Promotionsverfahren keine endgültig gescheiterten Promotionsverfahren vorausgegangen sind.

Stuttgart, den 27.11.2020
Ort, Datum

María Freiría López
Unterschrift

I would like to dedicate this thesis to my father, Juan Manuel Freiría Ballesteros, who taught me to love science.

Acknowledgements

Abstract

After the Fukushima accident, the interest of the scientific community in severe accident (SA) research has been renewed. Great efforts are being made internationally to reassess and strengthen the safety of nuclear power plants. The recriticality potential in debris beds formed after the core meltdown is one of the SA research issues that needs further attention, and it is also the focus of this work. An inadvertent criticality event may cause the release of nuclear radiation and have severe consequences. Thus, the criticality in debris beds must be evaluated to predict possible risks and establish the appropriate control measures if necessary.

The available criticality data for debris beds are still very scarce. Thus, the Japan Atomic Energy Agency has begun the ambitious task of building a criticality map for debris beds. That is an arduous enterprise, which requires the investigation of appropriate debris bed models and numerous computations under a broad range of possible conditions. A global effort and international cooperation are essential. The present work aims to contribute to this common endeavor by improving debris bed models, extending the criticality database, and facilitating future analyses.

Alternatives for modeling the debris bed characteristics with a potential influence on the criticality are discussed in this thesis, from the most conservative assumptions to more realistic approaches. Among other things, it was found that debris beds can be modeled with high accuracy as spheres regularly arranged in a water matrix if an adequate equivalent diameter d_{eq} is chosen. Besides, coupled neutronic-thermohydraulic calculations were proven to be not necessary for assessing the criticality of Fukushima debris beds.

This work also investigates the criticality characteristics of UO_2-concrete systems. The calculation results prove the good moderation capacities of concrete, which has a significant positive reactivity effect at very low porosities. Not only the bound water is capable of thermalizing neutrons but also the SiO_2, a major component of concrete. Consequently, MCCI products should be treated carefully in the criticality analyses.

A preliminary conservative criticality assessment of Fukushima debris beds has revealed safety parameter ranges, i.e., conditions for which recriticality can be excluded.

xii

On the one hand, dry debris beds cannot become critical under any conditions due to the lack of sufficient moderator. On the other hand, debris beds submerged in water will remain subcritical if the porosity is sufficiently low (< 0.24 for debris beds without concrete, < 0.1 if concrete is mixed with fuel), the mass is sufficiently small (< 124 kg), or the cooling water is sufficiently borated (> 2600 ppm B).

Finally, a statistical method is proposed as an alternative and more realistic way to evaluate the criticality in debris beds. A first exploratory analysis of the debris bed at Fukushima Unit 1 reveals that the probability of recriticality is extremely low. Additionally, the sensitivity analysis has concluded that the amount of control rod material (B_4C) mixed with fuel is by far the most relevant parameter. Other parameters with a strong correlation with k_{eff} are the percentage of fuel in the corium, the amount of debris in particulate form, and the debris bed spreading. Based on them, future areas of research and improvement are proposed.

Zusammenfassung

Nach dem Unfall von Fukushima wurde das Interesse der wissenschaftlichen Gemeinschaft an der Forschung zu schweren Unfälle intensiviert. Auf internationaler Ebene werden diverse Initiativen angestoßen, um die Sicherheit von Kernkraftwerken neu zu bewerten und zu erhöhen. Das Rekritikalitätspotential in Schüttbetten, die sich nach einer Kernschmelze gebildet haben, ist eines der Themen der Forschung innerhalb der schweren Unfälle, das weiterer Aufmerksamkeit bedarf, und welches auch im Mittelpunkt dieser Arbeit steht. Ein unbeabsichtigtes Kritikalitätsereignis kann zur Freisetzung von radioaktiven Partikeln und Strahlung führen und schwerwiegende Folgen für die Anlage haben. Daher muss die Kritikalität in Schüttbetten evaluiert werden, um mögliche Risiken vorherzusagen und gegebenenfalls die entsprechenden Kontrollmaßnahmen festzulegen.

Die verfügbaren Kritikalitätsdaten für Schüttbetten sind immer noch sehr spärlich. Daher hat die Japan Atomic Energy Agency mit der ambitionierten Aufgabe begonnen, eine Kritikalitätskarte für Schüttbetten zu erstellen. Das ist eine mühsame Aufgabe, die die Untersuchung geeigneter Schüttbettmodelle und zahlreiche Berechnungen unter einem breiten Spektrum möglicher Randbedingungen erfordert. Eine internationale Zusammenarbeit ist dabei unerlässlich. Die vorliegende Arbeit soll zu diesem gemeinsamen Unterfangen beitragen, indem sie die Schüttbettmodelle verbessert, die Kritikalitätsdatenbank erweitert und künftige Analysen erleichtert.

In dieser Arbeit werden Alternativen für die Modellierung der Schüttbettmerkmale mit einem potenziellen Einfluss auf die Kritikalität diskutiert, von den konservativsten Annahmen bis hin zu realistischeren Ansätzen. U.a. zeigen die Ergebnisse, dass Schüttbetten als regelmäßig in einer Wassermatrix angeordnete Kugeln mit guter Genauigkeit modelliert werden können, wenn ein adäquater äquivalenter Durchmesser d_{eq} gewählt wird. Außerdem erwiesen sich gekoppelte neutronen-thermohydraulische Berechnungen als nicht notwendig für die Beurteilung der Kritikalität von Fukushima Schüttbetten.

In dieser Arbeit werden auch die Kritikalitätseigenschaften von UO_2-Betonsystemen untersucht. Die Berechnungsergebnisse belegen die guten Moderationsfähigkeiten von Beton, der bei sehr niedrigen Porositäten einen signifikanten positiven Reaktivitätseffekt

hat. Nicht nur das gebundene Wasser ist in der Lage, Neutronen zu thermalisieren, sondern auch das SiO_2, ein Hauptbestandteil des Betons. Folglich sollten MCCI-Produkte in den weiteren Kritikalitätsanalysen sorgfältig behandelt werden.

Eine vorläufige konservative Kritikalitätsbewertung von Fukushima-Schüttbetten hat Sicherheitsparameterbereiche bzw. Bedingungen aufgezeigt, für die eine Rekritikalität ausgeschlossen werden kann. Einerseits können trockene Schüttbetten aufgrund des Mangels an ausreichendem Moderator unter keinen Bedingungen kritisch werden. Andererseits bleiben in Wasser eingetauchte Schüttbetten unterkritisch, wenn die Porosität ausreichend gering ist (< 0,24 für Schüttbetten ohne Beton, < 0,1, wenn Beton mit Brennstoff vermischt wird), die Masse ausreichend klein ist (< 124 kg) oder das Kühlwasser ausreichend boriert ist (> 2600 ppm B).

Schließlich wird eine statistische Methode als alternative und realistischere Methode zur Bewertung der Kritikalität in Schüttbetten vorgeschlagen. Eine erste explorative Analyse des Schüttbetts von Fukushima Unit 1 zeigt, dass die Wahrscheinlichkeit einer Rekritikalität extrem gering ist. Zusätzlich hat die Sensitivitätsanalyse ergeben, dass die Menge des mit dem Brennstoff vermischten Steuerstabmaterials (B_4C) bei weitem der relevanteste Parameter ist. Andere Parameter mit einer starken Korrelation mit k_{eff} sind der prozentuale Anteil des Brennstoffs im Corium, die Menge an partikelförmigem Schüttbett und dessen Ausbreitung. Auf dieser Grundlage werden zukünftige Forschungs- und Handlungsfelder abgeleitet.

Contents

List of Figures

List of Tables

Nomenclature

Roman Symbols

A	atomic number	[-]
c	Pearson's ordinary correlation coefficient	[-]
D	distribution of uncertain parameters	[-]
d	particle diameter	$[mm], [cm]$
E	neutron energy	$[MeV]$
e	error	[%]
f_e	erosion factor	[%]
h	height	[cm]
J	neutron current	$[n \cdot cm^{-2} \cdot MeV^{-1} \cdot s^{-1}]$
k	neutron multiplication factor	[-]
m	mass	$[g], [kg]$
N	angular neutron density	$[n \cdot cm^{-3} \cdot sr^{-1} \cdot MeV^{-1}]$
n	standard neutron density	$[n \cdot cm^{-3} \cdot MeV^{-1}]$
N_A	Avogadro's number	$[mol^{-1}]$
ND	number density	$[n \cdot cm^{-3}]$
nS	number of samples	[-]
nX	number of uncertain parameters	[-]

P	power	[W]
p	cell pitch	[mm]
Q	neutron source	$[n \cdot cm^{-3} \cdot MeV^{-1} \cdot sr^{-1} \cdot s^{-1}]$
R	radius	[cm], [m]
r	neutron position	$[cm]$
S	surface	$[cm^2]$
t	time	$[s]$
V	volume	$[mm^3], [cm^3]$
v	neutron velocity	$[cm \cdot s^{-1}]$
w	mass fraction	[%]
x, y, z	cartesian coordinates	[cm]

Greek Symbols

α	percentile	[-]
β	confidence level	[-]
χ	energy distribution	[-]
γ	Goodman and Kruskal's rank correlation coefficient	[-]
ν	mean number of neutrons	[-]
Ω	solid angle	$[sr]$
ϕ	scalar neutron flux	$[n \cdot cm^{-2} \cdot MeV^{-1} \cdot s^{-1}]$
ψ	angular neutron density	$[n \cdot cm^{-2} \cdot sr^{-1} \cdot MeV^{-1} \cdot s^{-1}]$
ρ_i	density of component i	$[g \cdot cm^{-3}], [kg \cdot m^{-3}]$
ρ	reactivity	[-]
ρ_S	Spearman's rank correlation coefficient	[-]
Σ	macroscopic cross section	$[cm^{-1}]$

σ	standard desviation	[%]
θ, φ	polar coordinates	[rad]
ε	porosity	[-]

Subscripts

∞	infinite
0	zero, nominal
a	absorption
c	radioactive capture
d	decay heat
DEFOR	DEFOR-A experiments
eff	effective
eq	equivalent
ext	exterior
f	fission
FARO	FARO L-28 experiments
hom	homogeneous model
i	target nucleus
ingot	ingot debris bed
inv	inventory
k	type of interaction
lat	lattice model
max	maximum
min	minimum
n	neutron generation

part	particulate debris bed
random	random model
real	real debris
ref	reference model
s	scattering
t	total
v	volume

Abbreviations

1FNPS	Fukushima Daiichi Nuclear Power Station
BCC	Body Centered Cubic
BE	Best-Estimate
BWR	Boiling Water Reactors
CC	Correlation Coefficient
ENDF	Evaluated Nuclear Data File
FCC	Face Centered Cubic
FCI	Fuel - Coolant Interaction
FP	Fission Products
GRS	Gesellschaft für Anlagen- und Reaktorsicherheit
HLRS	High-Performance Computing Center at the University of Stuttgart
IAEA	International Atomic Energy Agengy
ICSBEP	International Handbook of Evaluated Criticality Safety Experiments
IEA	International Energy Agency
IKE	Institut für Kernenergetik und Energiesysteme
IRID	International Research Institute for Nuclear Decommissioning

JAEA	Japan Atomic Energy Agency
JEFF	Joint Evaluated Fission and Fusion File
JENDL	Japanese Evaluated Nuclear Data Libraries
KTA	Kerntechnischer Ausschuss
LWR	Light Water Reactor
MCCI	Molten Corium - Concrete Interaction
MOS	Margin of Subcriticality
MPI	Message Passing Interface
NEA	Nuclear Energy Agengy
NPP	Nuclear Power Plant
NRA	Nuclear Regulation Authority of Japan
ORNL	Oak Ridge National Laboratory
PCV	Primary Containment Vessel
PDF	Probability Density Function
PSD	Particle Size Distribution
PWR	Pressurized Water Reactor
RCC	Rank Correlation Coefficient
RCS	Reactor Coolant System
RPV	Reactor Pressure Vessel
SA	Severe Accident
SAM	Severe Accident Management
SC	Simple Cubic
SF	Spontaneous Fission
SFML	Safe Fuel Mass Limit

SS   Stainless Steel

STACY   Static Experiment Critical Facility

TMI-2   Three Mile Island 2

USL   Upper Safety Limit

Zry   Zircaloy

Chapter 1

Introduction

1.1 Motivation and background

According to the last report of the International Energy Agency (IEA) [24], the global energy-related CO_2 emissions rose by 1.7% in 2018 and hit a new record of 33.1 Gt CO_2. The reason is a higher energy consumption caused by strong economic and population growth worldwide. Currently, the energy sector accounts for two-thirds of total greenhouse gases, and coal-fired electricity generation alone represents 30% of global CO_2 emissions. That makes coal the single largest source of global temperature increase. To mitigate climate change and its catastrophic consequences, the energy sector must make an effort to reduce emissions worldwide. The international trend is to evolve towards low-carbon energy mixes. The European Commission presented last year the European Green Deal, an ambitious package of measures with the final goal of becoming climate-neutral by 2050. In this EU roadmap towards a sustainable economy, *"further decarbonizing the energy system is critical to reach climate objectives in 2030 and 2050"* [22]. The energy transition pathways are country-specific, but there is a growing global consensus that renewable energy systems and nuclear energy will be key to meet decarbonization targets. In this regard, IEA has confirmed the impact of renewables and nuclear energy on the decoupling between energy demand and emissions in 2018, with emissions growing 25% slower than energy demand [24].

Despite the advantages of nuclear energy as a carbon-free energy contributor, after the Fukushima accident, some countries decided to phase out nuclear (Germany, Belgium, and Switzerland). The Fukushima accident has had a profound impact not only on energy policies but also on general public acceptance. Internationally, great efforts are being made to reassess and strengthen the safety of nuclear power plants (NPP). New and improved severe accident management (SAM) and release mitigation systems

are being investigated and implemented. The scientific community has recognized some severe accident (SA) research issues and weaknesses that need further attention. The International Atomic Energy Agency (IAEA) held a Training Meeting on "Post-Fukushima Research and Development Strategies and Priorities" at IAEA Headquarters, Vienna, Austria, December 15-18, 2015 [126]. The purpose of this meeting was to provide a platform for experts from the Member States and international organizations to discuss research and development areas regarding the Fukushima Daiichi accident and severe accidents in general that need to be further investigated. The possibility of recriticality in damaged reactors, which is the focus of the present work, appeared as one of the research issues that raises most interest and must be addressed. Similarly, the Nuclear Energy Agency (NEA) brought together a group of senior researchers to identify research opportunities post-Fukushima [5], which again recognized the recriticality issue as one of the knowledge gaps in nuclear safety that needs further consideration.

1.1.1 Recriticality in severe accidents

The term 'severe accident' refers to an event with an extremely low probability of occurrence but involving significant core degradation, which can lead to the release of radioactive products into the environment and have serious consequences. It is also called 'core melt accident'. SAs can occur only by an accumulation of malfunctions (equipment and/or human errors together with failure of safety procedures). Three important SAs happened in history: Three-Mile Island 2 (TMI-2) in 1979, USA; Chernobyl in 1986, Ukraine; and, more recently, Fukushima Daiichi in 2011, Japan.

SAs generally start when the decay heat produced in the reactor cannot be removed properly due to a cooling failure. They involve complex thermal, mechanical, physical, chemical, and radiological processes, which are commonly divided in two phases:

- **In-vessel phase**, which covers core heat-up, fuel degradation, material relocation inside the reactor vessel, and fuel-coolant interaction (FCI). If the cooling is not properly restored, the phase will ultimately end up with the vessel failure and subsequent release of molten corium into the containment building.

- **Ex-vessel phase**, which covers corium spreading at the reactor pit, molten corium-concrete interaction (MCCI), containment behavior (including transport of radioactive substances), and the source term release into the environment (worst-case scenario).

The term 'corium' refers to a molten mixture of fuel together with structural and control materials from the core. Once the corium solidifies, it forms the so-called 'debris bed'.

1.1.1.1 Recriticality scenarios

Nuclear criticality safety is defined as "*protection against the consequences of an inadvertent nuclear chain reaction, preferably by prevention of the reaction*" [17] and is generally achieved through the control of a limited set of macroscopic parameters such as mass, concentration, moderation, geometry, isotopic composition, enrichment, density, reflection, and neutron absorption [45].

In case of an accident, the reactor is immediately shut down and must be kept subcritical from this moment on. Recriticality would occur if a sufficient quantity of fissile material is arranged unintentionally into a critical configuration after the reactor shutdown. Light Water Reactors (LWRs) have some safety mechanisms to control the reactivity that maintain the fission process and, therefore, the reactor power at the desired level. These mechanisms are:

- Control rods: strong neutron absorbers (normally Ag-In-Cd or B_4C) that can be inserted fully or partially in the reactor core to regulate neutron flux.

- Inherent stability: LWRs are designed so that in the event of a power increase, the reactor self-stabilizes, and feedback mechanisms automatically reduce the reactivity (negative void reactivity coefficient and negative Doppler reactivity coefficient).

- Boron injection: Pressurized Water Reactors (PWRs) use borated water under normal operating conditions to adjust the power up and down. In Boiling Water Reactors (BWRs), boron is injected only in case of emergency.

During a SA, these mechanisms can be progressively lost, leading to a risky situation where recriticality could be an issue. Figure 1.1 represents the temperature regimes for extended liquid phase formation in a SA. The control rods meltdown earlier (1200-1400 °C) than UO_2 fuel (~2850 °C). This premature low-temperature failure of the absorbers may result in an early relocation, which would cause a physical separation between control rods and fuel. If this happens, the control rods would lose their original functionality. Under this scenario, the feedback mechanisms are not sufficient in themselves to guarantee the subcriticality. Thus, if a positive reaction insertion occurs (e.g., reflooding the core with unborated water for cooling purposes), recriticality is very likely to happen. As the accident progresses, the design geometry of the reactor core will also be gradually lost (stainless steel, cladding, and, finally, UO_2 will melt down progressively), and with it, the inherent stability. Fortunately, a destroyed core will never be as reactive as in its original form. While the fuel melts forming the corium, recriticality can be fairly dismissed since the moderation of neutrons is very difficult (any liquid water in contact
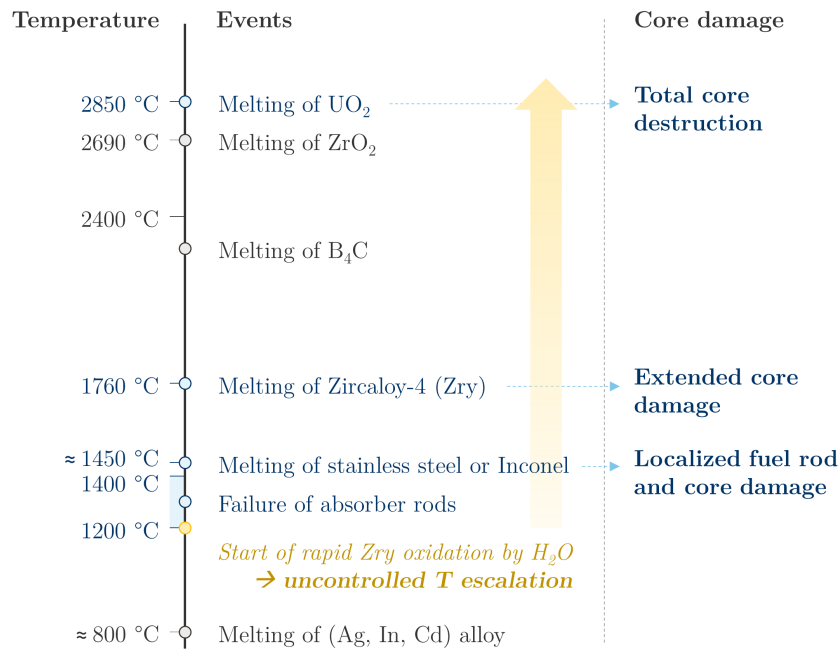
Figure 1.1: Temperature regimes for extended liquid phase formation in severe accidents [43]

with corium would evaporate immediately). Only after a while, when the reactor is cooled down and the corium solidifies forming the debris bed, recriticality becomes a concern again. At this point, boron injection into the coolant is the only mechanism remaining to control the criticality.

In summary, there are two potential recriticality scenarios (see Figure 1.2) that should be considered with special attention:

- **Recriticality after reflooding of a semi-intact core**. Recriticality may happen if reflooding of the reactor core with unborated water is performed after the separation between control rods and fuel in the early in-vessel accident phase.

- **Recriticality in debris beds**. Recriticality is possible after the solidification of the corium, when debris beds are formed either at the bottom of the vessel (in-vessel debris bed) or in the reactor containment (ex-vessel debris bed).

The recriticality potential in partially degraded cores after reflooding (first scenario) has been thoroughly investigated in several studies, for example, within the EU project SARA (Severe Accident Recriticality Analysis) [27] or by the U. S. Nuclear Regulatory Commission as part of its Accident Management Program [66].
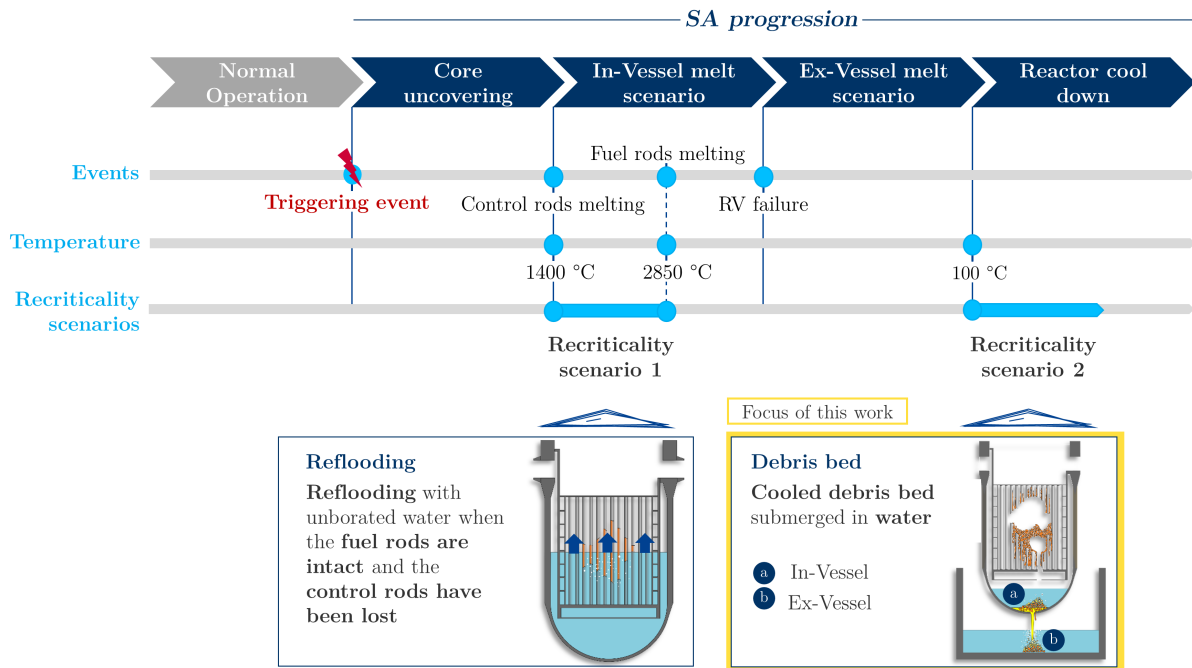
Figure 1.2: Recriticality scenarios during a severe accident

The criticality in debris beds (second scenario), which is the focus of the present work, was thoroughly investigated to assist the TMI-2 defueling activities (see Section 1.2.1), and, after years of inactivity, it has come to the fore again following the Fukushima accident. Unfortunately, the debris conditions at Fukushima are very severe, and the research team in charge of criticality safety has encountered serious obstacles to define the strategy that should be followed during the decommissioning. A criticality database of debris beds does not exist, neither a commonly accepted methodology nor a consensus about the most appropriate debris bed models and their applicability. This knowledge gap was evidenced after the Fukushima disaster and has been recognized by the scientific community [5]. All the aforementioned, coupled with the high uncertainty regarding the debris bed characteristics, make the criticality safety assessment at Fukushima a real challenge (see Section 1.2.2 for detailed information).

A recriticality event would cause the release of nuclear radiation that may be lethal for the nearby personnel. The generation of new fission products (FP) is the main concern and most potentially dangerous consequence of recriticality. After a SA, the safety barriers in the reactor that prevent the release of radiation into the environment may be severely damaged, resulting in a direct exposition of the public and workers. Thus, controlling the core subcriticality is one of the main accident management objectives. Based on the defense-in-depth concept, criticality control techniques that combine criticality

prevention, detection, and mitigation measures are necessary.

To prevent recriticality, SA mitigation measures prescribe the injection of emergency cooling borated water into the reactor core. However, this is not always feasible and will depend on the post-accident reactor conditions. In Fukushima damaged reactors, there is a major water problem that prevents this measure from being taken (see more details below in Section 1.1.1.2). Alternative prevention measures and enhanced detection and mitigation strategies must be investigated. Thus, performing a criticality evaluation of the debris beds is very important to predict possible risks and be able to establish the appropriate control measures if necessary.

1.1.1.2 Current situation in Fukushima

On March 11, 2011, the Great East Japan Earthquake of magnitude 9.0 on the Ritcher scale caused a big tsunami that led to a station blackout on the operating Units 1, 2, and 3 at Fukushima Daiichi Nuclear Power Station (1FNPS). The reactors were then isolated from their ultimate heat sink, resulting in a large core meltdown. Not only the cores but also the reactor pressure vessel (RPV) and the primary containment vessel (PCV) were damaged due to the failure of the cooling functions. As a consequence, a large amount of fuel debris was formed and is estimated to be distributed between the RPV (in-vessel scenario) and PCV (ex-vessel scenario). The tremendous damages caused also a significant release of radiation into the environment, either directly into the atmosphere or as contaminated water into the sea. The continuous leakage of the cooling water poured into the reactors as well as the inflow of groundwater into the damaged units became the main concern after the accident. The management of contaminated water has been the priority during the early years of Fukushima decommissioning activities.

Due to this 'water problem', maintaining a constant concentration of boron inside the damaged reactor buildings is very difficult.. Boron should be added endlessly, which is not feasible. Therefore, the debris beds in Units 1 to 3 are currently kept cool and stable by means of a continuous stream of non-borated water injected into these units. No active criticality control measure is implemented, but subcriticality is constantly being monitored by measurements of short-lifetime fission products gases (e.g., ^{133}Xe or ^{135}Xe) and water temperature. As no sign of criticality has been detected until now, the debris beds are assumed to be subcritical [118]. Nonetheless, any change in the reactors can endanger this apparently subcritical-stable condition. For that reason, it is a top priority to secure the subcritical state of the debris during the retrieval operations, when changes in the water level and debris structure are expected to occur. A boric acid injection system is already put in place to suppress nuclear fission in case of a

criticality event. Additional criticality prevention and monitoring technologies are also
being investigated as part of the strategic plan for a safe fuel debris retrieval, which is
underway [2, 46, 79]. A recriticality scenario would lead to the release of new fission
products with potentially severe consequences.

The Japan Atomic Energy Agency (JAEA), commissioned by the Nuclear Regulation
Authority of Japan (NRA), is currently working on a research program to support the
development of the criticality control system, which will be implemented during the fuel
debris removal activities at 1FNPS [119]. The program consists of three major activities:
definition of a method to evaluate the criticality risk, computation of basic criticality
characteristics of fuel debris, and validation of computation results through criticality
experiments. The final objective is to develop a criticality map that will be used to
reveal the recriticality potential of a debris bed taking the debris conditions as input
parameters.

1.2   State of the art

SA research started in the 1970s with the first probabilistic safety assessments. More
advanced research programs began at the beginning of the 1980s following the TMI-2
accident, which occurred in 1979, demonstrating that a nuclear core melt accident was
actually possible. The Chernobyl accident (1986) and, more recently, the Fukushima
disaster (2011) underlined the need to continue and extend research in this field. As a
result, a huge amount of R&D has been performed in the last decades internationally.
The complex processes involved in SAs have been extensively investigated numerically
and experimentally. As a result, large progress has been reached, although several issues
still need further attention to reduce uncertainties and consolidate the SAM plans. B.R.
Sehgal [102] provides a complete overview of SA research and phenomenology.

The recriticality issue in SAs was first taken seriously after TMI-2. The first criti-
cality analyses of debris beds were performed to ensure subcriticality during the TMI-2
defueling process (see Section 1.2.1). The investigations were abandoned afterward and
have been restarted recently after the Fukushima disaster. Since then, relevant progress
has been made (see Section 1.2.2). Currently, three complementary investigation lines
can be distinguished:

   1. **Numerical evaluation of criticality with neutronic codes**. Neutron trans-
      port codes (e.g., MCNP [31], Serpent [64], or MVP [76]) and cross section libraries
      (e.g., ENDF/B-VII [13] or JENDL-4.0 [105]) are used to model debris beds and

calculate the neutron multiplication factor of the system. The present work falls into this category.

2. **Experimental evaluation in critical facilities**. The computational models include some uncertainties that must be clarified by criticality experiments. The experimental database is very limited. Thus, new experiments that represent more closely real debris beds are planned and will be conducted by JAEA with the modified STACY (Static Experiment Critical Facility) and samples that simulate fuel debris compositions [35, 70, 106].

3. **Measurements in real accident scenarios**. Subcriticality is being monitored at 1FNPS damaged reactors through measurements of short-life time FP (^{133}Xe or ^{135}Xe) and water temperature. The Japanese International Research Institute for Nuclear Decommissioning (IRID) is developing additional advanced technologies to control the criticality during the fuel debris retrieval (e.g., criticality approach detection systems or FP gamma detector systems) [36].

The characterization of debris beds is also essential for the criticality assessment. Information on debris bed characteristics is needed to develop suitable debris bed models for the criticality computation as well as to generate appropriate debris bed simulant samples for the critical facilities. A realistic and accurate estimation of the recriticality potential will depend largely on the quality of debris bed data. There are three main ways to gain knowledge about debris beds:

1. **Numerical simulations with SA codes**. SA integral codes like MAAP [23], ASTEC [14], or MELCOR [28] simulate the entire accident with relatively low computing effort, from the initiating event to the possible release of source term to the environment and taking into account the main safety systems. SA detailed codes like ATHLET-CD [12] use best-estimate (BE) phenomenological models and provide a much more accurate simulation of the NPP behavior with higher computing times. Additionally, dedicated SA codes perform a finer simulation of specific phenomena (e.g., core degradation or hydrogen risks).

2. **Small-scale experiments** that reproduce specific phenomena: FCI experiments (e.g., DEFOR [53] or FARO [67]), debris spreading and sedimentation experiments (e.g., PDS-P [62]), MCCI experiments (e.g., OECD-MCCI [25] or VULCANO [16]), etc.

3. **Data collected from real accident scenarios** like TMI-2 [33], Chernobyl [89], and Fukushima (samples, visualization, etc).

Due to the high uncertainties of SA code results, the most reliable debris bed data is obtained from experiments and samples of accidents but also the most complicated. TMI-2 samples and examinations [33] have been especially valuable to gain knowledge.

The diagram in Figure 1.3 shows the whole process behind the criticality evaluation of debris beds and available resources.

1.2.1   TMI-2 criticality analysis

Nuclear criticality safety was one of the key safety issues during the recovery of TMI-2. The fuel partially melted and was retained in the RPV. A prevention-based approach was adopted to avoid recriticality. It was decided to increase the boron concentration in the coolant as much as necessary to maintain subcriticality for all conceivable core configurations ('infinite poison' concept [32]).

Numerous calculations of the shutdown margin were performed by criticality experts of the most important nuclear institutions in the United States. These analyses were based on very limited knowledge about the core configuration; thus, very conservative core disruptive models were used. Parametric criticality analyses were performed in parallel to identify worst-case parameter combinations, i.e., the most reactive compositions and configurations. The neutron multiplication factor (k_{eff}) criterion used to define the poison concentration for the reactor coolant system (RCS) was <0.99, i.e., a shutdown margin of at least 1%. That, coupled with a very conservative core model, provided an appropriate margin of safety. In 1984, the studies culminated with a report [32] that established a minimum boron concentration of 4350 ppm. For that, a lenticular design-basis model was employed, which included several inherent conservatisms (see Figure 1.4). The model assumed that the entire fuel inventory was accumulated at the bottom of the RPV, arranged in a double spherical segment shape (lenticular). The central region consisted of the highest enriched fuel (batch 3) and was surrounded by a mixture of the rest fuel batches (batches 1 and 2). No burnup credit was given. A spherical steel reflector supported the fuel, which was covered by borated water with an optimum fuel-to-moderator ratio. No structural nor poison materials were considered. The fuel debris was modeled as spherical UO_2 particles in borated water arranged in a dodecahedral lattice structure. The particle size was chosen to conserve the surface-to-mass ratio of a standard fuel pellet. For the criticality calculations, the three-dimensional multigroup Monte Carlo criticality code KENO V.a. [92] was used, which is the first criticality safety analysis tool in SCALE [95] system, developed by Oak Ridge National Laboratory (ORNL).

Additionally, criticality calculations were performed to design the defueling canisters
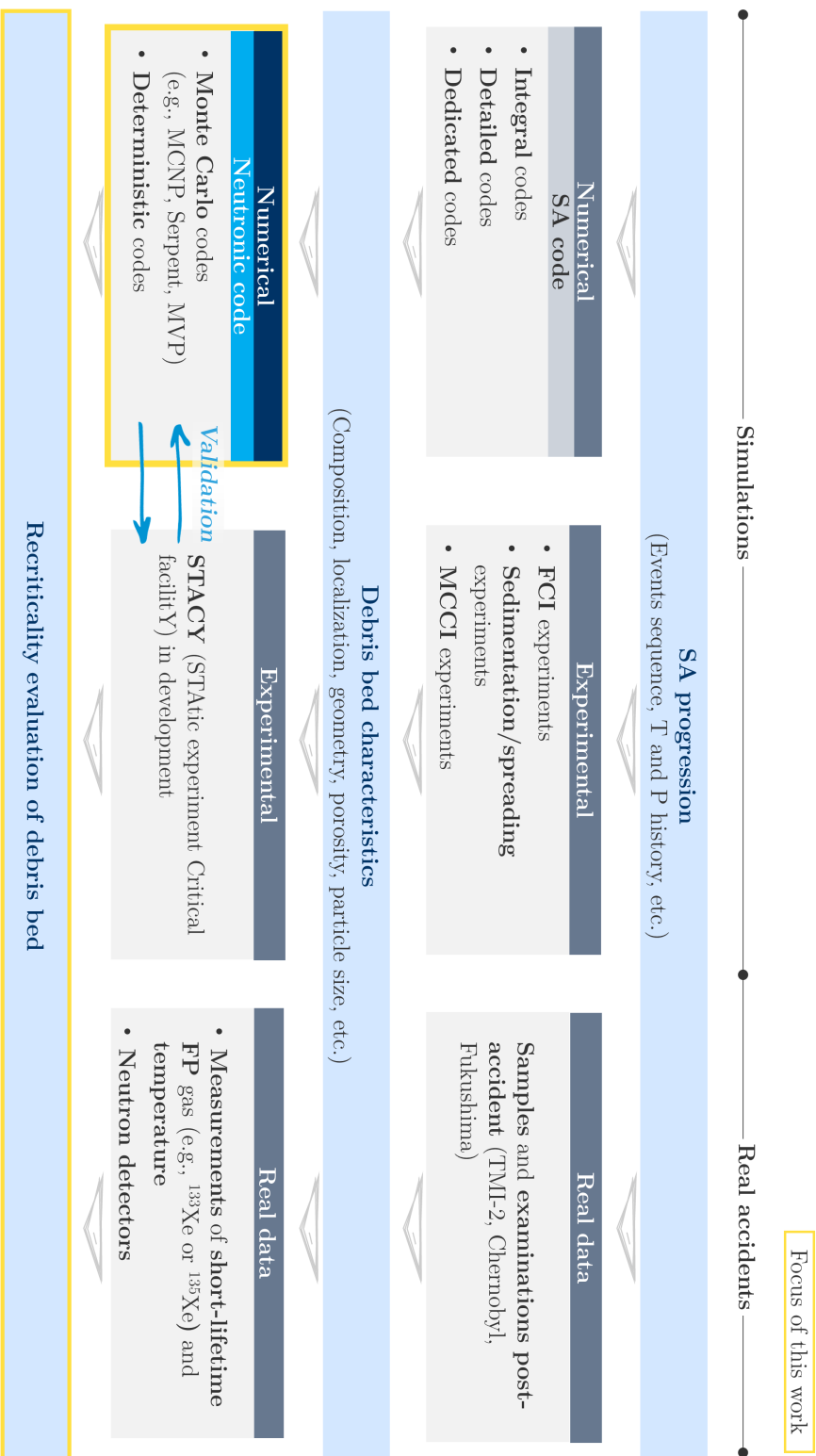
Figure 1.3: Overview of resources and research lines for the criticality evaluation of debris beds
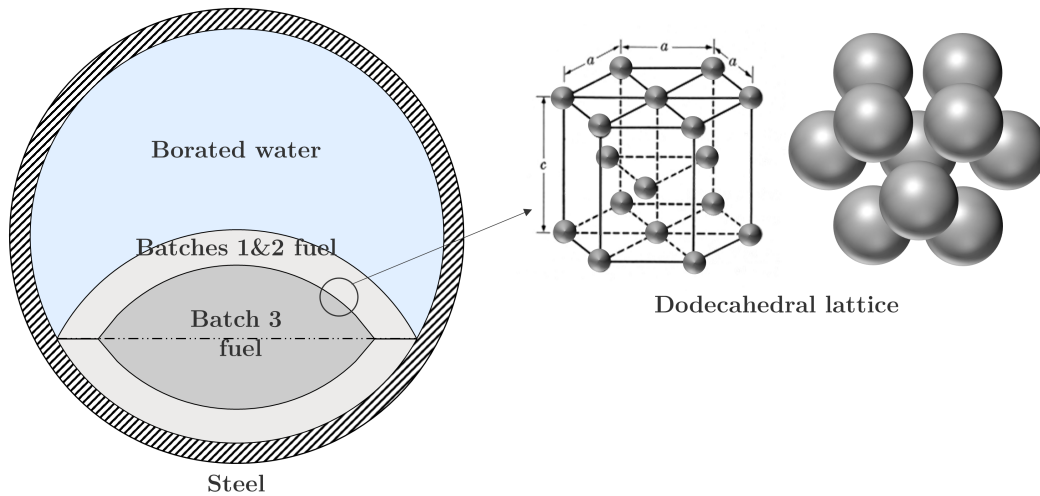
Figure 1.4: Lenticular debris bed model used for the TMI-2 RCS criticality report [32]

and canister-handling devices [38]. In these cases, a k_{eff} criterion of <0.95 was used to define the fixed poison requirements.

A computer code benchmark program was completed to determine an appropriate analytical uncertainty bias [32, 74]. A limited number of critical experiments were selected based on their similarity with the damaged TMI-2 core conditions in three aspects: fuel enrichment, soluble boron concentration, and neutron moderation. Conservatively, the worst case was taking as bounding value, and a bias of 2.5% Δk was adopted.

W. R. Stratton [111] and D. S. Williams et al. [124] provide an overview of the main criticality analyses done to support TMI-2 defueling.

The reactor defueling was successfully accomplished between 1985-1988, and no criticality event was detected. The Defueling Completion Report [33] describes in detail the conditions of the core before and after defueling as well as the defueling operations. Furthermore, a criticality assessment of the residual fuel is presented to demonstrate that unintentional criticality had been precluded in the facility.

1.2.2 Fukushima criticality analysis

As explained before in Section 1.1.1.2, the conditions at 1FNPS are very severe. Due to a water issue, boron injection cannot be used to prevent criticality. Consequently, a mitigation-based approach has been adopted [51].

The computation of basic criticality characteristics of debris beds is one of the major activities of the criticality control program developed by JAEA [119]. Due to the high uncertainty regarding the condition of the debris, a comprehensive criticality database
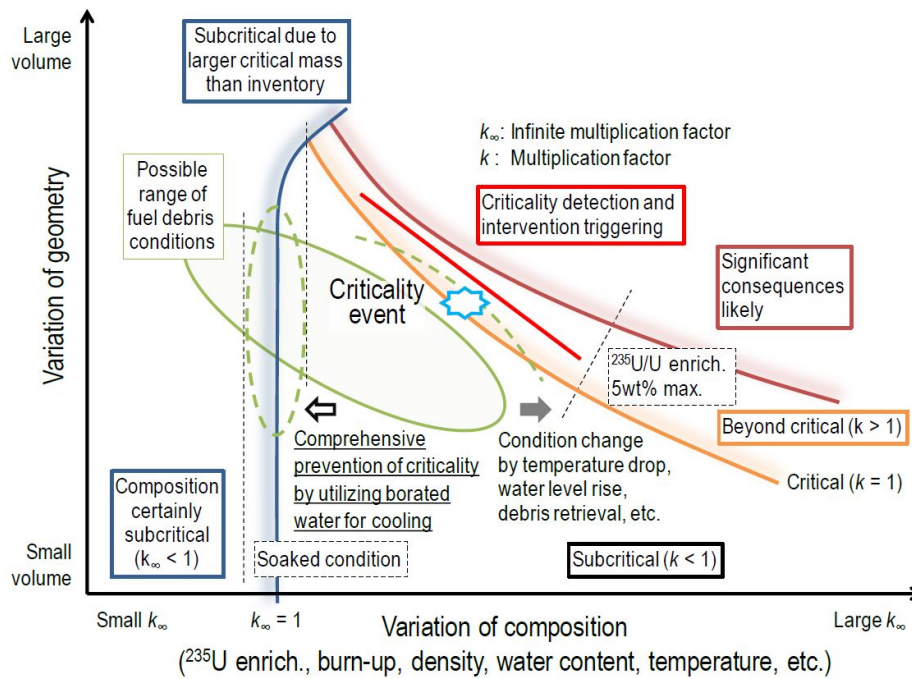
Figure 1.5: Criticality map concept developed by JAEA, taken from [51]

must be developed to cover any credible scenario. The criticality database or "criticality map" will be used to reveal the criticality situation of debris beds taking the debris conditions as input parameters. The "criticality map" concept is depicted in Figure 1.5 and shows a qualitative criticality assessment as a function of the debris bed composition and geometry. The criticality computations aim to find out the specific numbers or debris conditions, which are behind the lines that divide the map into subcritical, critical, and supercritical areas. For example, for which compositions debris beds would never be critical regardless of the geometry. In the future, once observations or sample analyses reveal the current debris bed conditions, they will be located on the map to evaluate the criticality risk. Additionally, it is also necessary to study how the criticality condition of a given debris bed can move on this map as a result of expected changes caused by defueling activities (e.g., temperature drop or debris relocation).

The criticality of UO_2-water composites has been computed in the past for many years to produce the criticality safety handbook [85], where the minimum critical masses for uranium-water homogeneous mixtures can be found. JAEA criticality safety group intends to extend this standard to wider conditions more typical of debris beds, e.g., UO_2-steel or UO_2-concrete composites. Several studies have been published, in which the MCCI products are modeled as a homogeneous mixture of fuel and concrete in form of spherical particles and submerged in water [49, 117] (see debris model in Figure
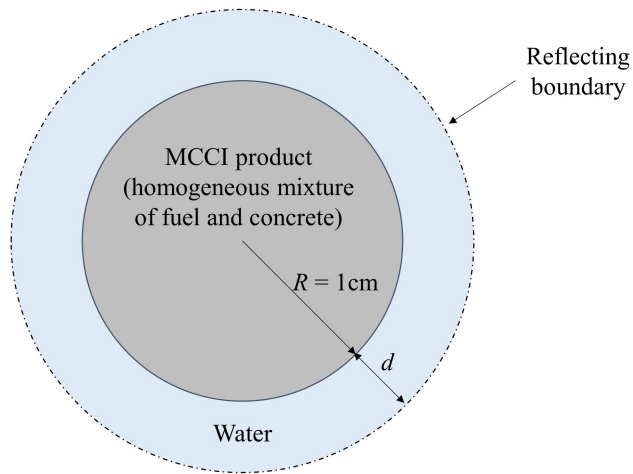
Figure 1.6: Debris bed model representing UO$_2$-concrete composites used by JAEA [49, 117]

1.6). Major parameters of these analyses are fuel composition, particle size, concrete volume fraction, and volume ratio between the water and the MCCI product. Infinite multiplication factors (k_∞) and critical masses were computed using the continuous-energy Monte Carlo code MVP [76] and the nuclear data library JENDL-4.0 [105]. Boron concentrations in water necessary to achieve k_∞=1 were also computed using the SRAC [82] code system and JENDL-4.0. The nuclide inventory of the BWR spent fuel was calculated with the SWAT burnup code system [112]. These studies prove the moderation capacities of concrete.

The aforementioned new criticality safety standards for fuel debris, including the computation models, must be validated by critical experiments. The experiment results available until now do not represent the conditions of debris beds properly. For that reason, JAEA is modifying the STACY critical facility and preparing critical experiments with simulated fuel debris samples [35, 107]. Currently, the feasibility of using a heterogeneous core arranging UO$_2$ rods and structural materials rods (e.g., SiO$_2$ simulating concrete) in water is being investigated [99].

In parallel with these activities, IRID is working on a statistical method for the evaluation of criticality at 1FNPS [72]. They work on the basis that a high conservatism may lead to excessive requirements for the criticality control system, so a methodology to evaluate the realistic status of the plants is proposed. The statistical method has three major steps: sampling of debris bed parameters that are defined by probability density functions (PDF), computation of k_{eff} with a Monte Carlo code, and statistical processing of results. Much of the success of this methodology is based on the information available

regarding the debris beds, which is still very limited. However, useful information about the fuel debris is expected to be collected by observations and future in-core investigations. Parameters with a strong correlation with the neutron multiplication factor can be also derived from these analyses. This information will allow concentrating future resources and efforts intelligently and efficiently. The first exploratory statistical calculations suggest that the criticality risk is extremely small. The distribution, amount, and composition of fuel debris were estimated with the SA code MAAP [23]. The Monte Carlo calculation code MVP [76] and the nuclear data library JENDL-4.0 [105] were used for the analyses.

1.2.3   TMI-2 vs. Fukushima criticality studies

Boration of the coolant water was practiced in TMI-2 and is the preferable way to control the criticality in debris beds. As illustrated in Figure 1.5, borated water bounds the criticality characteristics of debris beds into a small region and keeps it far from critical condition no matter how much temperature or geometry changes. The more severe situation in Fukushima has forced a much more complicated criticality safety approach, which requires an innovative risk assessment method and the backup of an extensive criticality database. A new experiment critical facility (STACY) is being developed to provide an adequate validation to on-going computations.

The criticality calculations and debris modeling in TMI-2 were also relatively simple. The most reactive possible configurations were first identified with parametric analyses and then used to develop extremely conservative models and estimate the boron concentration. In Fukushima, parametric calculations are necessary to investigate the impact of new parameters that have come to the fore, for example, the presence of MCCI composites. An excessive conservatism is being avoided, and more realistic assumptions are used in the debris bed models; even a statistical evaluation method is considered for a more realistic criticality evaluation of debris beds.

Table 1.1 shows a comparison between the main characteristics of the criticality computations performed after the TMI-2 and Fukushima accidents.

1.3   Aim and objectives

The present work aims to provide an approach to assess numerically the recriticality risks in debris beds and thus contribute to the development of a criticality map or database for debris beds. As already pointed out, a criticality map will allow identifying risk

Table 1.1: Overview of TMI-2 vs. Fukushima criticality computation analyses

	TMI-2	Fukushima
Accident date	1979	2011
Debris bed situation	Debris retained in RPV Up to 50 % core meltdown	Debris distributed between RPV and PCV (mostly in PCV) Up to 100 % core meltdown
Criticality safety approach	Prevention-based (boron injection)	Risk-informed, mitigation-based
Objective of analysis	Estimate amount of boron needed to secure subcritical state	Develop an extensive criticality database for debris beds
Type of analysis	Parametric analysis Conservative analysis	Parametric analysis Conservative analysis Statistical analysis
Debris bed model	Extremely conservative	Slightly conservative
Neutron transport code	KENO, XSDRNPM	MVP, MCNP
Burnup code	ORIGEN-S	SWAT, ORIGEN2
Library	ENDF/B-IV	JENDL-4.0, ENDF/B-VII
Validation	Computer code benchmark (bias = 2.5% Δk)	STACY critical facility in development
Results	4350 ppm B to maintain subcriticality	Recriticality potential low Database in development Further analysis needed
Impact	Successful defueling (1985-1988) No criticality event detected	Defueling planned for 2025 No sign of recriticality until now

situations rapidly, define prevention and mitigation measures, and apply them when necessary quickly and effectively. It will be a key tool for criticality safety during the decommissioning of Fukushima but also for the future design of safer SAM programs. The development of a criticality map is an arduous task that requires the investigation of appropriate debris bed models and numerous computations under a broad range of possible conditions. It is led by JAEA but a global effort and international cooperation are essential. Additionally, criticality safety evolves towards more realistic assessments for which more refined models and methods are necessary. Based on these motivations, the objectives of the present work are:

- Develop an adequate neutronic debris bed model for criticality calculations.

- Identify criticality safety parameter ranges for Fukushima debris beds.

- Study criticality characteristics of ex-vessel debris beds containing MCCI products, i.e., the effects of concrete on the criticality.

- Provide an alternative statistical method for a realistic criticality assessment in debris beds.

These objectives will specifically contribute to improve the debris bed models, extend the criticality database, and facilitate future analyses.

1.4   Structure of the thesis

This thesis is divided into seven chapters, including the present one, which has introduced the problem, the research gap, and the objectives of the work.

Chapter 2 is devoted to the methodology for the criticality evaluation of debris beds and provides some theoretical background about the criticality calculation with neutron transport Monte Carlo codes.

Chapter 3 discusses the modeling options for the debris beds characteristics that may be relevant for criticality, from the most conservative simplifications to more realistic approaches.

A conservative criticality evaluation of Fukushima debris beds is performed in Chapter 4 in order to identify criticality safety parameter ranges.

The criticality characteristics of uranium-concrete systems, which are representative of ex-vessel debris beds, are thoroughly investigated in Chapter 5.

Chapter 6 explains an alternative statistical method for a more realistic evaluation of debris beds.

Finally, Chapter 7 provides a brief summary of the accomplished work, followed by some recommendations for future research.

Chapter 2

Methodology

As explained in the previous chapter, this study will contribute to the global effort of developing a criticality database for debris beds that are formed during SAs in LWRs. Assessing the recriticality potential in debris beds numerically requires:

- quantifying the possible characteristics of debris beds.

- developing an adequate neutronic model for the criticality evaluation of debris beds.

- defining a procedure to compute the criticality as well as to process calculation results in order to provide some manageable conclusions (criticality safety ranges, probability of recriticality, etc.).

- finding appropriate criticality experiments for the validation of the computations.

This chapter describes the work performed to meet the aforementioned requirements. Figure 2.1 shows a schematic overview of the conducted work and methodology of the present thesis.

2.1 Pre-processing: debris bed data collection and modeling

Some preliminary work must be performed before computing the criticality of debris beds. This work consists of defining a realistic debris bed database together with an adequate debris bed model and will be the foundation upon which the criticality analyses will be performed.
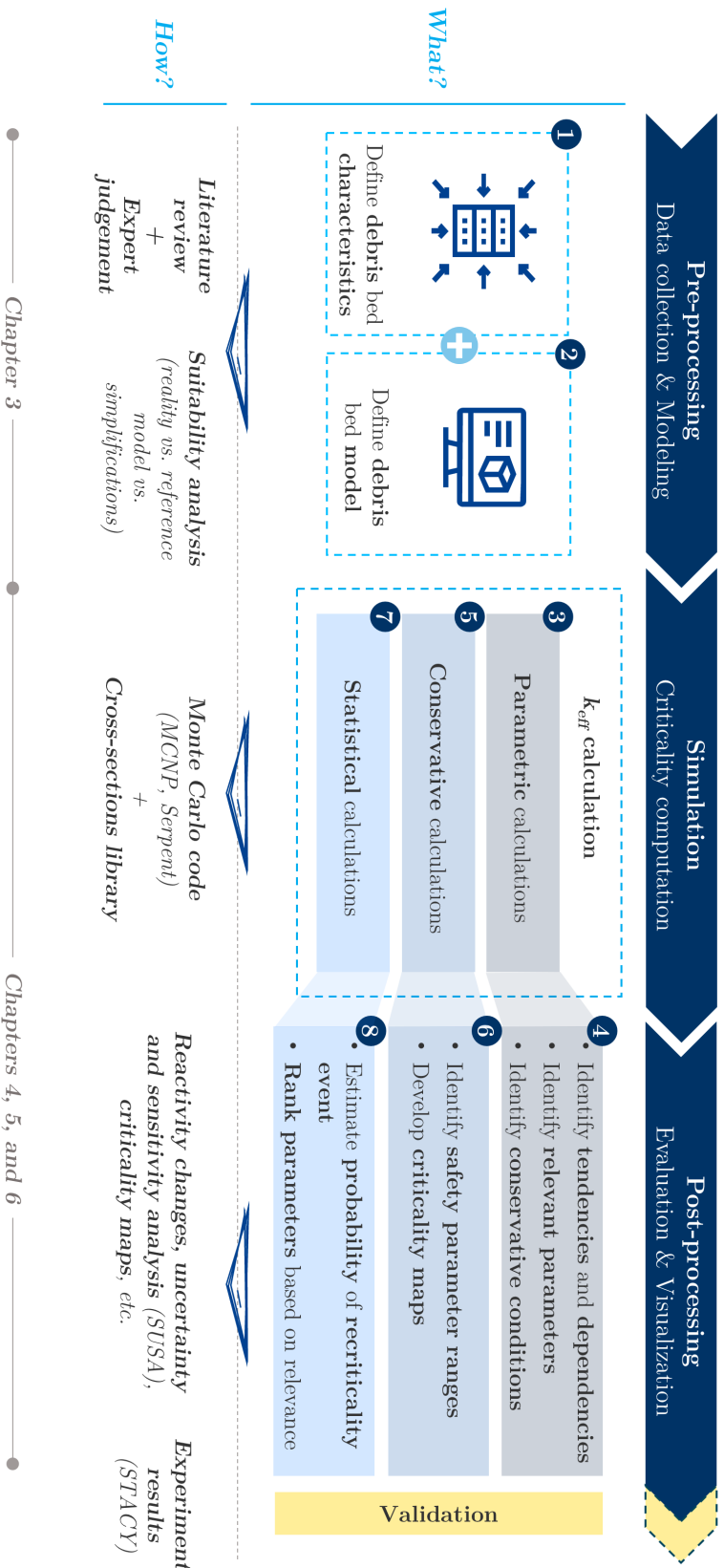
Figure 2.1: Overview of methodology to assess numerically the criticality in debris beds

An exhaustive literature review is needed to understand the formation process of debris beds and gather information about possible characteristics. In parallel, a pre-selection of parameters with a potential impact on the criticality must be done. Ideally, the final result of this groundwork would be a debris bed database with all the potentially relevant parameters and their uncertainty distributions. Unfortunately, the high uncertainties regarding the debris characteristics make this task a great challenge. Nonetheless, it is important to quantify the debris conditions and uncertainties as far as possible with the guidance of expert judgment. This information will be used to define the debris bed model and as input for the criticality computations.

Given the high complexity and uncertainty of debris beds, conservative assumptions and simplifications have to be adopted to achieve a computationally feasible debris bed model. An adequate compromise between model accuracy and simplicity must be found. For that, different possibilities of modeling should be investigated and compared.

Chapter 3 describes the debris parameters that should be taken into account for a criticality assessment, collects information about realistic debris bed conditions and discusses the different debris bed modeling options, from very conservative simplifications to more complex and realistic approaches.

2.2   Simulation and post-processing: numerical methods for criticality evaluation

A system containing fissile material (^{233}U,^{235}U, ^{239}Pu, or ^{241}Pu) is critical if it maintains a steady self-sustaining nuclear chain reaction. In a critical configuration, the population of neutrons remains constant in time, i.e., of the several neutrons produced by a single fission, an average of one leads to a new fission; the other neutrons are lost either by capture or leakage. This is a delicate balance that depends upon the composition, quantity, and configuration of the materials in the system and environment. A nuclear reactor is designed to operate in critical condition, which is characterized by a steady power level. Reaching criticality conditions inadvertently is not easy, but may happen. This work investigates under which conditions an inadvertent criticality event may occur in debris beds after SAs. To study this possibility, the balance of neutrons within the system must be calculated.

Basic notions of the neutron transport theory are presented below to introduce the criticality problem and the numerical methods available to solve it.

2.2.1 Neutron transport

The behavior of a nuclear system is governed by the distribution of neutrons in space, energy, and time. Neutrons are born from a source or fission and travel through a physical system interacting with other nuclei until they are eventually absorbed or leak out through a boundary. The neutron transport theory describes the neutron behavior through the study of the motions and interactions of the neutrons with materials. It can be considered as a specialized branch of the kinetic theory of gases developed by Boltzmann and his followers at the end of the 19th century; the basic ideas are common and can be found in classic references [6, 19, 21] and more recent publications [93, 110]. The neutron transport equation, often called the Boltzmann transport equation, describes mathematically the neutron balance in a system and can be used to calculate the neutron distribution.

2.2.1.1 The neutron transport equation

The conservation of the number of neutrons is a basic principle in the study of neutron transport. The neutron transport equation is the mathematical representation of this balance between neutron gain and losses in a system:

$$\frac{\partial N}{\partial t} = Production\,rate\,(Q) - Removal\,rate\,(R) - Leakage\,rate\,(L) \tag{2.1}$$

where $N = N(\boldsymbol{r}, \boldsymbol{\Omega}, E, t)$ is the angular neutron density. In a steady-state system, the rate of change of the angular neutron density is zero ($\frac{\partial N}{\partial t} = 0$).

Appendix A defines certain quantities, which are required to describe the neutron transport problem and derive the transport equation. Making use of these, the equation can be expressed in terms of the angular neutron flux $\psi = \psi(\boldsymbol{r}, \boldsymbol{\Omega}, E, t)$ as:

$$\frac{1}{v}\frac{\partial \psi}{\partial t} = Q - \Sigma_t \psi - \boldsymbol{\Omega} \cdot \nabla \psi \tag{2.2}$$

in units $[n \cdot cm^{-3} \cdot MeV^{-1} \cdot sr^{-1} \cdot s^{-1}]$, where:

- $\frac{1}{v}\frac{\partial \psi}{\partial t}$ is the rate of change of neutron density: $N(\boldsymbol{r}, \boldsymbol{\Omega}, E, t) = \frac{1}{v}\psi(\boldsymbol{r}, \boldsymbol{\Omega}, E, t)$

- $Q = Q(\boldsymbol{r}, \boldsymbol{\Omega}, E, t)$ is the neutron source, which includes external neutron sources Q_{ext}, production due to scattering from other energies and directions Q_s, and neutrons generated by fission events Q_f.

$$Q = Q_{ext} + Q_s + Q_f \tag{2.3}$$

$$Q_s = \int_0^\infty \int_{4\pi} \Sigma_s(\boldsymbol{r}, E' \to E, \boldsymbol{\Omega}' \to \boldsymbol{\Omega}, t)\psi(\boldsymbol{r}, \boldsymbol{\Omega}, E, t)dE'd\Omega' \qquad (2.4)$$

$$Q_f = \frac{\chi(E)}{4\pi} \int_0^\infty \int_{4\pi} \nu(E')\Sigma_f(\boldsymbol{r}, E', t)\psi(\boldsymbol{r}, \boldsymbol{\Omega}, E, t)dE'd\Omega' \qquad (2.5)$$

where $\Sigma_s(\boldsymbol{r}, E, t)$ and $\Sigma_f(\boldsymbol{r}, E, t)$ are the scattering and fission macroscopic cross sections respectively, $\chi(E)$ is the energy distribution of the outgoing fission neutrons (assuming isotropism), and $\nu(E)$ is the mean number of neutrons released in a fission event, typically 2.3.

- $R = \Sigma_t\psi$ represents the neutron losses due to all type of collisions, being $\Sigma_t(\boldsymbol{r}, E, t)$ the total macroscopic cross section.

- $L = \boldsymbol{\Omega} \cdot \nabla\psi$ is the neutron streaming term, which represents the neutron current $\boldsymbol{J}(\boldsymbol{r}, E, t)$ across a surface S with normal $\boldsymbol{n}$.

$$\int_S (\boldsymbol{J} \cdot \boldsymbol{n})dS = \int_V \nabla\boldsymbol{J}dV = \int_V \nabla[\psi\boldsymbol{\Omega}]dV = \int_V \boldsymbol{\Omega}\nabla\psi dV \qquad (2.6)$$

The neutron transport equation 2.2 depends on seven variables: space coordinates $\boldsymbol{r}(x, y, z)$, neutron motion direction $\boldsymbol{\Omega}(\theta, \varphi)$, energy E, and time t. With appropriate initial and boundary conditions, the transport equation can be solved, yielding the expected neutron distribution within the geometry; however, this is a formidable task. Only the most simple problems can be solved exactly; practical problems must be solved either approximately or numerically.

Deterministic vs. Monte Carlo methods From the 1950s, many different numerical methods have been investigated to solve the neutron transport equation [65, 68]. Essentially, two approaches can be distinguished: deterministic methods and stochastic techniques. Deterministic methods use approximate forms of the equation, discretize the problem, and solve the resulting system of algebraic equations analytically. Alternatively, stochastic (or Monte Carlo) methods are based on a probabilistic interpretation of the transport process and solve the problem by simulating the behavior of individual neutrons. The idea is that a sufficiently large number of individual histories simulations recovers the average behavior of the whole system. In other words, deterministic methods provide an exact solution to an approximate problem, while Monte Carlo methods provide an estimated solution with a statistical error to the exact problem.

For the calculations of the present thesis, the Monte Carlo method was chosen. Monte Carlo techniques do not use directly the Boltzmann equation to solve the transport problem; only a good knowledge of the involved physical phenomena such as scattering or absorption is required to simulate the particle transport properly. The main advantage of Monte Carlo over other methods is the ability to handle complex geometries and nuclear cross section data. In the early stages, multi-group Monte Carlo codes such as KENO [92] were developed; these divided the neutron energy spectrum into multi-groups due to the limited memory capacity. However, today's computers have larger memory capacity and faster processors that allow using a continuous neutron energy spectrum instead of a multi-group one. Among the most broadly used continuous-energy Monte Carlo codes are MCNP [31], MVP [76], or Serpent [64]. Therefore, Monte Carlo calculations are currently free of errors linked to any kind of approximation method. If the system geometry and nuclear data are known, the calculation results will contain only statistical errors[1]. These are inevitable but can be reduced to the desired level by increasing the number of simulated particles, and thus the calculation time. Additionally, the very nature of the method makes it ideal for parallel computation. The particle histories are independent of each other and can be run in parallel. On the contrary, deterministic methods require reasonable simple geometries and multi-group approximations to continuous energy neutron cross section data. Obtaining adequate multi-group cross sections for each specific problem may be a time-consuming task that remains the most significant obstacle to solving the transport problem deterministically in a reliable, efficient, and user-friendly manner [93].

2.2.1.2   The criticality problem

The neutron transport equation can be expressed in operator notation as follows:

$$\frac{1}{v}\frac{\partial \psi}{\partial t} + M\psi = Q_{ext} + F\psi \tag{2.7}$$

where M is the transport operator and F is the fission operator:

$$M\psi = \Sigma_t \psi + \boldsymbol{\Omega} \cdot \nabla \psi - \int_0^\infty \int_{4\pi} \Sigma_s(\boldsymbol{r}, E' \rightarrow E, \boldsymbol{\Omega}' \rightarrow \boldsymbol{\Omega}, t)\psi(\boldsymbol{r}, \boldsymbol{\Omega}, E, t)dE'd\Omega' \tag{2.8}$$

$$F\psi = \frac{\chi(E)}{4\pi} \int_0^\infty \int_{4\pi} \nu(E')\Sigma_f(\boldsymbol{r}, E', t)\psi(\boldsymbol{r}, \boldsymbol{\Omega}, E, t)dE'd\Omega' \tag{2.9}$$

---

[1]In practice, both Monte Carlo and deterministic calculations have adittional sources of errors: modeling errors, approximations in cross section values, etc.

In a critical system, the population of neutrons remains constant in time without the need for external sources. The production of neutrons due to fission exactly balances the loss of neutrons due to capture and leakage; then, a nonzero, steady-state neutron flux φ is possible and $\frac{\partial N}{\partial t} = \frac{1}{v}\frac{\partial \psi}{\partial t} = 0$. If no external neutron sources are considered, solving the neutron transport equation becomes an eigenvalue problem, also called criticality problem:

$$M\psi = F\psi \tag{2.10}$$

In the above form, only a critical system can be solved. To consider also subcritical and supercritical configurations, the above equation is transformed introducing a dimensionless factor k_{eff} that modifies the fission operator:

$$M\psi = \frac{1}{k_{eff}}F\psi \tag{2.11}$$

$$\psi = \frac{1}{k_{eff}}M^{-1}F\psi \tag{2.12}$$

The factor k_{eff} is the *effective multiplication factor* and allows altering the number of neutrons emitted by fission reactions in order to make the system critical. If $k_{eff} < 1$, the fission source must be increased so that a steady-state solution can exist; capture and leakage dominate fission, and the system is subcritical. If $k_{eff} > 1$, the fission source must be decreased to achieve critical conditions; fission dominates capture and leakage, and the system is supercritical. If $k_{eff} = 1$, capture and leakage exactly balance fission, and the reactor is critical [93].

Thus, the neutron balance of a nuclear system is characterized by k_{eff}, which in reactor theory is interpreted as the ratio between the number of neutrons of successive generations[2]:

$$k_{eff} = \frac{N_n}{N_{n-1}} = \frac{\text{number of neutrons in one generation}}{\text{number of neutrons in preceding generation}} \tag{2.13}$$

Neutron physicists use commonly another quantity derived from k_{eff} known as *reactivity*, which describes the deviation of an effective multiplication factor from unity:

$$\rho = \frac{k_{eff} - 1}{k_{eff}} \tag{2.14}$$

In practice, reactivity may take very small values and is commonly quantified in *per*

---

[2]A generation is the life of a neutron from birth in fission to death by escape, capture, or absorption leading to fission

cent mille (1 pcm = 10^{-5}).

The power iteration method   Above it has been shown how the criticality problem can be transformed into an eigenvalue problem, one of the most typical mathematical problems in science and engineering. The most common and well understood approach to solve equation 2.12 is the power iteration, a mathematical method for approximating the dominant eigenvalues and eigenvectors of a matrix [34, 87, 98]:

$$\psi^{(n+1)} = \frac{1}{k_{eff}^{(n)}} F M^{-1} \psi^{(n)}, \quad n = 0, 1, ..., \quad \text{given } \psi^{(0)} \text{ and } k_{eff}^{(0)} \tag{2.15}$$

Power iteration can be applied also with Monte Carlo techniques to solve k_{eff} eigenvalue problems. The process is described below in Section 2.2.2.

2.2.2   Criticality calculations with Monte Carlo codes

Stochastic or Monte Carlo methods estimate the collective behavior of particles in a system by sampling a large number of individual particle histories whose trajectories and interactions are simulated by a digital computer [37].

Particle transport is characterized by a very large number of particles undergoing random and independent histories. Each event of an individual particle history (scattering, absorption, etc.) occur in nature with the probability of occurrence determined by a cross section. Consequently, the global behavior of the whole system is predictable and can be estimated with a statistical error that decreases as the number of particles simulated increases (neutrons per cycle × number of cycles) [93]. The history of a particle refers to the events that occur during the particle's life. The life of a neutron begins at his birth, either from an external source or a fission event, and ends with absorption or leakage outside the system. Using random numbers, the computer generates a statistical history of simulated particles. The random numbers together with the cross sections determine when an interaction occurs, which type of interaction (absorption, fission, inelastic scattering, etc.) occurs, how much energy is lost, what is the new direction of the particle, or how many neutrons are generated in a fission event.

Monte Carlo techniques have been used to compute k_{eff} since the 1950s, and most of them use the standard power method (see equation 2.15), where each iteration n corresponds to a fission generation or k_{eff} cycle in the simulation [10]. The main steps of the process are:

1. Provide an initial neutron source ψ and an initial guess of k_{eff} (generation $n = 0$): $k_{eff}^{(0)}$, $\psi^{(0)}$.

2. Run M histories and save fission sites, which will be used as source in the next generation $\psi^{(n+1)}$: $\psi^{(n+1)} = \dfrac{1}{k_{eff}^{(n)}} M^{-1} F \psi^{(n)}$.

3. Estimate the new neutron multiplication factor $k_{eff}^{(n+1)}$: $k_{eff}^{(n+1)} = k_{eff}^{(n)} \dfrac{M^{-1} F \psi^{(n+1)}}{M^{-1} F \psi^{(n)}}$.

4. Repeat steps 1-3 until both $k_{eff}^{(n+1)}$ and $\psi^{(n+1)}$ have converged.

5. Continue iterating to compute tallies[3] of k_{eff} and reaction rates.

At the start of the calculation, the fundamental mode[4] of neutron production is not known, so an estimate is made. Normally, a flat or cosine distribution is assumed, and several hundred to several thousand neutrons per cycle are generated. These neutrons are started isotropically, and their random walks are simulated to estimate a new k_{eff} and source distribution. From the second cycle onward, the place where fission occurred in the previous cycle is saved in memory and will be assumed as the new neutron source distribution. This iteration is normally repeated for more than 100 cycles. As the number of iterations increases, the distribution of neutron production approaches the fundamental mode. Once the fundamental mode is reached (i.e., k_{eff} and neutron source distribution converge), the values of k_{eff} are accumulated to provide a final averaged estimation with a standard deviation (statistical error) [84]. Depending on the problem and desired accuracy, the user defines the initial neutron source (number of particles and spatial distribution), the initial estimate of k_{eff}, the total number of cycles to be run, how many of these cycles should be skipped, and the nominal source size N[5]. Most of the errors in criticality calculations with Monte Carlo codes are caused because the k_{eff} results start to be accumulated prematurely, i.e., before convergence. The power iteration process for Monte Carlo k_{eff} calculation is represented schematically in Figure 2.2. Figure 2.3 shows an example of a criticality calculation with MCNP code, where the k_{eff} value for each cycle is represented, and the convergence is clearly appreciated.

Most of the criticality calculations of this work were performed with MCNP6.1 [31], a continuous-energy Monte Carlo code developed by Los Alamos National Laboratory in the United States. MCNP is an internationally recognized and accepted code, used worldwide for decades, which has been verified and validated for numerous applications, including criticality safety calculations [73]. Serpent [64] is also a continuous-energy

---

[3]Tallying is the process of scoring the parameters of interest

[4]A stable mode where the distribution changes little from one cycle to the next

[5]The number M of histories varies from cycle to cycle but the total starting weight in each cycle is a constant N. In other words, the weight of each source particle is N/M, so all normalizations occur as if N rather than M particles started in each cycle.
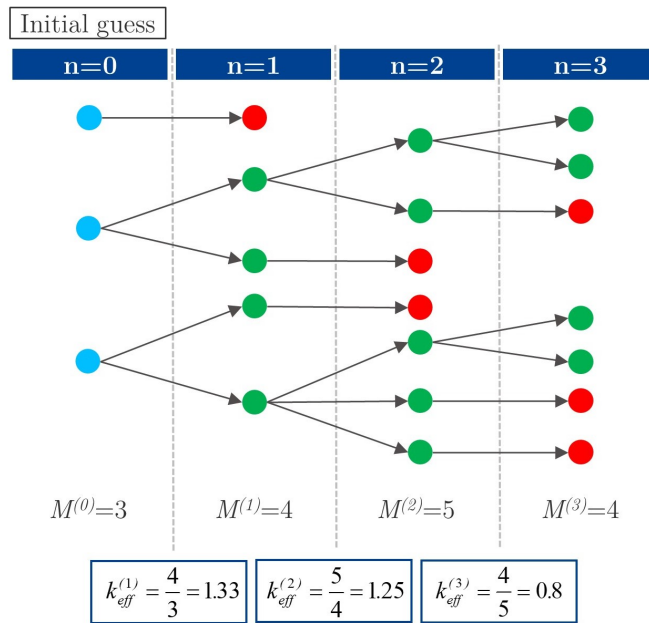
Figure 2.2: Power iteration for Monte Carlo k_{eff} calculation
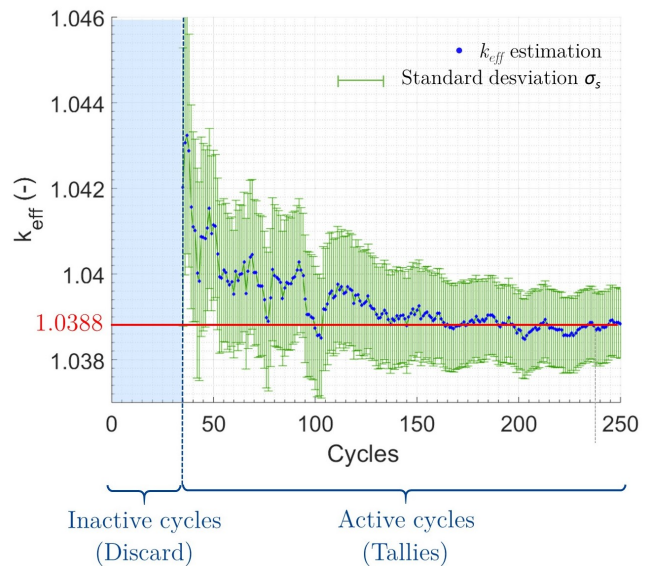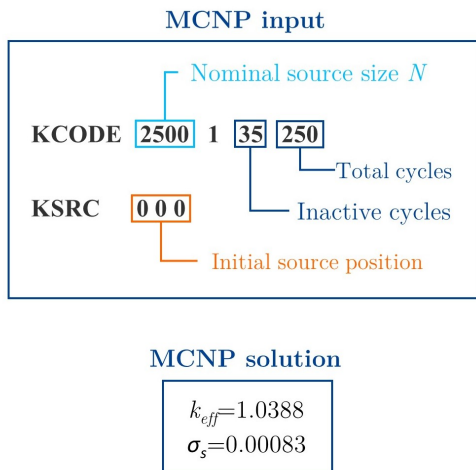
Figure 2.3: Example of k_{eff} calculation with MCNP

Monte Carlo code, developed at the VTT Technical Research Center of Finland and has been used for specific calculations.

2.2.2.1 Parallel calculations

As explained before, Monte Carlo transport is a natural candidate for multiprocessing and parallel calculations because the particle histories are independent, and the calculation accuracy increases with the number of particles tracked. MCNP6 supports two types of parallel computing, which can be used separately or together:

- **Shared memory parallelism (threading)**: OpenMP threading on a single multicore computer (e.g., laptop, office computer) or on a single node of a cluster.

- **Distributed memory parallelism (MPI)**: Message-passing between nodes on a cluster using some external MPI environment and libraries.

Most of the calculations of this thesis were performed at the supercomputer *Hazel Hen* of the High-Performance Computing Center at the University of Stuttgart (HLRS). *Hazel Hen*[6] was a Cray XC40 system and consisted of 7712 compute nodes. Each node had two Intel Haswell processors (12 cores) and 128 GB memory. This makes a total of 185,088 cores and a theoretical peak performance of 7.4 PFlops.

The computing time is strongly dependent on the type of problem, especially on the complexity of geometry, on the collision physics, and the kind, accuracy, and number of requested results. The criticality calculations performed through this thesis are relatively simple transport problems, and most of them run less than an hour in serial processing. Nonetheless, the number of calculations was quite high, and parallel processing with MPI was used to save computational time.

2.2.3 Criticality safety evaluation methods

After a SA, a criticality safety analysis must be performed to ensure that the formed debris beds do not pose a nuclear hazard for the public, workers, and environment. The possible conditions of the debris before, during, and after the defueling activities must be considered. Since there are great uncertainties, the assurance of adequate protection is normally provided through conservatisms, which can be introduced at different levels: conservative acceptance criteria, conservative model assumptions, conservative input conditions, etc. Extreme conservatism is often intentionally used because it simplifies

---

[6]The *Hazel Hen* system was shut down on 25th February 2020 and replaced by its successor *Hawk*

Conservative method
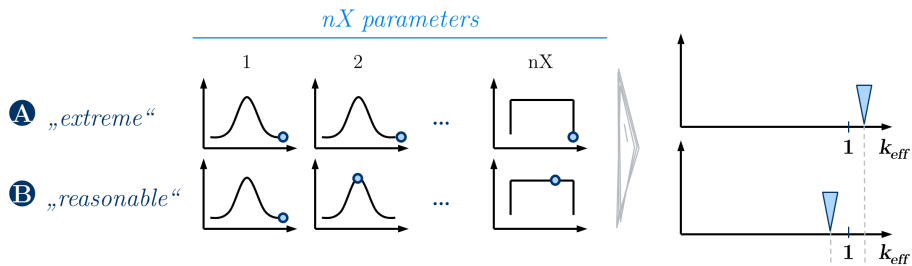
Statistical method
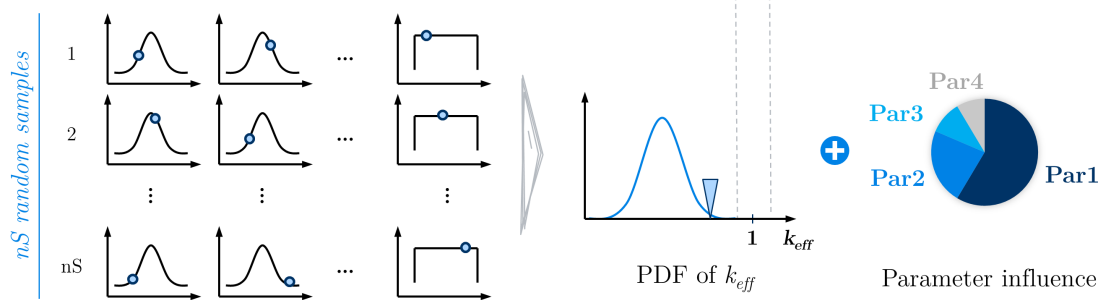
Figure 2.4: Overview of conservative model vs. statistical model

the analysis considerably, reducing efforts and times; however, an over-conservatism may lead to excessive requirements for the criticality control system and very high costs. A reasonable degree of conservatism must be sought, although this threshold is hardly recognizable in the absence of a detailed treatment of uncertainties. Even for expert analysts, it is easy to diverge to excessive conservatism when multiple conservative assumptions are used. For all these reasons, the current trend in nuclear safety analysis is to use realistic hypotheses rather than conservative, and estimate also the uncertainty. A statistical approach may be more laborious but provides a much more realistic picture of the situation and reasonable requirements.

The conservative and statistical methods are explained below in more detail and represented conceptually in Figure 2.4. Before employing any of them, preparatory or parametric calculations are normally performed, since they provide essential knowledge about the criticality behavior of the system.

2.2.3.1   Parametric criticality calculations

A parametric criticality study assesses the impact that changes of certain parameters have on the criticality of the system. The number of variables to perturb is usually small.

These are systematically varied over wide ranges in order to understand their effect on the neutron multiplication factor and analyze possible dependencies that are not obvious to the analyst. Once the tendencies and interdependencies are identified, these can be physically interpreted, which will allow a better understanding of the nuclear behavior of the system. Parametric calculations are commonly used with optimization purposes, i.e., to find out the combination of parameters that makes the system more reactive (worst-case scenario). Similarly, conservative parameter ranges can be derived from these calculations.

Former studies have extensively investigated the reactivity effects of parameters such as fuel enrichment, fuel burnup, fuel particle size, presence of impurities (e.g., boron, iron, zirconium, and cadmium), type of moderator (light water or heavy water), fuel volume fraction, void fraction in water, water boration, the total mass of fuel, fuel temperature, etc. After TMI-2, the parametric studies were essential to define the conservative debris bed model, which was then used to establish the boron concentration limits in the coolant system during the defueling operations [115, 122]. In Fukushima, the debris beds have particular characteristics that make it necessary to investigate new parameters whose impact is not yet fully known; one example is the presence of concrete mixed with fuel as a result of the MCCI at the pedestal floor. During this work, parametric calculations were performed to understand the effect of concrete on the criticality of debris beds and the relevance of the bound water inside the concrete (see Chapter 5).

2.2.3.2   Conservative criticality assessment

In safety analysis, conservatism is an approach in which the model, data, and assumptions are expected to lead to an outcome, which bounds the best-estimate on the safe side. Traditionally, conservatism has been mostly used because it is the most simple way to address uncertainty; however, recently there is a clear tendency to reduce the degree of conservatism in nuclear safety analyses. If calculation results are overly conservative, these may provide a poor basis for decision making leading to excessive requirements from an economic or technical point of view. Therefore, the degree of conservatism must be carefully chosen and adapted to the specific conditions of the evaluated case.

K. Jamali [52] covers this topic and provides recommendations for achieving a reasonable level of conservatism. The study proposes using mean values for most of the input parameters, in combination with bounding values (most conservative extremes) for one or two variables. Only a few selected parameters should be chosen at or near their bounding values; otherwise, the results would quickly become highly skewed representations of reality. This approach would ensure an output value comparable to the

actual 95th percentile and is the best alternative to complex statistical calculations.

A highly conservative approach was used for the criticality assessment in TMI-2, where it was decided to increase the amount of boron in the cooling water so that the system would remain subcritical under any conceivable condition. In this case, and given the situation encountered after the accident, the use of extreme conservatism was the most effective solution to the criticality problem. On the contrary, the situation in Fukushima is more complicated and criticality cannot be effectively controlled by adding boron to the coolant. The criticality assessment is much more complex and a more realistic approach is being sought, which will allow greater flexibility to design the criticality control system.

As part of this work, conservative calculations were performed to identify safety parameter ranges for Fukushima debris beds (see Chapter 4).

2.2.3.3 Statistical criticality assessment

In nuclear safety, there is an increasing interest in replacing the traditional conservative evaluation methods by best estimate calculations supplemented by uncertainty analyses. For that, the uncertainties due to imprecise knowledge of input parameters must be quantified in form of probability distributions. In other words, the input parameters are defined by their PDFs, which reflect the current state of knowledge, rather than by a discrete value only. The propagation of these uncertainties through the computer code calculations provides a probability distribution for the code outputs of interest. The upper limit of the output distribution is usually used to calculate the margin to acceptance criteria. Furthermore, uncertainty analyses are normally complemented by sensitivity analyses, which allow quantifying the correlations between inputs and outputs and, thus, identifying the most relevant parameters.

A statistical criticality assessment would provide a more realistic approach to the real situation in debris beds; however, this method has been barely used for this purpose. The huge uncertainties regarding the debris characteristics make it very difficult to define the probability distributions of input parameters rigorously. Y. Hayashi et al. [39] and Y. Morimoto et al. [72] propose statistical methods for the evaluation of criticality in Fukushima reactors.

Chapter 6 presents an alternative statistical procedure for the evaluation of criticality in debris beds based on the GRS (Gesellschaft für Anlagen- und Reaktorsicherheit) method. The tool for uncertainty and sensitivity analyses SUSA (Software for Uncertainty and Sensitivity Analyses) [57, 58], developed also by the GRS, was used to estimate the probability of a recriticality event in Fukushima Unit 1 and to identify the

relevant parameters.

2.3   Validation

The validation of the neutron transport methods used to evaluate criticality requires the comparison of computational results with critical experiments. Sensitivity and uncertainty analysis techniques can be used to perform a quantitative comparison. The difference between computational and experimental results is called bias and has an associated uncertainty. These, together with an additional margin of subcriticality (MOS), are used to establish an upper safety limit (USL). The nuclear system will be only considered subcritical if the calculated k_{eff} value is below USL:

$$k_{eff} < USL \tag{2.16}$$

$$USL = 1 + Bias - Bias\,uncertainty - MOS \tag{2.17}$$

For conservatism, normally only negative biases are considered (positive biases are set to zero).

Requirements and recommendations for the validation of neutron transport calculation methods applied to nuclear criticality safety analyses are provided in several standards [3, 20]. These references provide guidance for selecting benchmarks, estimating the bias and bias uncertainty, selecting appropriate margins, and documenting validation.

The critical experiments selected for the validation must be representative of the conditions of the system which is being modeled: similar neutron energy spectrum, fissionable materials, neutron absorbers, neutron reflectors, and geometries. Furthermore, a sufficient number of experiments should be selected to ensure feasible and statistically appropriate results. The *International Handbook of Evaluated Criticality Safety Experiments* (ICSBEP Handbook [81]) is generally recognized as the most extensively peer-reviewed source of criticality safety benchmark data available. ICSBEP Handbook contains criticality safety benchmark specifications derived from experiments performed worldwide. The benchmark specifications are intended to be used for the validation of calculation techniques and data.

As explained in Section 1.2.2, after the Fukushima accident, efforts are being made to evaluate the criticality characteristics of the debris beds at the damaged reactors. Numerous calculations are being performed and must be validated with critical experiments. However, debris beds contain structural materials that are not common in regular
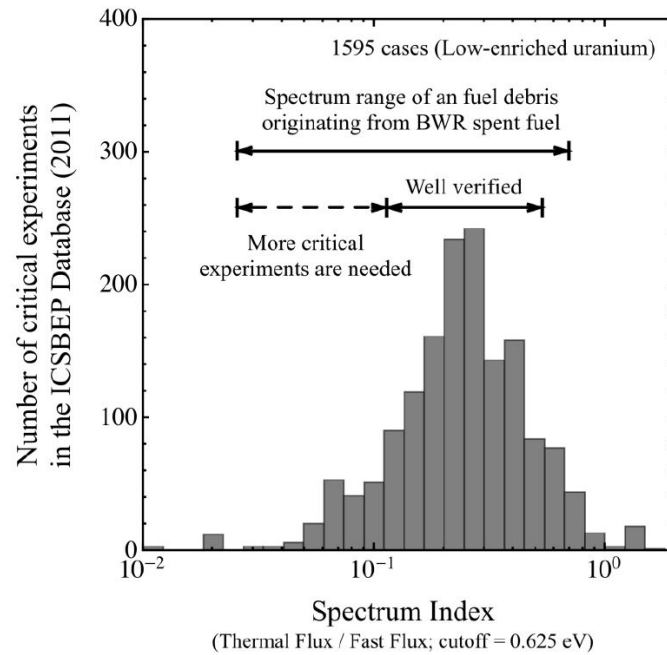
Figure 2.5: Spectrum range of debris bed from BWR against benchmark criticality experiments from ICSBEP database, taken from [48]

fuels, and only a small selection of the available experiments are representative. The criticality safety group of JAEA has assessed the usefulness of available benchmarks for this purpose [48]. Figure 2.5 shows the range of spectrum index[7] and the number of critical experiments with low-enriched uranium in the database of the ICSBEP Handbook 2011. The graph also indicates the spectrum range that is expected in debris beds of BWRs. It can be observed that only part of this spectrum is well verified and sufficiently represented by available critical experiments; for the lower part of the spectrum, more experiments are needed. JAEA is working to meet this need, and the STACY critical facility is being modified to provide adequate experimental results [99, 107]. Thus, the criticality calculations performed in within this work will be able to be validated in the near future once STACY criticality experiments are performed.

---

[7]The spectrum index is the ratio of thermal flux to fast flux.

Chapter 3

Debris bed model

Debris beds are the result of the corium solidification, and their characteristics are determined by complicated interactions of the core melt with the reactor structures and water. The FCI and the MCCI are examples of important SA phenomena with a decisive influence on the debris bed characteristics that are still being investigated. Thus, the conditions of the debris bed are very uncertain, can be very diverse, and strongly depend on the accident scenario.

SA codes simulate the accident progression and can be used to estimate some debris bed characteristics; however, the SA phenomena are extremely complicated, and such estimations involve great uncertainty. Experiments can also reproduce on a small scale the debris bed formation under different accident conditions and provide complementary data. Nevertheless, the most valuable source of information is found in real accident scenarios; debris samples, measurements, and an adequate exploration on-site are crucial to obtain reliable information and thus, reduce uncertainty.

Given the complexity and large uncertainties linked to debris bed systems, a great number of simplifications and assumptions must be used to model them and enable the criticality calculations. This chapter reviews the main parameters affecting the debris criticality and possible ways to model them, from the most conservative to more realistic approaches. Finding an appropriate debris model is a challenging task because the high uncertainties may easily lead to an excessive conservatism far from reality; nonetheless, certain conservatism may be useful to spare time and effort. The objective of this chapter is to share the state of knowledge and provide alternatives for adequate debris modeling.

3.1 Debris bed characteristics and modeling alternatives

Nuclear criticality safety guides provide general information for the prevention of criticality accidents, explaining, among other things, the factors affecting criticality [59, 94]. Based on that, the debris parameters that may have a relevant influence on the criticality are:

- Debris bed mass.

- Debris bed composition: corium composition, fuel enrichment, fuel burnup, and presence of structural materials like Zircalloy, steel, control rods, or concrete.

- Debris density.

- Debris temperature.

- Moderator/coolant conditions: type of water (light water, heavy water, seawater), temperature, void fraction, boration, etc.

- Physical configuration: internal structure (porosity, particle size, shape, and arrangement) and external structure (debris shape and surroundings, configuration of fuel, moderator, and reflector materials).

A qualitative analysis of these parameters is made below. Modeling concerns and modeling alternatives with several levels of conservatism are also discussed. Figure 3.1 summarizes them.

3.1.1 Debris bed mass

Increasing the debris mass has a positive reactivity effect because it reduces the neutron escape out of the system. The effective multiplication factor k_{eff} increases with the mass up to a certain limit where the mass is so large that the neutron leakage is negligible. At this point, the system is considered infinite and $k_{eff} = k_\infty$ (infinite multiplication factor). From a modeling and computing point of view, assuming that the debris has infinite extension is very simple and economical; it is achieved by using perfect neutron reflectors surrounding the nuclear system. On the other hand, such an assumption is excessively conservative in most cases. Thus, the possible mass accumulations inside the reactor should be estimated. The total debris mass will depend on the severity of the accident, i.e., the percentage of the core that melted down, and the initial core inventory.

———— *Reference* ————   ———— *Simplifications* ————

Debris Characteristics	Reality	Near-to-reality	„Realistic"	„Conservative"	„Very conservative"
1. Total debris mass	0 - 100% core (+extra: steel, concrete)	Typical estimated value	Typical estimated value	Max. estimated value	Infinite
2. Composition of debris	Heterogeneous	Heterogeneous	Homogeneous	Homogeneous	Homogeneous
i. Initial enrichment	mix. 2 - 5 wt% ^{235}U	Random mix.	Avg. value	Avg. value	> Avg. value
ii. Burn-up	mix. 3 - 40 GWd/t$_{\text{HM}}$	Random mix.	Avg. value	< Avg. value / No FP	No burnup credit*
iii. Structural materials	Mixed with fuel (grade?)	Mixed with fuel (grade?)	Mixed with fuel (grade?)	Homogeneously mixed	Homogeneously mixed
a) Zry, SS	Yes	Yes	Yes	Yes (?)	No
b) Control materials	Yes	Yes	Yes	No	No
c) Concrete	Yes (if MCCI)	Yes (if MCCI)	Yes (if MCCI)	Yes (if MCCI)	Yes (if MCCI)
3. Debris density	$< \rho_{theoretical}$ (internal porosity)	$< \rho_{theoretical}$ (internal porosity)	$< \rho_{theoretical}$ (internal porosity)	$\rho_{theoretical}$ (no internal porosity)	$\rho_{theoretical}$ (no internal porosity)
4. Debris temperature	T profile	T profile	T_{eq}	Cool (~25°)	Cool (~25°)
5. Coolant conditions	Heterogeneous	Heterogeneous	Homogeneous	Homogeneous	Homogeneous
i. Temperature	T profile	T profile	T_{eq}	Cool (~25°)	Cool (~25°)
ii. Void fraction	ρ profile	ρ profile	ρ_{eq}	No void fraction	No void fraction
iii. Boration	Depend on SA scenario	Depend on SA scenario	Depend on SA scenario	No	No
6. Geometry of debris					
i. Internal structure	Heterogeneous	Heterogeneous	Heterogeneous	Heterogeneous	Heterogeneous
a) Particle shape	Irregular	Spherical	Spherical	Spherical	Spherical
b) Particle size	mix. μm - 1-2 cm (*PSD*)	*PSD*	d_{eq}	d_{eq}	10.7 mm (real pellet)
c) Particle arrangement	Chaotic	Random	Random	Regular (BCC, FCC)	Regular (BCC, FCC)
d) Porosity	Irregular	Random mix.	ε_{eq}	Optimal	Optimal
ii. External geometry	Heap-like pile/mound-shaped	Heap-like pile/mound-shaped	Cone/Layer	Cone/Layer	Sphere

Analysis in Section 3.3 (Coolant conditions — Very conservative)

Analysis in Section 3.2 (Geometry of debris — Very conservative)

(?): unclear (further investigation necessary)

(*): burnup for which reactivity reaches a maximum (if burnable poisons)

Complexity / *Accuracy*   →   *Simplicity* / *Conservatism*

Figure 3.1: Modeling alternatives for the criticality evaluation of debris beds with different levels of conservatism

After a SA, several debris beds may exist in different locations: in-vessel (core region or lower head) and ex-vessel (at the pedestal floor inside or outside). With a few exceptions, the neutronic of in- and ex-vessel debris beds will be decoupled. If that occurs, the neutrons do not travel from one debris to another but get lost in between, and both nuclear systems can be considered independent. Consequently, the criticality could be studied separately, and the masses would not add up to a critical mass. After TMI-2, a conservative assessment demonstrated that if there was an ex-vessel debris, this and the in-vessel debris would be effectively neutronically decoupled mainly due to the large separation distances and the presence of significant separation materials between both debris accumulations [33].

In Fukushima reactors, the debris bed distribution has been estimated with SA codes, muon tomographies, and additional reactor data. First surveys and observations in the PCV have been accomplished; however, the radiation levels inside the reactor are extremely high, and incursions are still challenging. The estimated conditions inside the reactor are very severe: almost the whole core melted down (at least in Unit 1), and most of the debris beds are very likely accumulated at the pedestal floor in the three damaged reactors (ex-vessel scenario). Table 3.1 collects the estimation ranges of the debris mass at different core regions and the typical or most probable values for each case [47][79]. Future advances with on-site surveys will provide more accurate data and the estimations will be improved.

Table 3.1: Estimation of debris amount and distribution in Fukushima damaged reactors [47][79]

Location		Unit 1 (tons)	Unit 2 (tons)	Unit 3 (tons)
RPV	Core region	0-3 [0]	0-51[0]	0-31 [0]
	Lower head	7-20 [15]	25-85 [42]	21-79 [21]
PCV	Pedestal inside	120-209 [157]	102-223 [145]	92-227 [213]
	Pedestal outside	70-153 [107]	3-142 [49]	0-146 [130]
Total		232-357 [279]	189-390 [237]	188-394 [364]

[ ]: Typical value

For a conservative criticality assessment, the maximum values of the estimated mass ranges can be used; the typical values of debris bed masses would provide more realistic results.

3.1.2 Debris bed composition

Debris beds mainly consist of fuel, structural materials, and to a lesser extent control materials, which are also the major components of LWR cores. PWR cores contain mainly UO_2 (78 wt%) and Zircaloy (16 wt%). Stainless steel, Inconel, Ag-In-Cd control rod material, and Al_2O_3 used in the burnable poison rods comprise the remaining 6 wt%. For a BWR, the major components are also UO_2 (68 wt%) and Zircaloy (24 wt%). The remaining materials (8 wt%) are primarily stainless steel and B_4C from control rods [44].

In very severe accidents such as Fukushima, not only the core structures meltdown, also other major components of the reactor as the reactor vessel may collapse and become part of the corium. Similarly, if the corium falls on the pedestal, it may cause the ablation of concrete, and large quantities of this material may also mix with the fuel.

From the point of view of criticality safety, four relevant points concerning the debris composition should be treated carefully:

- Characteristics of fuel at the moment of the accident, i.e., original inventory and burnup history. The fuel isotopic composition is the base of any criticality calculation.

- Neutron absorbers closely mixed with fuel, i.e., control materials (Ag-In-Cd or B_4C) and burnable poison (e.g., Gd_2O_3). Even very small quantities of these materials can make a dramatic difference in the criticality results.

- Extent of MCCI. The presence of concrete in the debris bed may enhance the neutron fission under specific circumstances.

- Heterogeneity of the system. In particular, the grade of mixing of certain materials with fuel may have a significant impact on the criticality results.

In relation to the last point, a stochastic geometry capability has been implemented in most Monte Carlo codes, e.g., MVP [71], Serpent [96], and MCNP [1]. Although these capabilities were originally developed to improve the modeling of pebble bed reactors, they can also be used to model debris beds. They allow generating geometrically random distributed fuel particles within a matrix. Thus, the heterogeneous composition of debris beds can be modeled by assuming different fuel/material batches within a water matrix.

3.1.2.1 Fuel

The type of fuel most widely used today in nuclear reactors is low-enriched uranium dioxide (UO_2). Less common is the use of MOX fuel, which consists of a mixture of

plutonium and uranium oxides (UO_2/PuO_2). The neutronic behavior of both fuels is different [120]. Besides the type of fuel, the initial uranium enrichment and burnup at the moment of the accident will determine the isotopic composition of the fuel in debris beds. These vary depending on the reactor type, the specific fuel design, the fuel management scheme, and the kind of burnable poison used.

Fukushima damaged reactors contained 9x9 STEP-3 BWR fuel assemblies (see Table 3.2).

Table 3.2: Fuel type and number of assemblies in Fukushima reactors [78]

Reactor	No. assemblies	Fuel	Mass (t_{HM})
Unit 1	400	UO_2	69
Unit 2	548	UO_2	94
Unit 3	548	UO_2 + MOX*	94

(*) 32 assemblies

Fuel enrichment The original core design determines the enrichment of the fuel. To achieve an optimal power distribution in LWRs, fuel rods with several enrichments, typically between 3 to 5 wt%, are loaded and graded spatially.

The original loading of Fukushima reactor cores included six different initial enrichments that make an average of 3.7 wt% ^{235}U (see initial inventory in Table 3.3).

Table 3.3: Initial inventory of assemblies in Fukushima reactors [77]

Enrichment (wt% ^{235}U)	Mass (kgU)
4.9	9.6
4.4	76.8
3.9	28.8
3.4	19.2
2.1	9.6
3.4 (Gd)*	26.9
Total	170.9

(*) Rods containing 5 wt% Gd_2O_3

Heterogeneous models with several fuel batches randomly distributed may be used for a very realistic representation [72]. Nonetheless, in the absence of evidence pointing to the contrary, considering the average enrichment is a good approach for criticality safety analysis in debris beds. In the criticality evaluations performed after the TMI-2

accident, the enrichment of the fuel was that corresponding to the homogeneous mixture of the different fuel batches. Later on, defueling records and debris samples analyses indicated that the assumed homogeneity of the core debris was appropriate [33]. An increase in the fuel enrichment (i.e., atomic density of fissile isotope ^{235}U) has a strong positive effect on the reactivity of the system; thus, considering an enrichment higher than average would be conservative.

Fuel burnup The irradiation of nuclear fuel during the reactor operation leads to a reactivity reduction. The most important reactivity effects due to the transmutations occurring during fuel burnup are:

- Destruction of fissile atoms.

- Production of neutron-absorbing nuclides (fission products and non-fissile actinides).

- Production of fissile actinides such as ^{239}Pu and ^{241}Pu.

- Destruction of burnable poison if present (e.g., Gd).

All effects contribute to the reactivity reduction except the production of fissile actinides and the destruction of burnable poisons, which add positive reactivity to the system but not enough to outweigh the negative contributions of the other effects [84].

In the past, assuming fresh fuel was a common practice in criticality safety analysis because it was conservative and made the evaluation much easier. Currently, there is a clear tendency to run away from excessive conservatism, and taking credit for the burnup in irradiated fuels is recommended. For that, the spent fuel composition must be determined using depletion analysis. To facilitate the analyses, and depending on the level of detail/accuracy desired, several categories of burnup credit can be used. These are (from most conservative to most accurate): accounting for fissile depletion only, actinide depletion only, actinide depletion with limited FPs, or all isotopes.

Given the above, the fuel isotopic composition can be accurately calculated at any time if the operation history of the reactor is well known. This composition is heterogeneous within the reactor core and depends on the reactor loading pattern, but an average value can be considered for the criticality calculations in debris beds. The adequateness of this assumption will depend on the melted assemblies and the mixing grade during the accident progression. The defueling experience at TMI-2 showed that assuming a homogeneous debris composition was a right approach [33], at least for this particular debris. Recent studies have incorporated debris models with random distributions of different fuel batches [39, 72]; no significant differences were appreciated between the

heterogeneous and homogeneous fuel models. In conclusion, assuming an average burnup value with certain conservatism (e.g., considering actinide depletion with limited fission products) seems to be a reasonable solution to this modeling issue.

The current fuel burnup achieved in reactors is up to about 50 GWd/t. In Fukushima reactors, the average burnups at the moment of the accident were: 25.8 GWd/t in Unit 1, 23.1 GWd/t in Unit 2, and 21.8 GWd/t in Unit 3 [78]. More detailed data about the burnup conditions of Fukushima reactors are found in Table 3.4. Very detailed estimations of fuel composition at different times after the Fukushima accident in the damaged reactors have been already performed by JAEA [78]. The corresponding isotopic compositions are given in Appendix B, together with a brief explanation of the nuclides considered for the criticality safety calculations performed through this work.

Table 3.4: Burnup conditions in Fukushima reactors [78]

Unit 1 (GWD/t : no. assemblies)	Unit 2 (GWD/t : no. assemblies)	Unit 3 (GWD/t : no. assemblies)
5.2 : 64	3.3 : 116	4.7 : 148*
15.2 : 64	15.8 : 116	15.5 : 112
24.2 : 80	26.0 : 120	28.5 : 140
33.3 : 68	35.2 : 120	36.2 : 112
37.5 : 64	40.6 : 76	40.5 : 36
40.2 : 60		

(*) Includes 32 MOX assemblies

3.1.2.2   Impurities

Impurities are all those materials other than fuel that are present in debris beds. Most of them are structural materials from the reactor, and a small part consists of control material from control rods or burnable poison.

The presence of impurities has normally a negative reactivity effect. Nonetheless, recent studies warn about the good moderation capacities of concrete, which may add positive reactivity to the system in some circumstances [49, 117]. In any case, if credit is taken for impurities, a more reasonable representation of the debris bed criticality characteristics will be achieved.

Table 3.5 shows quantitative estimations of the possible amount of impurities in the debris beds at Fukushima Unit 1 made by IRID [47, 79] (also available for Unit 2 and Unit 3). It is noteworthy the great proportion of impurities, especially in the ex-vessel debris bed.

Table 3.5: Estimation of debris distribution and composition in Fukushima Unit 1 [47, 79]

Location		Estimation range [Typical value] (ton)				
		Fuel (UO_2)	Struct. mat.	Concrete	Total	%
RPV	**Core region**	0-3 [0]	0 [0]	0 [0]	0-3 [0]	0
	Lower head	1-11 [9]	6-9 [6]	0 [0]	7-20 [15]	5
PVC	**Pedestal inside**	31-55 [45]	34-53 [34]	55-101 [78]	120-209 [157]	56
	Pedestal outside	12-32 [22]	22-53 [33]	36-68 [52]	70-153 [107]	38
Total		76 [76]	62-15 [73]	91-169 [130]	232-357 [279]	100
%		27	26	47	100	

Structural materials Major structural parts of water reactor cores are made normally of stainless steel (SS) and Zircaloy (Zry). Stainless steel has better physical and mechanical properties, and it is used in most LWR vessels. Zircaloy has better nuclear properties (the neutron absorption is about twelve times smaller than steel), and it is normally preferred as cladding. Consequently, the presence of Zircaloy in debris beds does not provide a significant reactivity effect. On the contrary, the stainless steel does have a negative contribution, and it should be considered in realistic criticality assessments, particularly if the SA involves damages of the RPV, in which case the debris may contain a significant amount of iron.

A recent study has demonstrated that the mixing ratio of stainless steel with fuel in the debris bed has a strong negative reactivity effect [72]. Thus, assuming that fuel and stainless steel are mixed homogeneously is not conservative and should be taken into account when modeling.

In ex-vessel accident scenarios, the molten corium may interact with the concrete at the pedestal floor, forming debris beds with a significant amount of concrete. The major ingredient of concrete is silicon dioxide (SiO_2), which has a small neutron absorption cross section but also some moderator capacities, as recent studies demonstrated [49, 117]. These studies assumed conservatively standard concrete, which has bound water inside. The bound water is actually released during MCCI, and more realistic assessments should not consider it (see Chapter 5).

The presence of structural materials estimated in Fukushima debris beds is very high ($> 50\%$) [47, 79], especially in Unit 1 (see Table 3.5), where the conditions are most severe. The failure of the RPVs and subsequent concrete abrasion have caused a great accumulation of structural materials, which have mixed with corium forming the debris beds. In case of a less severe accident where the debris bed is retained in-vessel, the

proportion of impurities expected inside the debris would be much lower. That was the case at TMI-2, where debris samples revealed 27-28% of impurities against 72-73% of UO_2 [33].

Control materials Control rods are made of strong neutron absorbers such as silver-indium-cadmium alloy (generally 80% Ag, 15% In, and 5% Cd) or boron carbide (B_4C). The presence of small amounts of these materials in a nuclear system reduces the recriticality potential considerably.

Additionally, LWRs use burnable poisons to compensate for the effects of fuel burnup. These are generally compounds of boron or gadolinium (e.g., Gd_2O_3) that are homogeneously mixed with the fissionable material or shaped into separate lattice pins or plates. Due to the burnup of the absorption material, the negative reactivity of the burnable poison decreases over core life.

While burnable poisons are expected to coexist with fuel inside the debris, the distribution of control materials like boron is not well known. On the one hand, all the TMI-2 samples evaluated after the defueling activities contained some amount of impurities, which were present as an integral part of the debris, including the boron [33]. Conversely, experimental investigations claim that oxide and metal would separate and that major portions of uranium would be in the oxide phase, where the boron very rarely resides [4]. For such a case, considering that boron coexists with fuel may lead to an underestimation of the recriticality potential. Thus, analyzing real samples of the debris beds under investigation is recommended to reduce the uncertainty and perform a more accurate criticality assessment. Research is underway in order to find adequate technologies able to provide a detailed spatial distribution of boron in debris [54].

The sensitivity analysis performed in Chapter 6 demonstrates the drastic negative reactivity effect of boron and, consequently, the relevance of modeling it properly.

3.1.3 Debris density

An increase in debris density has the same effect as an increase of fuel enrichment; in both cases, the result is more fissile atoms per unit volume, which up to a point has a positive effect on the reactivity. The theoretical density of UO_2 fuel is 10.97 g/cm^3, while production density is about 95% of that value, but there is no way a priori to know how the atoms/molecules will pack together in a crystal lattice in a debris bed.

The debris density can be estimated if a composition is assumed, with all components and corresponding atomic densities. Based on FCI experiments [61, 67, 75, 109], the true density of the debris is always lower than this value due to the internal porosity of the

system, which can be even reach 30-40% in some cases. The internal pores reduce the concentration of fissile nuclei and have a negative effect on reactivity.

Until now, no data about debris density is available for Fukushima debris beds.

3.1.4 Debris temperature

The thermohydraulic parameters of the debris bed, such as temperature and density, are intimately related and will determine the neutronic behavior of the system, and vice versa. The system neutronics (decay heat, fission rate, ...) determines the temperature of the debris. Simultaneously, the cross sections of nuclear reactions vary with temperature. If the temperature increases, the nuclei move at higher speeds, increasing the probability of resonance capture of epithermal neutrons (Doppler effect) and, therefore, decreasing the reactivity. Additionally, the temperature directly affects the density; an increase of temperature causes a decrease of density, which in turn, inserts negative reactivity. No significant density changes due to temperature are expected in the solidified materials that compound debris beds but in the moderator and coolant (changes in the void fraction).

Temperature, density, and power profiles in the debris bed, as well as k_{eff}, can be determined with coupled neutronic-thermohydraulic calculations. A realistic example was calculated in Section 3.3 using the available data of Fukushima debris beds. The objective of this analysis was to evaluate the impact of realistic thermohydraulic characteristics on the criticality and find out to what extent it is recommended to describe them accurately.

3.1.5 Coolant/moderator conditions

Light water can be a very efficient moderator in relatively small volumes and reduce substantially the minimum amount of fissile material required to sustain a chain reaction or even make recriticality possible in otherwise subcritical systems. For that reason, SAM measures prescribe the use of borated water for cooling the damaged core; that allows keeping the debris cool and stable without compromising the criticality safety. Nonetheless, maintaining a constant concentration of boron is not always possible (see Section 1.1.1.2). If debris beds are submerged in non-borated water, as in Fukushima, the recriticality can be an issue and should be addressed carefully.

It is important to note that water is also a very good neutron reflector. A water layer of approx. 30 cm thick reflects the neutrons completely; thus, if water covers the debris bed, the neutron fission will be also enhanced.

3.1.5.1 Water temperature and density

As explained before in Section 3.1.4, the temperature and density (or void fraction) of the water covering the debris are closely related and can be calculated with coupled neutronic-thermohydraulic calculations. As the temperature of the coolant increases, its density decreases. Since the concentration of atoms is lower, neutrons suffer fewer collisions and are more likely to escape from the debris and less likely to reach thermal temperatures (negative reactivity effects). At the same time, the absorption rate in moderator and coolant also decreases (positive reactivity effect); however, that effect only becomes relevant if there is poison in the coolant or moderator (e.g., boric acid). In such a case, the effect of any density change is magnified, and important positive reactivity injections may occur.

In Fukushima, the temperatures in the water pool are monitored, and values under 26°C are registered. Nevertheless, a more detailed estimation of the temperature and density profiles has been performed (see Section 3.3), concluding that assuming water with full density may be a reasonable conservative approach for Fukushima debris beds.

3.1.5.2 Boration

^{10}B is maybe the most important neutron absorber and appears as boron carbide (B_4C) in control rods or as boric acid (H_3BO_3) in solutions with coolant water. The injection of boron in the reactor cooling system is the preferred criticality safety measure in case of a nuclear accident. When reliance is placed on neutron-absorbing materials (e.g., boron or cadmium), their continued presence and intended distributions and concentrations must be controlled to ensure their effectiveness. That is not always an easy task; therefore, solutions of absorbers must be used carefully.

In Fukushima, a boron injection system is put in place and will be used only in case of a criticality event. Meanwhile, the debris beds are cooled with unborated water.

3.1.6 Debris bed configuration

Taking into account the geometrical configuration of the debris bed is fundamental for an adequate criticality assessment. Morphological information is generally not predicted by the SA codes. Thus, current knowledge has been mostly gained with experiments that reproduce the debris bed formation at low scale under different accident conditions. Also, data collected during TMI-2 defueling activities have provided valuable information.

3.1.6.1 Internal structure

The topology of a debris bed depends on the debris formation process and, very specially, on the interactions between the melted corium and water. The FCI process has been extensively investigated in numerous experiments, which have provided limited information about prototypical configurations of debris beds and other characteristics. FCI experiments reproduce at small scale the penetration of the molten corium into the water accumulated at the lower plenum or cavity during a hypothetical SA, and its subsequent settling at the bottom of the RPV or at the pedestal floor. In CCM [109], COTELS [75], FARO [67], and DEFOR [88] experiments two fundamental types of debris beds were observed:

- **Particulate debris bed**: porous debris bed consisting of particles.

- **"Cake" or ingot debris bed**: compact monolithic debris with low internal porosity in the form of small cavities, crevices, and channels.

Both debris types were also found at TMI-2 [33]. Considering the criticality safety, particulate debris beds are generally more dangerous because the spaces between the particles may be filled with water, enhancing the neutron moderation.

Another important and common conclusion from experiments and real samples is that debris beds are very heterogeneous systems, with particles of very different shapes and sizes, irregularly arranged and non-homogeneous porosity. Numerous assumptions must be made to model these complex structures. Traditionally, heterogeneous nuclear systems were always homogenized in criticality safety. The homogenization facilitates the modeling but yields non-conservative results. More recently, regular lattices and random models are commonly used. In Section 3.2, a comprehensive analysis is carried out, where different modeling possibilities are investigated as well as the impact of several simplifications on the criticality. From these analysis, it was concluded that particulate debris beds can be modeled with a reasonable good accuracy assuming spherical particles regularly arranged in a lattice if and adequate equivalent diameter d_{eq} is chosen (a methodology for the calculation of d_{eq} is presented in Section 3.2.3.2).

If no data about the particle size distribution is available, $d_{eq} = 10.7$ mm (equivalent size of a real pellet) can be used. Experiments have demonstrated that particles smaller than the standard pellet are more representative of debris beds; thus, such assumption will be conservative in most cases.

Porosity   The fraction of hollow space in the debris bed is called porosity:

$$\varepsilon = \frac{V_{hollow}}{V_{total}} \tag{3.1}$$

According to particle packing theory, the porosity of a bed of monosized spheres varies from 0.26 to 0.46 depending on the packing structure. In an unarranged configuration, the porosity may vary locally and the mean value is around 0.39 [101].

In real debris beds, the irregular particle shapes and sizes also affect porosity. The irregular shapes yield larger holes and thus higher porosity. On the other hand, different particle sizes reduce the porosity because the smaller ones can fill the holes formed between the bigger particles. The porosities measured in debris beds of FCI experiments varied from 0.5 to 0.7 with most cases around 0.6 [53, 67, 109]. That means that the porosity of prototypical debris beds may be substantially higher than the value predicted by the particle packing theory. Furthermore, the porosity is not uniform, and debris beds may be more compacted in the lower area.

If the debris is submerged in water, the hollow space will be filled with water, enhancing the neutron moderation. In these cases, the porosity has a positive effect on the reactivity up to a point where the maximum k_{eff} is reached. In conservative assessments, the optimal porosity is considered. Alternatively, an equivalent value ε_{eq} can be used if supported by additional data.

3.1.6.2   External structure

Debris shape   The shape of the debris bed affects how easily neutrons can escape from it. A shape with a large surface area, such as a thin slab, favors leakage and is safer than the same amount of fissile material in a small, compact shape such as a cube or sphere.

Several experiments have studied the debris particle settling and sedimentation [15, 55, 60, 62]. They found that the boiling water and two-phase flow inside the bed may act as a mechanical energy source and cause the spread of the particles in the so-called "self-leveling" phenomenon. Depending on that, the debris may form a steep-angled heap-like pile or rather a low-sloped mound-shaped bed.

Fuel/moderator/reflector configuration   In criticality safety, it is not only important to know which are the materials in the debris but how they are distributed. The same material may act neutronically very differently depending on its configuration and location in the debris bed system. For example, water may behave as moderator if it is

intimately mixed with fuel or as reflector if it covers the debris externally. The same occurs with steel, which may act as neutron absorber when coexists with fuel or as reflector if it surrounds the debris (e.g., in-vessel debris surrounded by reactor vessel). Similarly, concrete is one of the most common materials used for neutron shielding; however, if mixed with fissile material, it may be a pretty good moderator.

Some conservatism may be introduced in the modeling of the debris geometry, for example, by adding a perfect reflector surrounding the system.

3.2 Modeling the internal structure of debris beds

This section aims to find an appropriate model for the complex internal porous structure in debris beds. The influence of the particle shape, particle size distribution, and particle arrangement on the neutron multiplication factor is investigated as well as the impact of possible simplifications. Different modeling alternatives are considered, and, based on the results, their applicability ranges are discussed.

Particle shape Particles in real debris beds have irregular and very different shapes. The effect of particle shape on the neutron multiplication factor is shown in Figure 3.2. Particles were modeled as spheres, cylinders, and cubes arranged in a regular infinite cubic lattice. The graphics illustrate the reactivity changes caused by the particle shape for different porosities and using the spherical particles as reference. A negative correlation between k_∞ and the surface-to-volume ratio of the particles is appreciated.

Thus, assuming spherical particles is highly recommended because it simplifies greatly the debris modeling and yields conservative results. This simplification is very common in criticality safety and will be used throughout all this study.

Particle size Debris beds are composed of particles of different sizes, commonly from few μm to 2-3 cm. Each debris bed has a unique particle size distribution (PSD), which can be defined by a discrete or continuous mathematical function that provides information about the relative amount (typically by mass) of the particles according to their size. Experiments performed in test facilities as DEFOR, KROTOS, or FARO provided data about the PSD in debris beds under several formation conditions.

In this study, two hypothetical debris beds with the averaged particle size distributions provided by DEFOR-A tests (PSD_{DEFOR}) [61] and FARO L-28 experiments (PSD_{FARO}) [67] were considered (see Table 3.6). These debris beds were modeled in three different ways: as a heterogeneous system of particles having a range of sizes (poly-
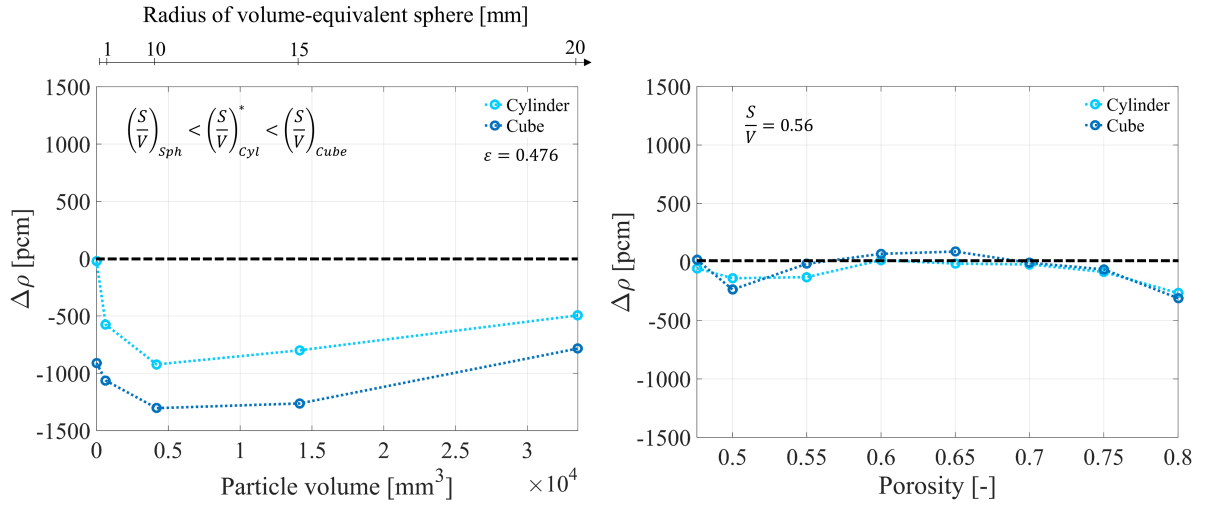
Figure 3.2: Reactivity changes as function of the particle volume and porosity for different particles shapes (Reference: system with spherical particles)

disperse system), as a heterogeneous system of particles with uniform size (monodisperse system), and as a homogeneous system. The appropriateness of every model is analyzed in Section 3.2.3.

Particle arrangement In a real debris bed, the particles are arranged chaotically in space. Models with particles randomly distributed, as well as simplified systems with particles regularly arranged, were analyzed and compared (see Section 3.2.3.3).

Nowadays, Monte Carlo codes offer several features to reproduce stochastic particle packings. In Serpent, the explicit particle fuel model reads the coordinates and radius of the particles from a separate file and represents them explicitly, without any approximation [96]. In MCNP, the stochastic geometry capability provides a random displacement of the spheres within a cubical matrix cell [1].

3.2.1 Possible simplifications

As explained before, debris beds are very complex systems that must be simplified to reduce the computational effort associated with the criticality calculation. To model the internal structure, simplifications at three different levels (particle shape, size, and spatial distribution) were applied. Figure 3.3 depicts the models considered in this study for a suitability analysis:

Realistic model Very realistic model, which consists of particles with different sizes (defined by a *PSD*) chaotically distributed in water. The particles are assumed to

Table 3.6: Particle size distributions [61, 67]

DEFOR distribution (PSD_{DEFOR})			FARO distribution (PSD_{FARO})		
d_{min} (mm)	d_{max} (mm)	Cumulative mass fraction (%)	d_{min} (mm)	d_{max} (mm)	Cumulative mass fraction (%)
7.1	12	100	10	15	100
5.6	7.1	96.9	6	10	85.6
4.7	5.6	88.7	4	6	68.3
4	4.75	81.9	2	4	58.5
3.55	4	69.9	1	2	38.59
2.8	3.55	62.6	0.71	1	24.81
2.36	2.8	45.6	0.5	0.71	18.99
2	2.36	36.2	0.355	0.5	13.02
1.8	2	26	0.25	0.355	8.42
1.4	1.8	21.2	0	0.25	5.51
1	1.4	12.3			
0.5	1	6.1			
0.25	0.5	1.9			
0.1	0.25	0.7			
0	0.1	0.2			

be spherical.

Random model All particles have spherical shape and uniform size. The coordinates of each particle are generated randomly, resulting in a chaotic distribution.

Regular lattice model The fuel particles are monosized spheres regularly arranged in space. Typical 3-D regular lattices are SC (Simple Cubic), BCC (Body-Centered Cubic), or FCC (Face-Centered Cubic).

Homogeneous model Fuel and water are homogeneously mixed, forming a system with uniform composition and properties.

Based on the literature review, the preferred and most used models are the homogeneous and the regular lattice, which are also the most simple; however, the application borders are still not clear. A suitability analysis is needed to clarify to what extent they are appropriate. A better understanding of the models will allow less conservative and more realistic criticality results.
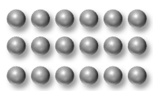
Real debris	Debris models				
	Representation	Id	Description	Simplifications	Accuracy/Simplicity
Fuel particles of different shapes and sizes chaotically arranged in water		**Realistic** model	Polydisperse system with spherical particles and chaotic distribution	▪ Particle shape	*Max. Accuracy*
		Random model	Monodisperse system with spherical particles and chaotic distribution	▪ Particle shape ▪ Particle size	
		Regular lattice model	Monodisperse system with spherical particles and regular distribution	▪ Particle shape ▪ Particle size ▪ Particle distribution	
		Homogeneous model	Homogeneous system	▪ Complete (particle size → 0)	*Max. Simplicity*

Figure 3.3: Possible simplifications for the neutronic modeling of the debris beds internal structure

3.2.2   Reference model

To assess the adequacy of the simplified models described before, it is necessary to develop a near-to-reality model (reference model), whose higher fidelity results could be used as a reference to evaluate the accuracy of each candidate. The reference model chosen for this study is defined as follow:

Reference model Near-to-reality model with only two simplifications: the particles are considered to be spheres, and those with diameters equal or lower than 0.5 mm ($d \leq d_{hom}$ = 0.5 mm) are mixed homogeneously with the water. It is thereby essentially the realistic model (see Figure 3.3) with a minimal partial homogenization that enables the computation.

A simple simulation program was developed to generate the packing of the particles. The program was designed in the following way:

- Input: dimensions of the cubic box where particles are packed, particle size distribution (*PSD*), and porosity.

- Body: the box is filled with spheres until the desired porosity and *PSD* are reached. For that, spheres of each size interval are generated until the target mass fraction is reached. The simulation starts with the particles belonging to the biggest-size interval and finishes with the smallest ones. The particle coordinates are

generated randomly within the limits of the cubic box and without considering the gravity effects. Similarly, the particle radii are generated randomly within the size limits of the corresponding interval. Overlapping is not allowed. On the contrary, truncation in the box borders is possible, which ensures a uniform porosity distribution through the whole structure.

- Output: particle sizes and coordinates.

To avoid the extremely large computing times required for the simulation of the smallest particles (when the particle size $d \to 0$, the number of particles $n \to \infty$), a diameter threshold d_{hom} was defined, so that:

- All the particles with diameters equal to or lower than the diameter threshold ($d \leq d_{hom}$) were homogenized.

- The effect of this partial homogenization on the neutron multiplication factor (k_{∞}) was negligible.

Based on the conclusions obtained after the analysis of the homogeneous model (see Section 3.2.3.1), a diameter threshold of 0.5 mm (d_{hom}= 0.5 mm) was considered to be appropriate.

Taking into account the minimal simplifications applied, the reference model is expected to reflect with high accuracy the criticality characteristics of a real debris bed.

The reference model was simulated in a 100 mm side cubic box for different porosities and fulfilling two particle size distributions: PSD_{DEFOR} and PSD_{FARO} (see Table 3.6). Figure 3.4 illustrates an example of the generated packings.

The Monte Carlo code Serpent [64] was used to model the simulated random packings explicitly[1] and calculate the neutron multiplication factor k_{ref}. It is important to note that generating such an accurate system is not efficient. Large memories and computing times are required. Although, in principle, the total number of entries (particle positions) in Serpent is unlimited, memory or running time may become a limiting factor if the number exceeds several million. The reference model is not an effective way for computing the criticality in debris beds; it is just a tool to find out an adequate simpler model.

---

[1]The explicit fuel particle model is a feature available in Serpent, which reads the coordinates and radius of the particles from a separate file and represents them explicitly, without any approximation
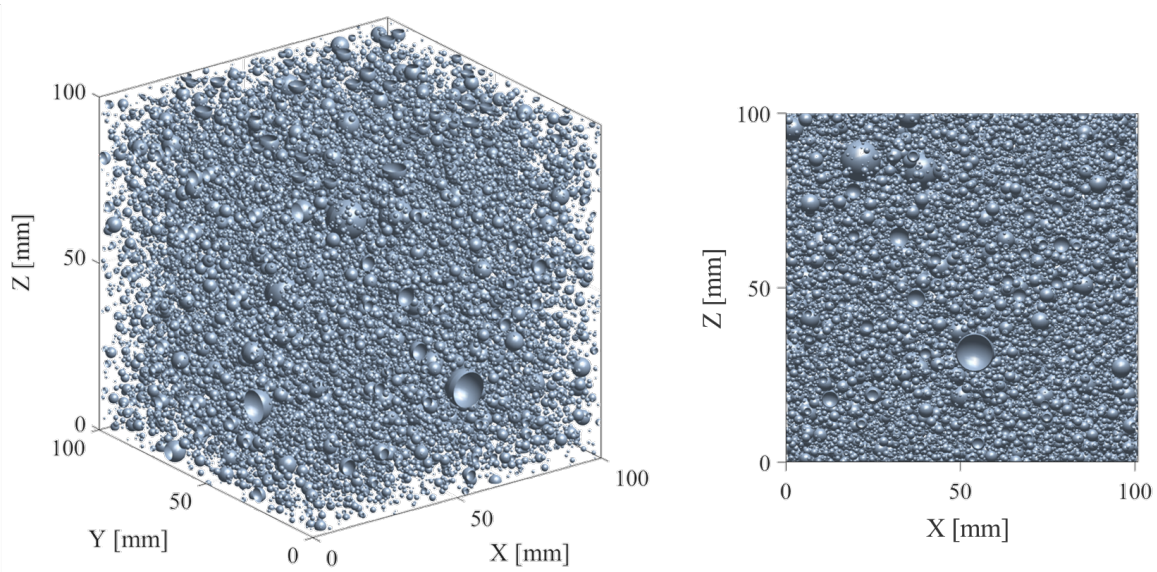
Figure 3.4: Example of reference model sphere packing simulation for a porosity of 0.9 and PSD_{DEFOR}

3.2.3 Suitability analysis

This section analyzes the suitability of the simplified debris bed models described before by comparing the results with those obtained with the reference model. The objective is to identify the most suitable model, i.e., the model with the best compromise between accuracy and simplicity. Figure 3.5 presents an overview of the models that are compared.

The neutron multiplication factors, which were considered and compared in this study, are:

k_{real} Unknown criticality value of the real debris bed that is being modeled.

k_{ref} High fidelity criticality value of the reference model, calculated with the explicit model for stochastic geometries of Serpent. This model is characterized by the *PSD*. Although slightly conservative, it is representative of the unknown k_{real}.

k_{random} Criticality value of the random model, calculated with the stochastic geometry capability of MCNP6.1. This model is characterized by the particle size d, which was varied from 0.5 mm up to 20 mm.

k_{lat} Criticality value of the regular lattice model, calculated with MCNP6.1 (BCC structure was chosen). This model is characterized by the particle size d, which was varied from 0.5 mm up to 20 mm.
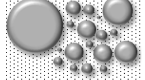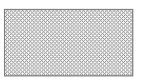
Debris bed characteristics						
Particles characteristics			Porosity	Composition	Geometry	k_∞
Shape	Size	Arrangement				
Real debris Irregular	PSD_{DEFOR} PSD_{FARO}	Chaotic				k_{real}
Reference model Sphere	PSD_{DEFOR} PSD_{FARO}	Chaotic		▪ Fuel: Fresh UO_2 fuel with 3.7% wt U^{235} (10.4 g/cm³)	Infinite (reflective boundary conditions)	$k_{ref} \sim k_{real}$
Random model Sphere	Monosize: d_{eq}	Chaotic	[0.35-0.9]			$k_{random} \sim k_{ref}$ $\sim k_{real}$
Regular lattice model Sphere	Monosize: d_{eq}	Regular (BCC lattice)		▪ Water: H_2O (1 g/cm³)		$k_{lat} \sim k_{ref} \sim$ k_{real}
Homogeneous model N/A	N/A	N/A				k_{hom}

Figure 3.5: Characteristics of the debris bed models used for the suitability analysis

$\boldsymbol{k_{hom}}$ Criticality value of the homogeneous model calculated with MCNP6.1. The homogeneous configuration may be identified with the zero-size limit of a heterogeneous configuration ($d \to 0$ mm).

In all the cases, the neutron multiplication factor was calculated for different porosity values ranged from 0.35 up to 0.9. Since the debris shape was irrelevant in this analysis, only infinite media were considered (k_∞). That was achieved by applying the reflective boundary condition in the Monte Carlo codes. Thus, the debris beds were modeled as infinite UO_2-water systems. Fresh UO_2 fuel with 3.7 wt% ^{235}U and pure water at a temperature of 20 °C were considered. The standard deviations were always kept below 0.1% for all the calculations in this study[2].

3.2.3.1   Regular lattice vs. Homogeneous model

Figure 3.6 shows the results delivered by the homogeneous model (k_{hom}) and the regular lattice model (k_{lat}) for different particle sizes (from 0 to 20 mm). Up to a point, the neutron multiplication factor increases with the particle size. The optimal particle size[3] is above 20 mm for the most typical porosities in debris beds (< 0.7). That means

---

[2]The standard deviations are too small to be clearly appreciated in the graphs. Consequently, no error bars are included.

[3]Paticle size value at which the neutron multiplication factor reaches a maximum
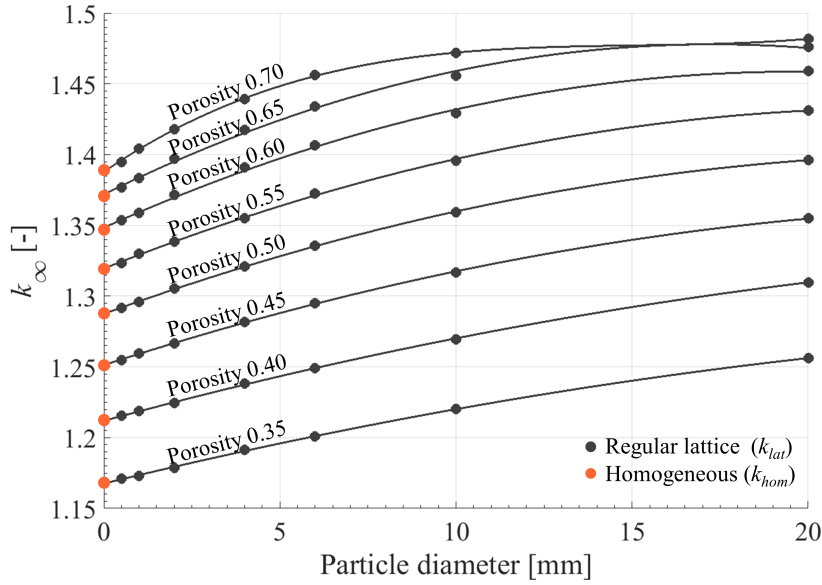
Figure 3.6: Evolution of k_{hom} and k_{lat} as a function of the particle size and porosity

that the neutron multiplication factor increases monotonically with the particle size for the porosity and particle size ranges of interest. This positive reactivity is dominated by the increase of the resonance escape probability [83], which in turn is determined largely by the fuel-moderator arrangement and the enrichment of the fuel. The self-shielding effect is a phenomenon connected with the heterogeneity of a nuclear system (i.e., the separation between fuel and moderator), and it causes a significant increase in the resonance escape probability. As the particle size decreases, the self-shielding effect becomes less important; consequently, the neutron multiplication factor decreases until reaching a minimum value when $d \to 0$ mm (homogeneous system). Figure 3.7 illustrates the positive reactivity changes caused by increasing particle sizes in comparison with the homogeneous model.

Homogenization   Like any other simplification, the homogenization of a heterogeneous nuclear system is linked to an error, which in this case is negative (non-conservative).

From a practical point of view, a debris bed can be homogenized when the particle size is small enough that only a negligible error is introduced. Equation 3.2 shows the definition of homogenization error:

$$e_{hom}(\%) = \frac{k_{hom} - k_{lat}}{k_{lat}} \times 100 = \frac{k(d=0) - k(d_{lat})}{k(d_{lat})} \times 100 \qquad (3.2)$$
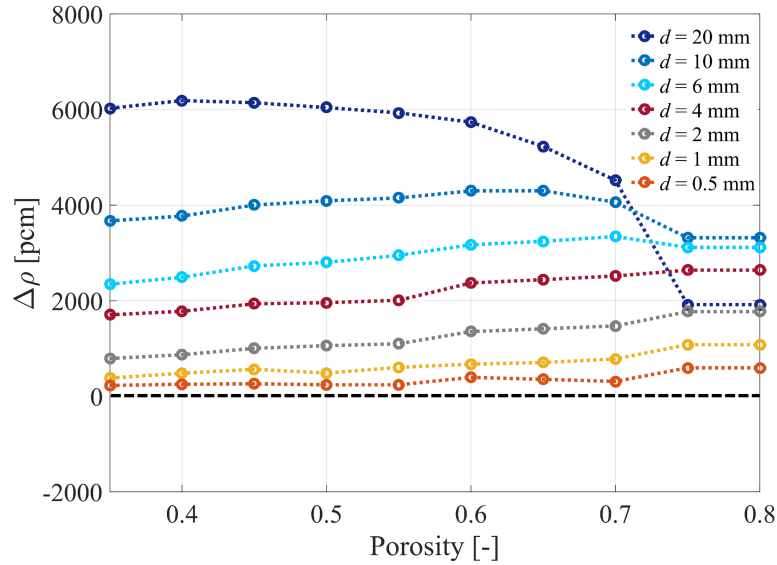
Figure 3.7: Reactivity changes as a function of the particle size and porosity (Reference: homogeneous model)

where k_{hom} is the neutron multiplication factor of the homogeneous system, and k_{lat} is the neutron multiplication factor of the heterogeneous system that can be regarded as homogeneous introducing an error e_{hom}. d_{lat} is the particle size of such a system.

Figure 3.8 shows those heterogeneous systems for which a complete homogenization would introduce an error in the neutron multiplication factor of 0.5%, 1%, 1.5%, 2%, and 3%. The heterogeneous systems are defined by the porosity and size of the particles.

As might be expected, e_{hom} decreases significantly as the particle size gets smaller. Additionally, for a given particle size, the error introduced becomes smaller for lower porosities. Taking into account the typical range of particle sizes in a debris bed (from few μm up to 2-3 cm), a total homogenization of debris beds may introduce in some cases an unacceptably high and non-conservative error. Consequently, homogenization should be used carefully, and more realistic alternatives for modeling should be investigated.

3.2.3.2 Regular lattice vs. Reference model

For each debris bed with porosity ε and particle size distribution *PSD*, there is a criticality-equivalent debris bed consisting of monosized spheres. The particle size that characterizes this equivalent regular lattice system is the so-called equivalent diameter d_{eq}:

$$d = d_{eq} \iff k_{lat}(d, \varepsilon) = k_{ref}(PSD, \varepsilon) \tag{3.3}$$
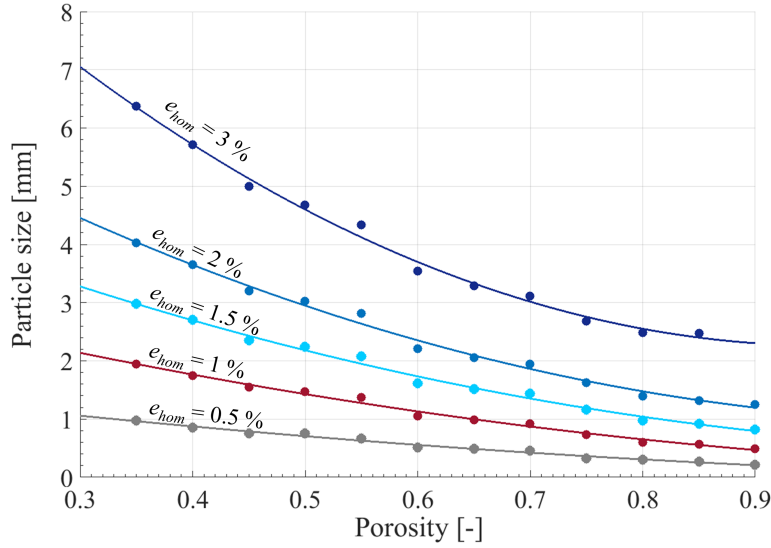
Figure 3.8: Particle sizes of systems that can be regarded as homogeneous and associated error e_{hom}

d_{eq} was calculated as a function of the porosity ε for the two distributions considered in this study: PSD_{DEFOR} and PSD_{FARO} (see Figure 3.9). In both cases, d_{eq} becomes smaller as the porosity of the simulated debris bed increases; however, this effect is more pronounced for the debris with PSD_{FARO}. A high d_{eq} variance means that it will be very difficult to find a unique simplified model adequate for representing the debris bed in the whole considered porosity range.

Equivalent diameter calculation   A methodology for the calculation of the equivalent diameter d_{eq} has been presented before. The downside of this procedure is the necessity of developing a reference model, which is very time-consuming. Thus, finding an alternative, simpler, and faster way to estimate d_{eq} would be very useful. The possibility of defining the d_{eq} as a mathematical function of the *PSD* is discussed below.

The mean diameters of a distribution of unequally-sized spherical particles were considered as possible candidates to be used as d_{eq}: count diameter, length diameter, surface diameter, and volume diameter. These can be calculated with the following general formula:

$$d_{p,q} = \left(\frac{\sum n_i d_i^p}{\sum n_i d_i^q} \right)^{1/p-q} \tag{3.4}$$

where n_i and d_i are the number and diameter of the spherical particles in a specific size fraction i, respectively. The parameters p and q receive different values depending
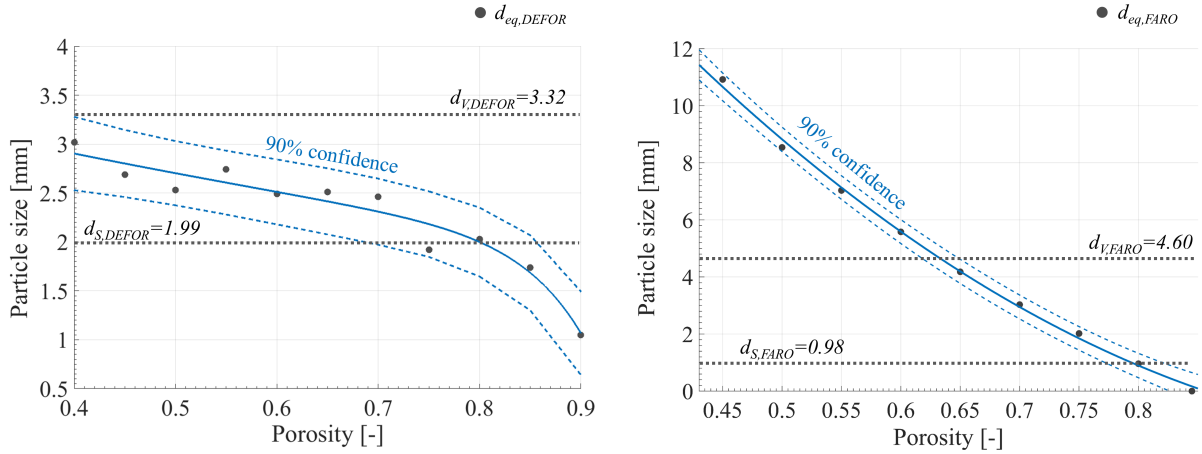
Figure 3.9: Equivalent diameter d_{eq}

on the mean diameter being calculated (see Table 3.7).

Table 3.7: Mean diameter values

Symbol	Name	p,q	DEFOR Value (mm)	FARO Value (mm)
d_n	Count mean diameter	1,0	0.07	0.15
d_l	Length mean diameter	2,1	0.39	0.23
d_s	Surface mean diameter	3,2	1.99	0.98
d_v	Volume mean diameter	4,3	3.32	4.60

Table 3.7 also shows the mean diameter values calculated for the PSD_{DEFOR} and PSD_{FARO}.

The results delivered by the reference model (see Figure 3.9) estimate a $d_{eq,DEFOR}$ within the range [0.6-3.3 mm]. The value of the volume mean diameter $d_{v,DEFOR}$ is 3.32 mm, just at the upper limit of the range. Consequently, d_v is a good candidate to be used as d_{eq} for the criticality evaluation of such debris bed. On the other hand, $d_{eq,FARO}$ was estimated to be within a much wider range, [0-11.5 mm]. The volume mean diameter $d_{v,FARO}$ is 4.60 mm, which corresponds to the estimated $d_{eq,FARO}$ for porosities between 0.6 and 0.65. At lower porosities, $d_{v,FARO}$ will provide non-conservative results.

Figure 3.10 compares the results delivered by the reference model (k_{ref}) with those delivered by a several regular lattices with different particle sizes (k_{lat}), and the homogeneous model (k_{hom}). For the PSD_{DEFOR}, there is a very good agreement ($| \Delta\rho | < 700$ pcm) between the results of the reference model ($k_{ref,DEFOR}$) and the regular lattice model with a particle diameter equal to the volume mean diameter ($k_{lat,d_v=3.32}$). Consequently, an adequate equivalent diameter was found for the DEFOR debris bed:
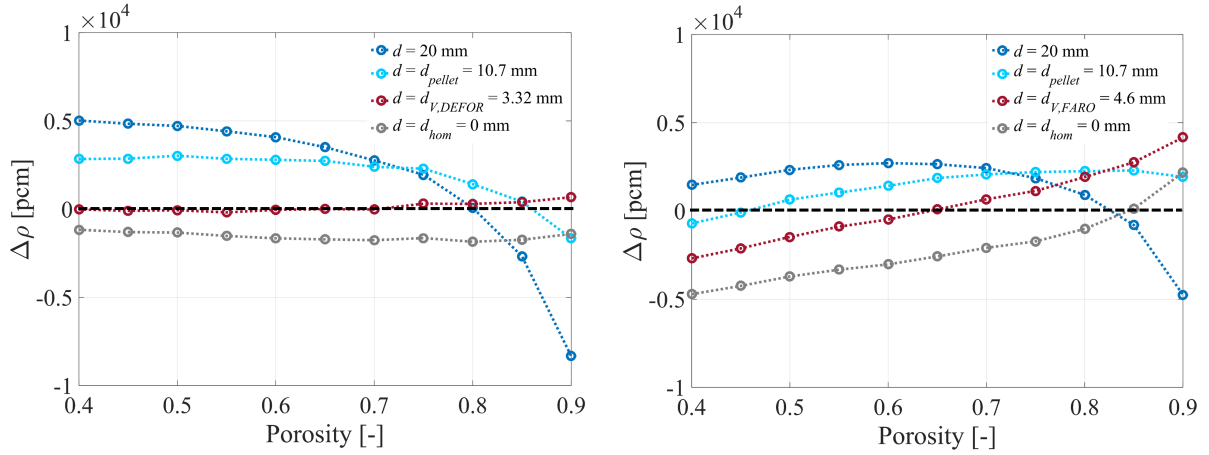
Figure 3.10: Reactivity changes introduced by different modeling alternatives for debris beds with PSD_{DEFOR} and PSD_{FARO} (Reference: Reference model)

$d_{eq,DEFOR} = d_{v,DEFOR} = 3.32\,mm$. However, the results obtained with PSD_{FARO} differ significantly. In that case, no simplification approximates the real criticality behavior of the debris bed for the whole porosity range. Different $d_{eq,FARO}$ values should be considered depending on the porosity range of interest if very accurate results are desired. Nonetheless, taking into account the uncertainties regarding the debris characteristics, assuming a diameter $d = d_{pellet} = 10.7\,mm$ would provide reasonable results and conservative over most of the porosity spectrum.

After the presented results, it can be concluded that polydisperse debris can be modeled as monosized spheres if an adequate d_{eq} is chosen. However, it was proved that not always the same value is adequate for the whole porosity range. Further particle size distributions should be investigated as well as new debris models in order to find out if there is a possible way to represent debris beds in the whole porosity range providing conservative results.

3.2.3.3   Regular lattice vs. Random models

SC, BCC, and FCC are common cubic structures used in crystallography to describe the periodic arrangement of atoms in a crystal. These sphere packings can also be used to describe idealistically the position of the particles forming a debris bed. Regular lattice models can be built very easily in Monte Carlo codes; furthermore, a high efficiency is achieved in the neutron tracking routines.

The BCC lattice was chosen for the criticality calculations of the suitability analysis presented before. In this section, new debris bed models with SC and FCC structures are used to analyze the possible impact of the lattice on the neutron multiplication factor.
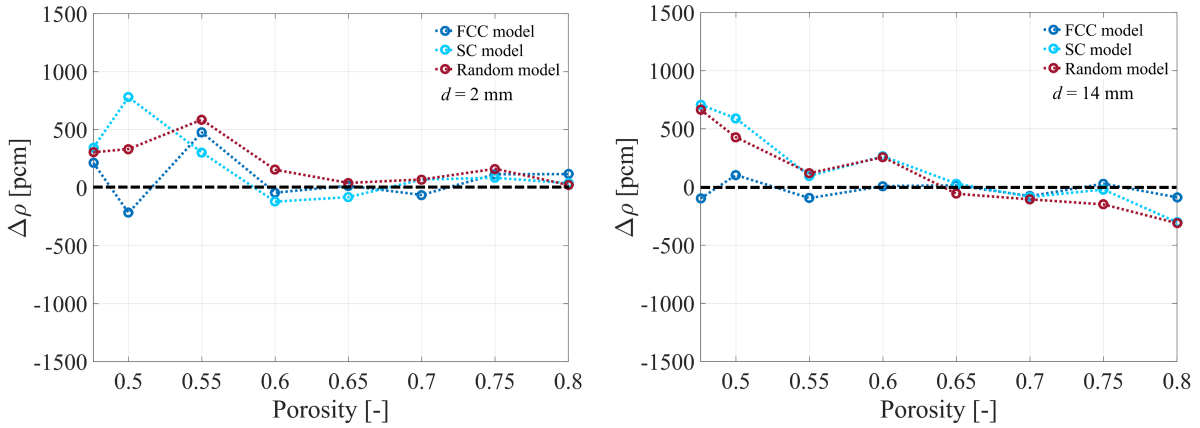
Figure 3.11: Comparison between different lattices and a random model (Reference: BBC model)

Additionally, a random model was generated using the stochastic geometry capability[4] in MCNP (random particle translations) and is also compared with the regular lattices[5].

The neutron multiplication factor was calculated as a function of the porosity and particle size for each system. The porosity was varied from 0.476 (minimum porosity for a SC lattice, when all the fuel spheres are in contact) up to 0.8. In Figure 3.11, the reactivity changes are plotted for two different particle sizes and taking the BCC lattice model as reference.

The results of the BCC model are very similar to those obtained with the other alternatives ($|\Delta\rho| < 700$ pcm). Overall, it can concluded that the particle size has a higher impact on the criticality of the debris than its spatial distribution. Based on that, any of the proposed options can be used for assessing the criticality in debris beds if an adequate particle size is chosen. Nonetheless, it is important to take into account that SC lattice cannot cover porosities smaller than 0.476; consequently, its use for the modeling of debris beds is limited. BCC reaches a minimum porosity of 0.32, which is considered small enough in most cases since debris beds with lower porosities are not usual. The minimum porosity physically achievable with monosized spheres is 0.26 (highest density packing) and can be reached with a FCC lattice. New options should be investigated to model very compact debris beds ($\varepsilon < 0.26$). Additionally, it is important to underline that the stochastic capability used for the random model provides only a limited randomness; thus, new random models with completely chaotic distributions should be considered in the future.

---

[4]The URAN card provides a limited capability of modeling stochastic geometry in MCNP6

[5]The random model was based on a SC lattice but includes some random transformation to the geometry each time a neutron enters the lattice element (debris particles).

3.3   Modeling the thermohydraulic characteristics of debris beds

In this section, coupled neutronic-thermohydraulic calculations are performed to obtain realistic temperature, density, and power profiles in debris beds. The objective is to evaluate the effect that simplifications in thermohydraulic characteristics (i.e., temperature and density) may have on the criticality. That will determine whether the coupled calculations are meaningful for assessing the criticality of debris beds.

The thermohydraulics and neutronics of a nuclear system are interdependent. Both temperature and density play a decisive role in the criticality assessment and are required as input parameters for the neutronic calculations. They can be calculated with a thermohydraulic code, which, in turn, needs as input the power profile resulting from neutronic simulations. The exchange of data between both codes is required to solve this problem.

The neutronic code MCNP6.1 was coupled with COCOMO [11], a thermohydraulic code developed at IKE (Institut für Kernenergetik und Energiesysteme), at the University of Stuttgart. COCOMO is a calculation tool able to simulate the processes occurring during the melt relocation into a water-filled reactor cavity, including melt jet fragmentation, melt-water mixing, debris bed formation, and cooling by means of integrated modeling covering all the relevant interactions. Figure 3.12 shows a scheme of the coupling and calculation process.

The scope of this thesis is limited to stationary calculations. Consequently, only subcritical configurations can be considered for the coupled calculations. In this case, the feedback effect of the neutronics on the thermohydraulics is determined by the decay heat P_d and a power component P, which is mainly produced by fission reactions of the neutron source present in the debris bed. Coupled calculations will only be meaningful if the the power P generated by the neutron source is comparable with the order of magnitude of the decay power P_d for which thermohydraulic analyses still make sense (e.g., evaporation still occurs in the packed bed).

As an example, coupled calculations were perfomed for the debris beds at Fukushima. A closer view to the main calculations and results is provided below.

3.3.1   Decay heat in debris bed

After the accident, once the reactor shuts down, the main source of heating is the energy released by radioactive decay. The decay heat varies with time after the shut-down and
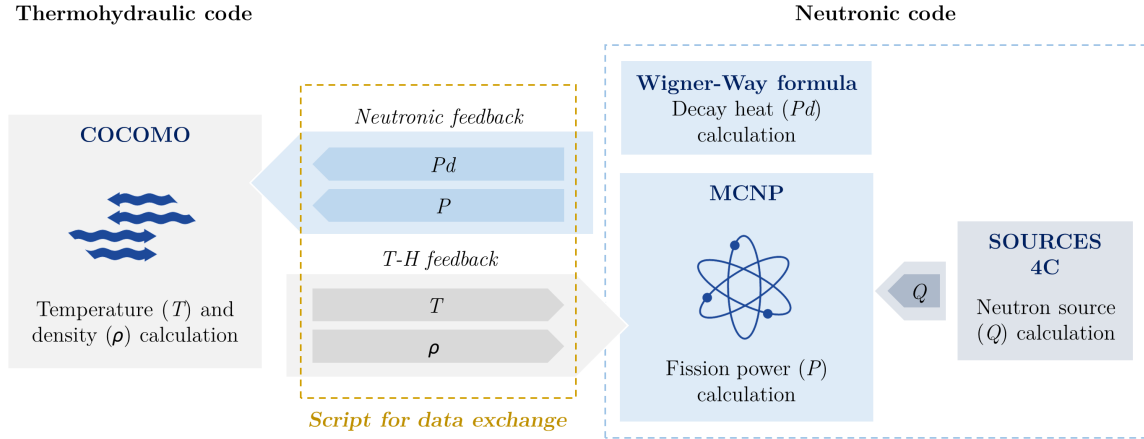
Figure 3.12: Calculation process for MCNP-COCOMO coupling

can be calculated theoretically from known nuclear data; it depends on the reactor power history and fuel type. JAEA calculated the decay heat in Fukushima damaged reactors and spent fuel pools for different times after the accident [78].

The decay power inside the debris bed can also be estimated with the Wigner-Way formula [121]:

$$P_d(t) = 0.0622 \cdot P_0 \cdot \left[t^{-0.2} - (t - t_o)^{-0.2} \right] \tag{3.5}$$

where $P_d(t)$ is thermal power generation due to beta and gamma rays, P_0 is the nominal power before the shutdown, t_0 is the irradiation time of fuel before the shutdown, and t is the time elapsed since the shutdown.

This formula uses a single half-life that represents the overall decay of the core over a certain period of time and provides a rough approximation.

Figure 3.13 shows the decay heat values calculated by JAEA after the accident in Fukushima damaged reactors. The values of Unit 2 and 3 are practically identical and overlap each other. They are slightly higher than the decay heat of Unit 1, which is a smaller reactor with lower thermal power. These values were used as initial debris power density to start the calculations.

3.3.2   COCOMO calculations

COCOMO provides the temperature and density profiles within the debris bed once the power density and some boundary conditions are given:

- Total debris mass: conservatively, the total core masses were considered to be packed as debris bed, i.e., 78.29 t in Unit 1 and 106.65 t in Unit 2 and 3.
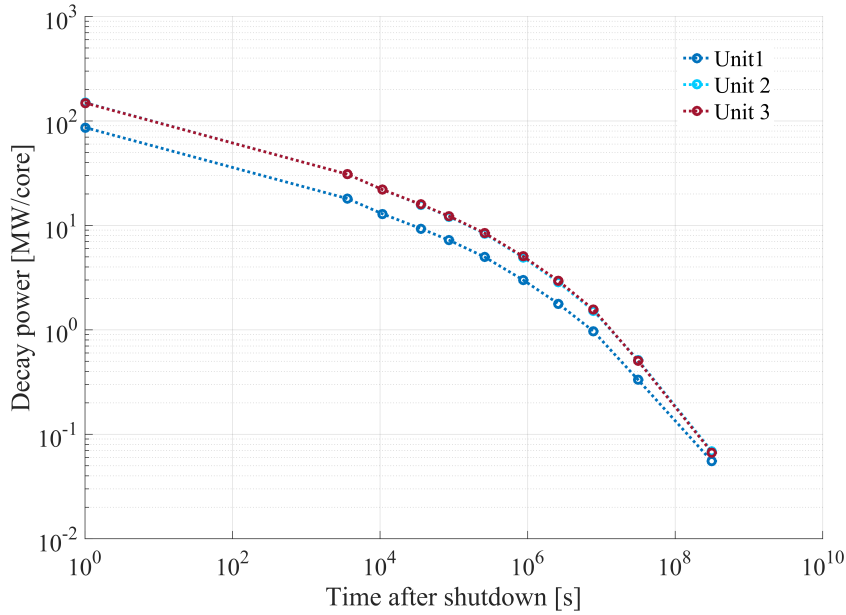
Figure 3.13: Decay heat $P_d(t)$ at Fukushima damaged reactors after the accident [78]

- Debris density: conservatively, a debris bed without structural materials and an averaged density of 10.43 g/cm^3 was considered.

- Final debris shape: a conical shape with 30° repose angle was chosen for the calculations and a flat surface radius of 1 m.

- Debris porosity: an averaged porosity of 0.38 was assumed.

- Particle diameter: an equivalent diameter of 3 mm was used.

- Reactor cavity dimensions: 6 m diameter and 8 m height.

- Water height: 5 m.

- Calculation grid: a cylindrical mesh was chosen ($\triangle R = 0.2\,m$; $(\triangle z)_{debris} = 0.1\,m$; $(\triangle z)_{water} = 0.1\,m$; $(\triangle z)_{air} = 0.2\,m$; one cell in azimuthal direction φ).

For the first calculations, only the decay heat $P_d(t)$ calculated by JAEA and uniformly distributed was considered (i.e., no neutronic feedback).

Figure 3.14 shows the debris bed model in COCOMO for Fukushima Unit 1. The cylindrical grid is illustrated as well as the three main zones of the model: debris bed, water pool, and air. Some examples of temperature and void fraction profiles are plotted in Figure 3.15. Nowadays (about ten years after the accident), the impact of the decay heat in the temperature and void fraction is very small. The decay heat has decreased
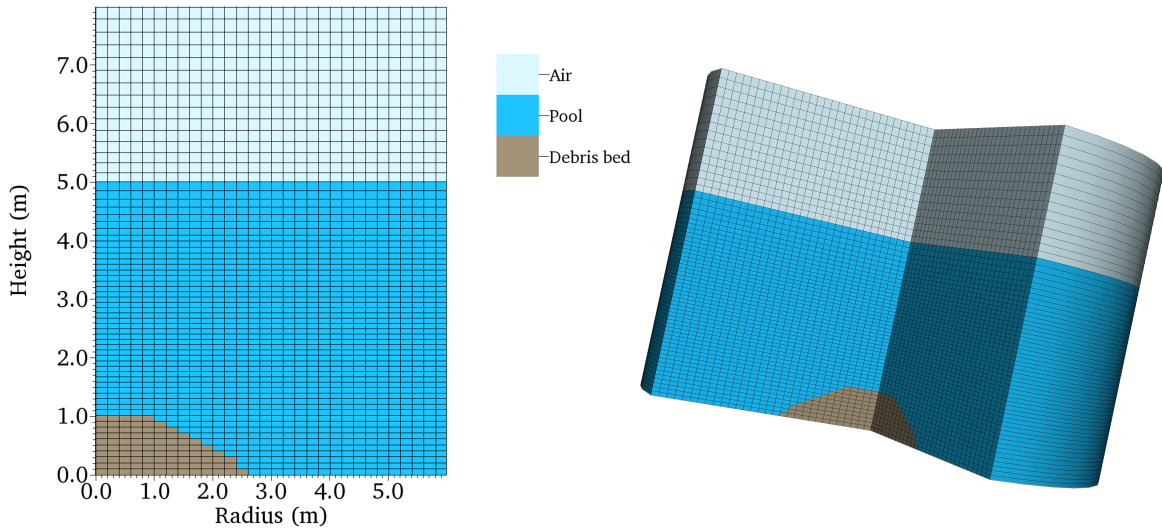
Figure 3.14: Debris bed model in COCOMO

so much that the void fraction in water is practically negligible, and the temperature inside the debris is only two degrees higher than the room temperature.

The results obtained for Unit 1, 2, and 3 debris beds at different times after the Fukushima accident were input in MCNP to calculate the neutronic characteristics of such systems. For that, a program was generated to automatize the data transfer between both codes.

3.3.3   Neutron source in debris bed

The main power component P that determines the feedback from neutronics into thermohydraulics is mostly due to fission reactions of the neutron source in the debris bed.

The neutron source is generated by:

- **Spontaneous fission (SF)**: form of radioactive decay that is found in very heavy chemical elements (radionuclides of high mass number A $\geq$ 230, i.e., actinides such as Cm). SF involves the spontaneous non-induced splitting of the nucleus into two nuclides or fission fragments and the simultaneous emission of more than one neutron on average.

- **(α,n) reactions**: the alpha radiation emitted from the decay of the uranium (and its decay products) can initiate this type of nuclear reaction after knocking some low-atomic-weight isotopes (target nucleus, e.g., isotopes of Li, Be, B, C, N, and

t = 1 day after the accident

t = 10 years after the accident

Temperature [K]

Temperature [K]
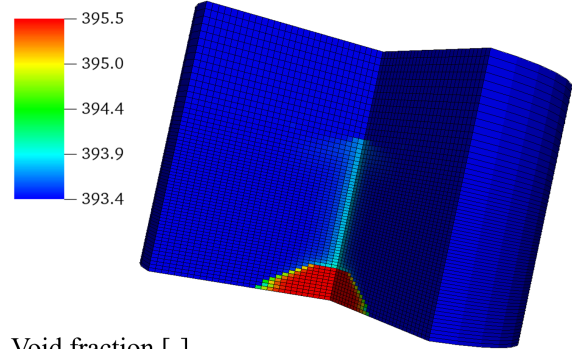
Void fraction [-]
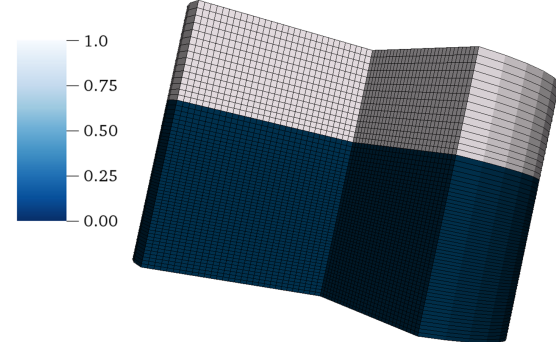
Void fraction [-]

Figure 3.15: Temperature and water void fraction profiles in ex-vessel debris bed at Fukushima Unit 1 calculated with COCOMO

O), which are transformed into other nuclides while emitting a neutron. This neutron source becomes significant when the alpha emitter is finely interspersed within the absorber or target material.

SOURCES 4C [125] is a computer code that determines neutron production rates and spectra from (α,n) reactions, spontaneous fission, and delayed neutron emission due to radionuclide decay. The code provides the magnitude and spectra of the resultant neutron source as well as an analysis of the contributions by each nuclide in the problem. It was used to calculate the neutron source in the debris beds at 1FNPS based on the estimated core compositions of the damaged reactors [78].

The values of the neutron sources at Fukushima Unit 1 are shown in Table 3.8 as well as the contributions of the different isotopes. Only ^{17}O and ^{18}O were considered relevant target nucleus of the (α,n) reactions (elements such as Li, Be, B, C, or N are not expected to be closely mixed with fuel in Fukushima reactors). The flux of neutrons per unit volume is provided, assuming an averaged density of 10.43 g/cm^3. These values

were used to input the neutron source in MCNP6 code together with the temperature and density profiles delivered by COCOMO.

Table 3.8: Neutron source at 1FNPS Unit 1 calculated by JAEA [78] and SOURCES 4C

Alpha sources	SOURCES 4C	JAEA [n/s]					
	1h	1h	30d	180d	1y	5y	10y
^{238}U		$6.91 \cdot 10^3$	$6.91 \cdot 10^3$	$6.91 \cdot 10^3$	$6.91 \cdot 10^3$	$6.91 \cdot 10^3$	$6.91 \cdot 10^3$
^{238}Pu		$1.19 \cdot 10^8$	$1.21 \cdot 10^8$	$1.25 \cdot 10^8$	$1.28 \cdot 10^8$	$1.26 \cdot 10^8$	$1.21 \cdot 10^8$
^{239}Pu		$1.38 \cdot 10^7$	$1.39 \cdot 10^7$	$1.39 \cdot 10^7$	$1.39 \cdot 10^7$	$1.39 \cdot 10^7$	$1.39 \cdot 10^7$
^{240}Pu		$1.82 \cdot 10^7$	$1.82 \cdot 10^7$	$1.82 \cdot 10^7$	$1.82 \cdot 10^7$	$1.82 \cdot 10^7$	$1.82 \cdot 10^7$
^{241}Am		$1.46 \cdot 10^7$	$1.53 \cdot 10^7$	$1.91 \cdot 10^7$	$2.36 \cdot 10^7$	$5.55 \cdot 10^7$	$8.74 \cdot 10^7$
^{243}Am		$5.76 \cdot 10^5$	$5.76 \cdot 10^5$	$5.76 \cdot 10^5$	$5.76 \cdot 10^5$	$5.82 \cdot 10^5$	$5.82 \cdot 10^5$
^{242}Cm		$3.23 \cdot 10^9$	$2.87 \cdot 10^9$	$1.52 \cdot 10^9$	$6.90 \cdot 10^8$	$2.07 \cdot 10^6$	$6.63 \cdot 10^5$
^{243}Cm		$9.98 \cdot 10^5$	$9.96 \cdot 10^5$	$9.87 \cdot 10^5$	$9.74 \cdot 10^5$	$8.84 \cdot 10^5$	$7.83 \cdot 10^5$
^{244}Cm		$8.35 \cdot 10^7$	$8.32 \cdot 10^7$	$8.19 \cdot 10^7$	$8.04 \cdot 10^7$	$6.90 \cdot 10^7$	$5.69 \cdot 10^7$
Total [n/s/cm^3]	**283.20**	**292.12**	**261.37**	**148.82**	**80.11**	**24.00**	**25.13**

SF	SOURCES 4C	JAEA [n/s]					
	1h	1h	30d	180d	1y	5y	10y
^{238}U		$8.28 \cdot 10^5$	$8.28 \cdot 10^5$	$8.28 \cdot 10^5$	$8.28 \cdot 10^5$	$8.28 \cdot 10^5$	$8.28 \cdot 10^5$
^{238}Pu		$1.94 \cdot 10^7$	$1.97 \cdot 10^7$	$2.04 \cdot 10^7$	$2.08 \cdot 10^7$	$2.06 \cdot 10^7$	$1.98 \cdot 10^7$
^{242}Pu		$9.57 \cdot 10^7$	$9.58 \cdot 10^7$	$9.58 \cdot 10^7$	$9.58 \cdot 10^7$	$9.58 \cdot 10^7$	$9.59 \cdot 10^7$
^{242}Cm		$3.40 \cdot 10^7$	$3.40 \cdot 10^7$	$3.40 \cdot 10^7$	$3.40 \cdot 10^7$	$3.40 \cdot 10^7$	$3.40 \cdot 10^7$
^{244}Cm		$1.01 \cdot 10^{10}$	$1.00 \cdot 10^{10}$	$9.87 \cdot 10^9$	$9.68 \cdot 10^9$	$8.30 \cdot 10^9$	$6.86 \cdot 10^9$
^{246}Cm		$3.99 \cdot 10^7$	$3.99 \cdot 10^7$	$3.99 \cdot 10^7$	$3.99 \cdot 10^7$	$3.99 \cdot 10^7$	$3.98 \cdot 10^5$
^{252}Cf		0	0	0	0	0	0
Total [n/s/cm^3]	**2261.00**	**2174.39**	**2021.68**	**1459.67**	**1108.17**	**712.91**	**590.99**

In subcritical systems, the neutron source is amplified by a factor $\frac{1}{1-k_{eff}}$. That means, that the P component will only be considerable for k_{eff} values very close to 1.

3.3.4 MCNP calculations

The previously calculated neutron rates and spectra were introduced in MCNP6.1 as neutron sources for the respective systems. At the same time, the material density

and temperature profiles provided by COCOMO were processed and coupled also with MCNP6.1. Fuel and water were homogenized and no structural materials were considered. Spent fuel with the estimated compositions in Units 1, 2, and 3 after the accident were used for the calculations (see isotopic compositions in Appendix A). Once the debris bed models were created, the energy deposition was calculated for every mesh cell.

The results of this analysis are presented in Figure 3.16. The integral values of the power P deposited in the whole debris were calculated and compared with the decay heat P_d in the debris at different times after the accident. The power generated by the neutron source is always at least two orders of magnitude lower than the power released by radioactive decay. Based on this results, it can be concluded that the neutronic feedback would be so small that is not worth considering.

Additionally, the values of k_{eff} over time are plotted in Figure 3.17. k_{eff} is in all cases lower than 0.93. These values are not close enough to 1 to make it worthwhile to consider the effects of coupling.

Because of the aforementioned findings, further coupled calculations are not meaningful in the scope of this thesis. Room temperature and pure water with no void fraction will be assumed for all the criticality calculations further on.
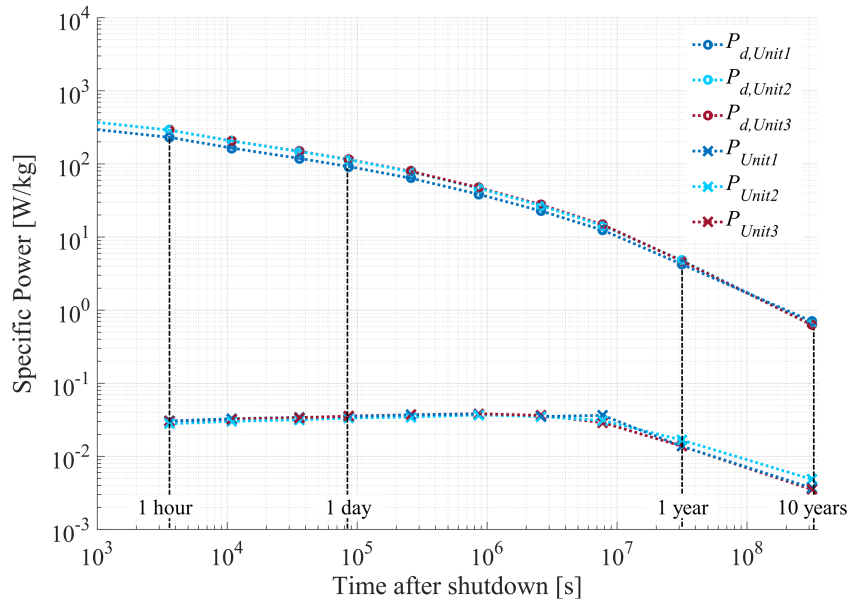
Figure 3.16: Comparison between decay power P_d and neutron source additional power P for several times after the accident
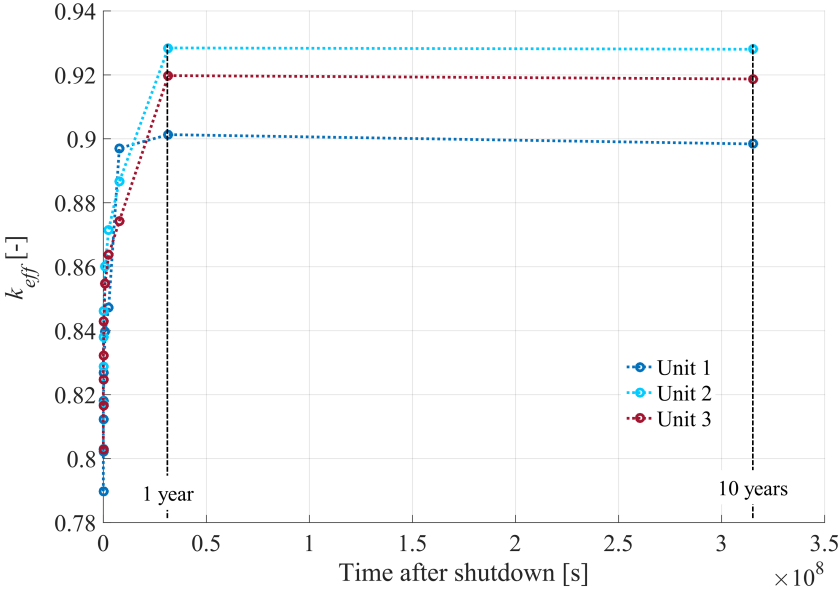
Figure 3.17: k_{eff} values in Fukushima damaged reactors at several times after the accident

Chapter 4

Conservative criticality evaluation of debris beds

In this chapter, a conservative criticality evaluation of the debris beds at Fukushima Daiichi is performed. Several of the most influencing parameters on the neutron multiplication factor were studied: particle size, porosity, debris size/mass, fuel composition, and boration of water. As the fuel debris conditions are still uncertain, wide ranges of the selected parameters were considered to cover any possible debris bed configuration, and conservative assumptions were applied. The presence of concrete in the debris beds is not contemplated in this chapter. Given the importance of concrete in the criticality assessment of ex-vessel debris beds that are formed after the MCCI, a complete chapter was devoted to this topic (see Chapter 5).

The results show under which conditions the criticality safety is ensured (safety parameter ranges) or the quantity of boron that should be added to the coolant to prevent it.

4.1 Calculation model

4.1.1 Geometrical model

4.1.1.1 Infinite debris bed

Figure 5.1a shows the debris bed model used for the computation of the infinite neutron multiplication factor (k_∞). The debris is represented as a heterogeneous structure consisting of fuel particles submerged in water. The infinite extension is achieved by applying the reflection boundary conditions in the neutronic code MCNP6.1 [31].

(a) Infinite debris model   (b) Finite debris model
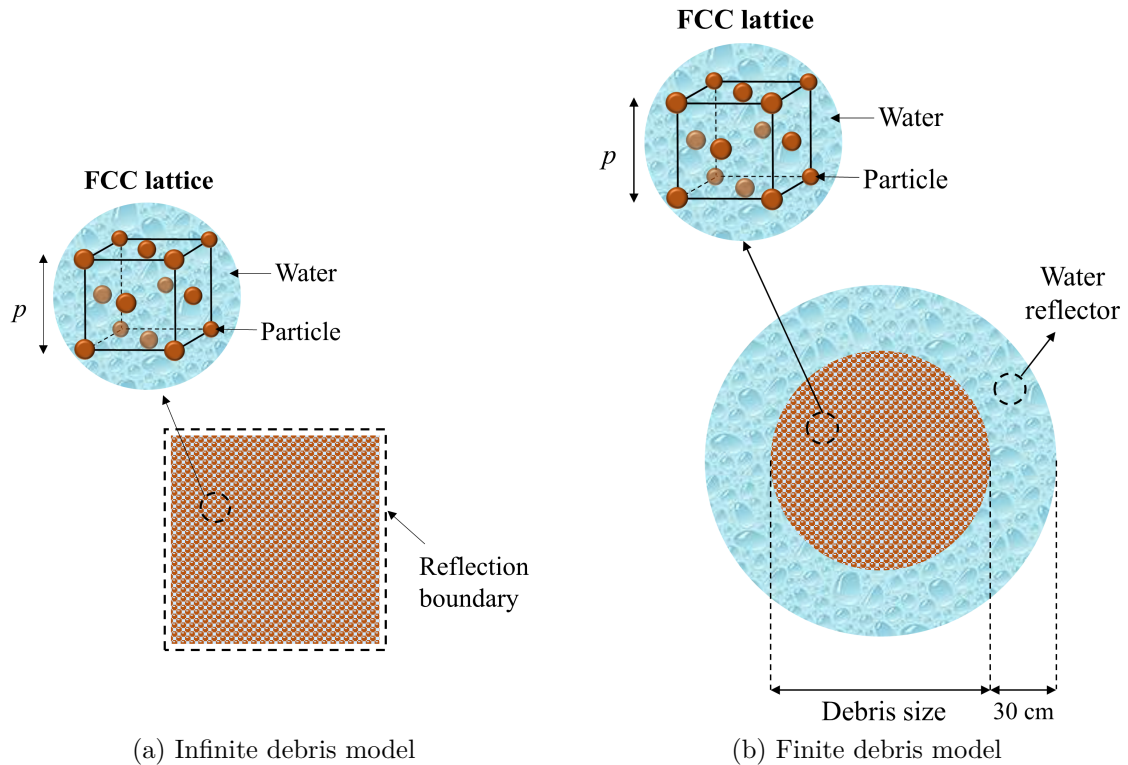
Figure 4.1: Debris bed models

Regarding the internal porous structure of the debris, the following simplifications were applied:

- The particles are spherical.

- All particles have the same size.

- The particles are regularly arranged in the space following an FCC lattice.

The suitability of these simplifications was demonstrated in the previous chapter (Section 3.2). In this study, the particle size was a parameter, and the pitch p of the FCC unit cell was used to vary the porosity of the debris. It is important to note that the minimum porosity physically achievable for an FCC system is 0.26 (when all the fuel spheres are in contact). To model systems with lower porosities, the density of the water was reduced accordingly. It was proved that reducing the water density has the same effect on the neutron multiplication factor as reducing the water volume, i.e., the porosity. Alternative ways for the modeling of very compact debris bed systems need to be further investigated in future works.

4.1.1.2   Finite debris bed

Figure 5.1b shows the model used to represent finite debris beds and calculate the effective neutron multiplication factor (k_{eff}). The internal structure is identical to the one described before, but now it is contained in a limited area. For conservative results, the shape of the whole debris bed was spherically arranged to minimize the neutron leakage and the critical mass. Surrounding the fuel debris, there is a water reflector of effectively infinite thickness (approx. 30 cm). Outside this area, there is only void. The debris size was also varied to analyze the evolution of the k_{eff} and to calculate the safe fuel mass limit (SFML) for different scenarios.

4.1.2   Debris bed composition

Several types of fuel were considered for the calculations in this study:

- Fresh fuel with enrichment ranged from 2 up to 5 wt% ^{235}U (based on the initial uranium inventory of "BWR STEP3" assembly resumed in Table 3.3).

- Spent fuel with burnup ranged from 12 up to 50 GWd/t$_{HM}$ (based on the burnup history of 1FNPS reactors resumed in Table 3.4).

The isotopic compositions used for the calculations are collected in Appendix B. For the spent fuel, the nuclide compositions were taken from the international burnup calculation benchmark report for the "BWR STEP3" fuel assembly published by NEA [77], and the estimation of fuel compositions in 1FNPS published by JAEA [78]. Both actinides and FPs were considered in the calculations (for details about the selection of nuclides see Appendix B).

It was conservatively assumed that there was nothing present in the fuel debris but fuel pellets and water. Thus, the negative reactivity effects due to the possible presence of cladding, fixed absorbers, and structural materials were ignored. The presence of concrete and formation of MCCI products is investigated in detail in Chapter 5.

4.1.3   Coolant composition

Light water was used as coolant/moderator. Room temperature and standard atmospheric pressure were assumed for all the calculations of this study. Based on the results obtained in Section 3.3, no void fraction was considered. Thus, the density of the water was set to 0.997 g/cm^3.

Boron was added in every scenario in order to know the required concentration that would guarantee the subcritical condition of the debris.

4.2 Criticality calculations

Criticality calculations were performed for multiple scenarios using the calculation models described before. Five parameters were investigated: particle size, porosity, debris size, fuel composition, and water boration. The parameters and ranges of variation are summarized in Table 5.2.

Table 4.1: Parameter and ranges for the criticality calculations

Parameter	Range	Boundary value
Particle size	2 - 30 mm	10.7 mm
Porosity	0 - 0.9	Optimal porosity
Debris size	10 - 300 cm	Infinite
Fuel composition		
- Enrichment	2 - 5 wt% ^{235}U	Spent fuel with 12 GWd/t$_{HM}$
- Burnup	0 - 50 GWd/t$_{HM}$	
Water boration	0 - 15000* ppm B	0

* Not practicable. The maximum solubility is about 12000 ppm B in water

To analyze all the possible dependencies between these parameters, they all were combined by pairs resulting in a total of ten possible combinations or calculations sets. In each calculation set, the paired parameters were varied over their whole ranges, while the rest of parameters had a fixed conservative boundary value (see Section 4.2.1). The neutron multiplication factor was then calculated for all the possible combinations. In total, more than 10,000[1] simulations were carried out using MPI parallelism at *Hazel Hen* supercomputer.

Table 5.3 sums up the criticality calculations of this study. Gray cells show the variation ranges of the paired parameters for each calculation set. The values of the remaining parameters, which define the boundary conditions of a given set, appear in the white cells. For example, in the calculation set 2, the particle and debris size are combined; particle size varies from 1 to 30 mm and debris diameter from 10 up to 300 cm. k_{eff} is calculated for all the possible combinations of these two parameters, while the rest maintain their boundary values: porosity is set to the optimal value that maximizes the k_{eff}, no boration is considered, and the fuel composition is the corresponding to Fukushima fuel with 12 GWd/t$_{HM}$.

---

[1]Many of these calculations were aimed at calculating the optimal porosity for each of the parameter combinations

Table 4.2: Criticality calculations matrix

Calc. Set	Particle size [mm]	Porosity [-]	Debris size [cm]	Fuel composition		Water boration [ppm B]
				Enrichment [wt% ^{235}U]	Burnup [GWd/t$_{HM}$]	
1	2 - 30	0.32 - 0.9	Inf.	-	12	0
2	2 - 30	Opt.	10 - 300	-	12	0
3	2 - 30	Opt.	Inf.	0 - 5	12 - 50	0
4	2 - 30	Opt.	Inf.	-	12	0 - 3000
5	10.7	0.32 - 0.9	10 - 300	-	12	0
6	10.7	0.32 - 0.9	Inf.	0 - 5	12 - 50	0
7	10.7	0.32 - 0.9	Inf.	-	12	0 - 3000
8	10.7	Opt.	10 - 300	0 - 5	12 - 50	0
9	10.7	Opt.	10 - 300	-	12	0 - 3000
10	10.7	Opt.	Inf.	0 - 5	12 - 50	0 - 15000

MCNP6.1 code [31] and ENDF/B-VII.1 [13] cross section libraries were used to perform the criticality calculations. The standard deviations of the neutron multiplication factors were always kept below the 0.1%. For that, a neutron source of 4000 histories per cycle with a total of 300 cycles (100 skipped) was used for every single calculation.

4.2.1   Parameter conservative assumptions

Each calculation set studies the influence of two parameters on the k_{eff}. The rest of parameters are then set to conservative values (conservative boundary conditions).

The boundary value of the particle size was set to 10.7 mm in order to preserve the normal pellet surface-to-volume ratio. This value is not the optimum that maximizes the k_{eff}. In fact, previous analyses have demontrated that the optimal particle size for UO$_2$ particles moderated with water is greater than a standard-size fuel pellet (see Section 3.2.3.1). However, defueling experience and debris formation experiments have indicated that particles much smaller than standard size pellets are representative of the debris bed [61, 67, 75, 109].

The conservative value of the porosity was set to the optimal porosity that maximizes the k_{eff}. This value is different for every scenario and was calculated separately every time. The porosity in debris beds can change easily and considerably over time, for example, during the defueling activities. For that reason, taking the most conservative approach was considered appropriate in this case. Appendix C explains the evolution of the optimal porosity in dependence of several parameters.

Regarding the debris size, an infinite configuration was considered as conservative boundary condition.

Spent fuel with a burnup of 12 GWd/t$_{\text{HM}}$ was chosen as boundary value for the fuel composition. This value is significantly lower than any of the averaged burnups at Fukushima reactors (25.8 GWd/t$_{\text{HM}}$ in Unit 1, 23.1 GWd/t$_{\text{HM}}$ in Unit 2, and 21.8 GWd/t$_{\text{HM}}$ in Unit 3). Assuming fresh fuel is more conservative, but the results would be very far from reality.

Finally, the amount of boron in water was conservatively set to zero. Assuming pure water without boron and no void fraction maximizes the neutron multiplication factor.

Based on the theory of K. Jamali [52] (see Section 2.2.3.2), the results obtained with these assumptions are expected to be very conservative, since more than one or two relevant parameters are always set to their bounding values (most conservative extremes)[2].

4.2.2 Criticality acceptance criterion

An acceptance criterion of $k_{eff} < 0.95$ (USL) was applied throughout all this work, i.e., a 5% margin to criticality (MOS) (see equations 2.16 and 2.17). That means that the calculated neutron multiplication factor k_{eff} must be less than 0.95, including all uncertainties and tolerances, to ensure subcriticality. Any modeling uncertainties are covered by setting relevant parameters to pessimistic values (conservative evaluation). In the absence of experimental data, the bias was assumed to be zero; this value should be reassessed in the future once data is available. That is the conventional criterion for subcriticality assessment, recommended also by the Nuclear Safety Standards Commission (Kerntechnischer Ausschuss, KTA) [80].

4.3 Results

Some of the most important results of the previously explained criticality calculations will be shown and discussed in this section.

Figure 4.2 corresponds to the calculation set 4 and shows the evolution of the neutron multiplication factor as a function of the particle size and the water boration. Two different representations of the results can be distinguished: a 3D criticality surface on the left side and a contour criticality plot on the right side.

---

[2]The calculation sets 1, 5, 6, 7 (see table 5.3) can be non-conservative if there is concrete in the debris bed (see Chapter 5).
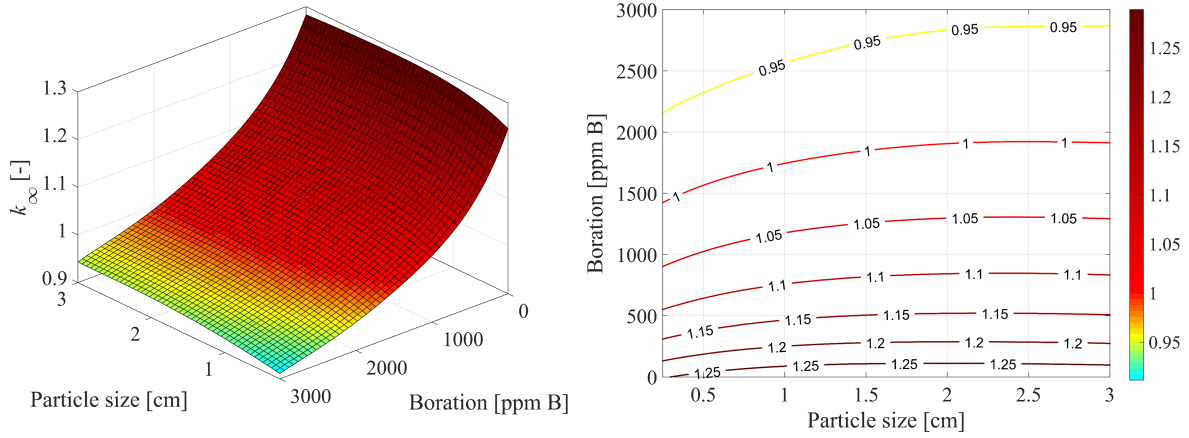
Figure 4.2: Evolution of k_∞ as a function of the particle size and boron concentration in water

k_∞ decreases slightly as the size of the debris particles gets smaller reaching a minimum value for the homogeneous system ($d \to 0\,cm$). If the debris is submerged in non-borated water, k_∞ reaches its maximum value for a particle size of 1.94 cm. This optimal particle size increases slightly with the water boration. In any case, the contour curves are almost flat for particle sizes larger than 2 cm, i.e., the changes in the neutron multiplication factor with the particle size are practically negligible. Consequently, although noticeable, the effect of the particle size on the neutron multiplication factor is far from being the most important.

On the other hand, boron is a good neutron absorber, especially for thermal neutrons, and causes a significant decrease in the k_∞. If for safety reasons the critical level is conservatively set to 0.95, the contour line $k_\infty = 0.95$ would indicate the boron content required to secure subcriticality. Thus, 2900 ppm B are necessary to guarantee subcriticality conditions of the debris bed independently of the particle size.

Figure 4.3 provides criticality data depending on the porosity (calculation set 7). k_∞ increases with the porosity until a maximum is reached for the so-called optimal porosity. At this point, the moderation conditions are optimal. The optimal porosity moves to lower values as the boron concentration increases. In a system without boron, the optimal porosity is 0.75; however, if the debris bed is submerged in water with 2600 ppm B, this value decreases to 0.41. In that case, a higher porosity would not only mean a better capacity to moderate neutron but also more quantity of boron absorbing neutrons. More details about how the optimal porosity changes in dependence of debris bed parameters such as water boration or the fuel enrichment are collected in Appendix
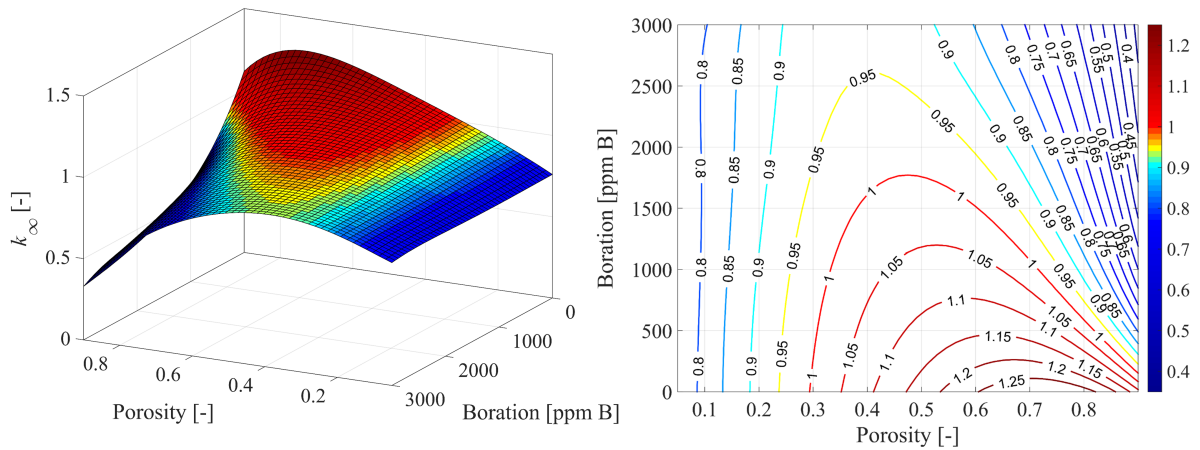
Figure 4.3: Evolution of k_∞ as a function of the porosity and water boration
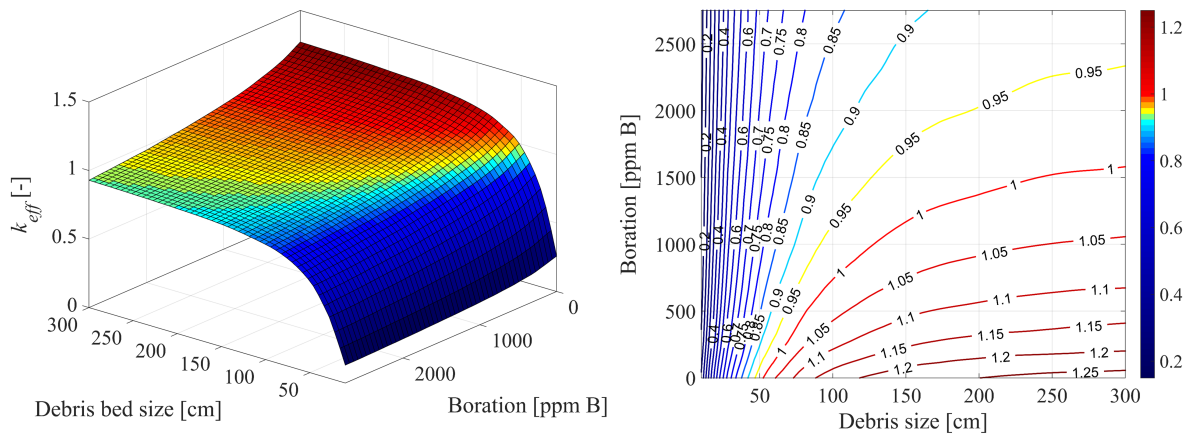
Figure 4.4: Evolution of k_{eff} as a function of the debris size and water boration

C. The porosity has a strong influence on the criticality characteristics of a debris bed and, consequently, must be treated very cautiously.

The contour line $k_\infty = 0.95$ (critical level) indicates that 2600 ppm B are enough to keep the fuel debris subcritical under the boundary conditions considered and independently of the porosity. Additionally, systems with porosities lower than 0.24[3] cannot become critical since there is not enough moderator in the system.

Figure 4.4 represents the calculation set 9 and provides information about the criticality conditions of a debris bed depending on its size. The neutron multiplication factor increases drastically with the debris size until an almost stable value is reached.

Assuming the critical value on 0.95, the minimum critical size of the debris bed is 45 cm. For these conditions, the optimal porosity was calculated to be 0.75, resulting

---

[3]This statement is only valid for systems without concrete. For more details see Chapter 5
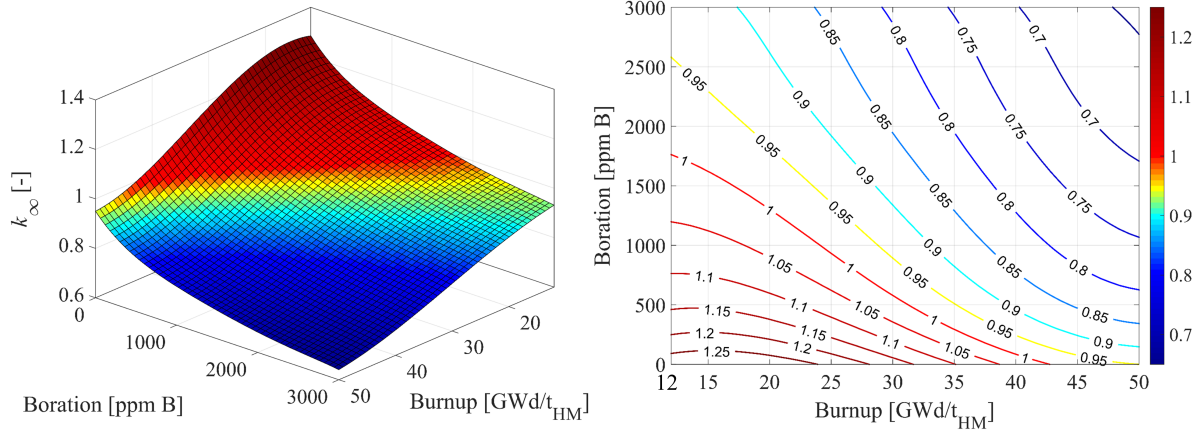
Figure 4.5: Evolution of k_∞ as a function of the fuel burnup and water boration

in a corresponding critical mass of 124 kg. Taking into account that the total mass of the reactor core of Unit 1 (the smallest of the damaged reactors) is about 92 tons, the previously calculated critical mass represents less than 1% of the core. Therefore, any fuel debris in the damaged units 1, 2, and 3 easily exceeds the minimum mass required to reach criticality. Nevertheless, these results are useful for the design of the caskets and transport devices that will be used during the debris retrieval. The contour line $k_\infty = 0.95$ (critical level) shows the quantity of boron necessary to secure subcriticality for different sizes.

Figure 4.5 shows the evolution of k_∞ as the fuel burnup varies (calculation set 10). As it was expected, the neutron multiplication factor decreases with the burnup. Debris beds with a burnup higher than 50 GWd/t_{HM} would be intrinsically subcritical, although such high values are never reached (in averaged). One more time, it can be appreciated that 2600 ppm B would ensure the subcritical conditions of the debris.

The effect of fuel enrichment on the criticality was also analyzed (see Figure 4.6). k_∞ increases significantly and almost linearly as the wt% ^{235}U in the system gets higher. The addition of boron has firstly a very negative effect on the system reactivity; however, as the boron concentration increases, its capacity to control the criticality diminishes. That occurs because the optimal porosity values are very low for fresh fuel systems with a high concentration of boron.

Table 4.3 gathers the concentrations of boron required to guarantee subcritical conditions for different fuel compositions. The differences are significant, which means that it is very important to investigate further the debris composition and the mixing process of the melted fuel assemblies to delimit the realistic ranges.
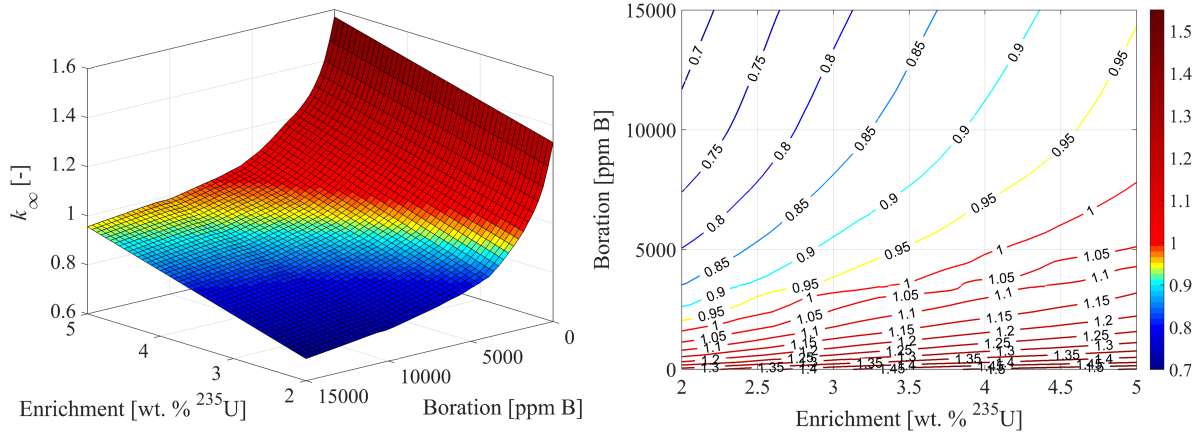
Figure 4.6: Evolution of k_∞ as a function of the fuel enrichment and water boration

Table 4.3: Amount of boron required to secure subcriticality for different fuel compositions

Fuel type	Characteristics	Concentration of natural boron in water ($k_\infty = 0.95$)
Fresh fuel 5 wt.% ^{235}U	Averaged enrichment in fuel assembly	14000 ppm B
Fresh fuel 3.7 wt.% ^{235}U	Maximum enrichment in fuel assembly	7200 ppm B
Spent fuel 12 GWd/t$_{HM}$	Highest reactivity of intact assembly	2600 ppm B
Spent fuel 23.1 GWd/t$_{HM}$	Averaged burnup in Unit 2	1600 ppm B
Spent fuel 25.8 GWd/t$_{HM}$	Averaged burnup in Unit 1	1300 ppm B

4.3.1 Safety parameter ranges

To conclude, the safety parameter ranges of the conservative model investigated are collected in Table 4.4.

Table 4.4: Safety parameter ranges (spent fuel with 12 GWd/t$_{\text{HM}}$ burnup)

Parameter	Safety range $(k_\infty, k_{eff} < 0.95)$
Porosity	< 0.24*
Debris size/mass	< 45 cm / < 124 kg
Boration	> 2600 ppm B*

* Not valid for debris beds containing concrete

The porosity range is not realistic for particulate debris beds, where porosities higher than 0.4 are expected; however, it may apply in case of very compacted monolithic or ingot debris as long as the fuel is not mixed with concrete.

The range of safety debris sizes or masses covers only very small debris accumulations. It may be useful for debris transportation purposes.

The safety burnup range is not realistic since 50 GWd/t$_{\text{HM}}$ is about the maximum value reached nowadays in LWRs.

Finally, the boration safety value is feasible and may be useful to guarantee the criticality safety during the retrieval activities.

The calculations must be validated once the results of the on-going critical experiments are available. These results can contribute to the criticality database that is being developed. However, for the criticality assessment of Fukushima debris beds, the presence of concrete should be evaluated if the MCCI is confirmed (see Chapter 5).

Chapter 5

Effect of MCCI products on debris bed criticality

This chapter investigates the criticality conditions of debris beds that have been formed through the molten corium–concrete interaction (MCCI). These were modeled as UO_2-concrete systems submerged in water. A big amount of this kind of composite is estimated to be present in the PCV of Fukushima damaged reactors, at least in Unit 1 and 3 [97, 114]. During the accident, the failure of the RPV caused the relocation of a large part of the corium into the reactor cavity (ex-vessel scenario). As a result, the molten corium very likely reacted with the concrete forming the so-called MCCI product.

The criticality characteristics of this type of composites were first investigated after the Fukushima accident [49, 117]. These studies prove the good moderation capacities of concrete and highlight the need for further research. Standard concrete was considered for the calculations; however, during the MCCI process, the concrete decomposes and does not preserve its original state anymore. Among many other things, the very high temperatures cause the release of the bound water as steam. Consequently, MCCI products can only conserve a residual quantity of the initial bound water, if any. Reducing the water content may have significant negative reactivity effects that should be evaluated to complement the previous work. The goal of this chapter is to meet this need providing a more realistic approach to the current situation of ex-vessel 1FNPS debris beds. The obtained results will contribute to the development of a criticality database for a safe decommissioning of 1FNPS.

For a better understanding, the calculations are introduced by a brief explanation of the MCCI process and the particular characteristics of debris beds containing MCCI products.

5.1   The Molten Corium - Concrete Interaction

In a SA, if the molten core is not retained in-vessel, it will be poured onto the reactor pit basemat. Energy is generated in the corium from radioactive decay and chemical reactions, which can be removed either by conduction via the adjacent concrete or by radiative heat transfer through the top surface. Typically, the thickness and low conductivity of concrete result in an initial corium heating phase followed by continuous erosion of concrete. Concrete starts melting around 1100 to 1250 °C, and the surface is ablated at a typical rate of several centimeters per hour [7].

Since the concrete is made up mainly of SiO_2, $CaCO_3$, and H_2O, its decomposition leads to the release of gases (H_2O and CO_2) and the melting of residual oxides (SiO_2 and CaO), which are added to the corium pool. The corium pool, therefore, contains heavy oxides from the reactor core (UO_2 and ZrO_2), light oxides from the concrete (mainly SiO_2 and CaO), and metals (Fe, Cr, Ni, and Zr) [50]. The gas bubbles from the decomposing concrete enter the pool and agitate it, inducing the mixing of the liquids. Depending on the gas flow rate, the configuration of the pool may be a single layer (oxide and metal mixed) or two-layer (oxide and metal stratified according to their respective densities).

Overall, the molten corium-concrete interactions are characterized by the coupling of very complex phenomena that include thermohydraulic, thermochemical, and mechanical processes. A very simple picture of the prototypical phenomenology has been provided before (for detail information about the MCCI, see [7, 103]); nonetheless, the interactions will depend on the specific reactor and accident scenario. Even though extensive research has been undertaken to understand MCCI processes, simulating them and predicting their behavior are still challenging tasks. In general, the reliability and validation of the MCCI models are insufficient, and code results are linked to high uncertainties [102].

5.1.1   MCCI product

Knowing the characteristics of the corium and MCCI products is essential for a proper and safe decommissioning of severely damaged reactors.

Currently, there is very limited knowledge about the MCCI product characteristics. Comprehensive data from real accident scenarios are not available (in TMI-2, MCCI did not occur; in Chernobyl, the lava-like fuel-containing materials differ significantly from the MCCI product that would be found in a LWR; in Fukushima, sampling is still pending). Besides, most MCCI experimental and numerical research has focused until now on the concrete ablation phenomena. Nonetheless, some MCCI test products

have been analyzed in experiments during the last years [26, 102]. Recently, VULCANO MCCI tests were performed under conditions similar to Fukushima Unit 1 [8, 56]. The purpose of this JAEA/CEA collaboration was to obtain prototypical corium samples and analyze them to characterize the real debris.

5.1.1.1 Amount of concrete

The proportion of corium and concrete in an MCCI product depends on the extent of the interactions, i.e., the volume of the ablated concrete. Consequently, an approximate value can be obtained if an estimation of the ablation time (or ablation depth) is done.

During the molten core-concrete interaction, the melt will be continuously enriched in concrete decomposition products (mainly CaO and SiO_2). In the first hours of MCCI, the mass fraction of "concrete oxides" in the pool is less than 25%. After 5-15 hours, the mass fraction grows up to around 50% [50]. Beyond 15 hours of MCCI, silica and/or calcia may become the major constituents of the melt, as it occurred during the Chernobyl accident.

The extent of MCCI at Fukushima Unit 1 was estimated with MAAP code by TEPCO [116]. The results shows an erosion of approx. 65 cm depth in axial and radial directions in each sump pit, which is equivalent to 20-30 tons of concrete mixed with fuel. Assuming 25 tons of ablated concrete with density $\rho_{concrete} = 2300\,kg/m^3$ and 78 tons of UO_2 (initial inventory of Unit 1) with density $\rho_{UO_2} = 10400\,kg/m^3$, the concrete volume fraction (of erosion factor) can be calculated as follow:

$$\rho_{MCCI} = \frac{1}{\frac{w_{UO_2}}{\rho_{UO_2}} + \frac{w_{concrete}}{\rho_{concrete}}} = \frac{1}{\frac{78\,t/103\,t}{10400\,kg/m^3} + \frac{25\,kg/103\,kg}{2300\,kg/m^3}} = 5607\,kg/m^3 \tag{5.1}$$

$$f_e = \frac{V_{concrete}}{V_{MCCI}} \cdot 100 = \frac{\rho_{MCCI} \cdot m_{concrete}}{\rho_{concrete} \cdot m_{MCCI}} \cdot 100 = \frac{5607\,kg/m^3 \cdot 25\,t}{2300\,kg/m^3 \cdot 103\,t} \cdot 100 = 59\% \tag{5.2}$$

That is just a guide value to get an idea of the magnitude of the MCCI interaction in a real scenario and, thus, chose meaningful ranges for the calculations.

5.1.2 Concrete characteristics

Concrete is a composite material mainly made of cement, water, and aggregates. There are many types of concrete depending on the aggregates, which normally consist of variable proportions of silica (SiO_2) and limestone ($CaCO_3$).

The concrete used in the construction of Fukushima plants is of the siliceous type, which contains mainly SiO_2. The composition was estimated from samples picked up from Fukushima Unit 1 reactor building [86]. Table 5.1 shows the composition of regular siliceous concrete [69], which is close to the estimated at Fukushima reactors, and it was used for all the calculations with concrete through this work.

Table 5.1: Regular siliceous concrete composition (Density: 2.3 g/cm³ [69])

Element	Atomic number density [atoms/barn/cm]
H	0.013742
O	0.046056
Na	0.001747
Al	0.001745
Si	0.016620
Ca	0.001521
Fe	0.000347

The characteristics and behavior of concrete at high temperatures are described in detail in [7, 103]. Within the scope of this thesis, it is particularly important to know the behavior of the bound water inside the concrete since a minimal presence of water in the debris bed may have dramatic effects on the criticality.

5.1.2.1   Bound water inside the concrete

Two types of water can be distinguished [103]:

- Evaporable water: free and physically bound (absorbed) water. This water is released at 105 °C and completely eliminated at 120 °C.

- Chemically bound water: forming hydrates, e.g., $Ca(OH)_2$ or $3CaO_2 \cdot SiO_2 \cdot 3H_2O$. They are released between 100 and 850 °C.

Since the concrete starts melting around 1100-1250 °C, it is very unlikely to find any water in the concrete forming the MCCI products.

5.2   Calculation model

5.2.1   Geometrical model

As in the previous chapter, two debris bed models were used: infinite and finite (see Figure 5.1). A debris bed with infinite extension was conservatively assumed for most of the calculations in this study, while the finite model was used to calculate the SFML.

(a) Infinite debris model   (b) Finite debris model
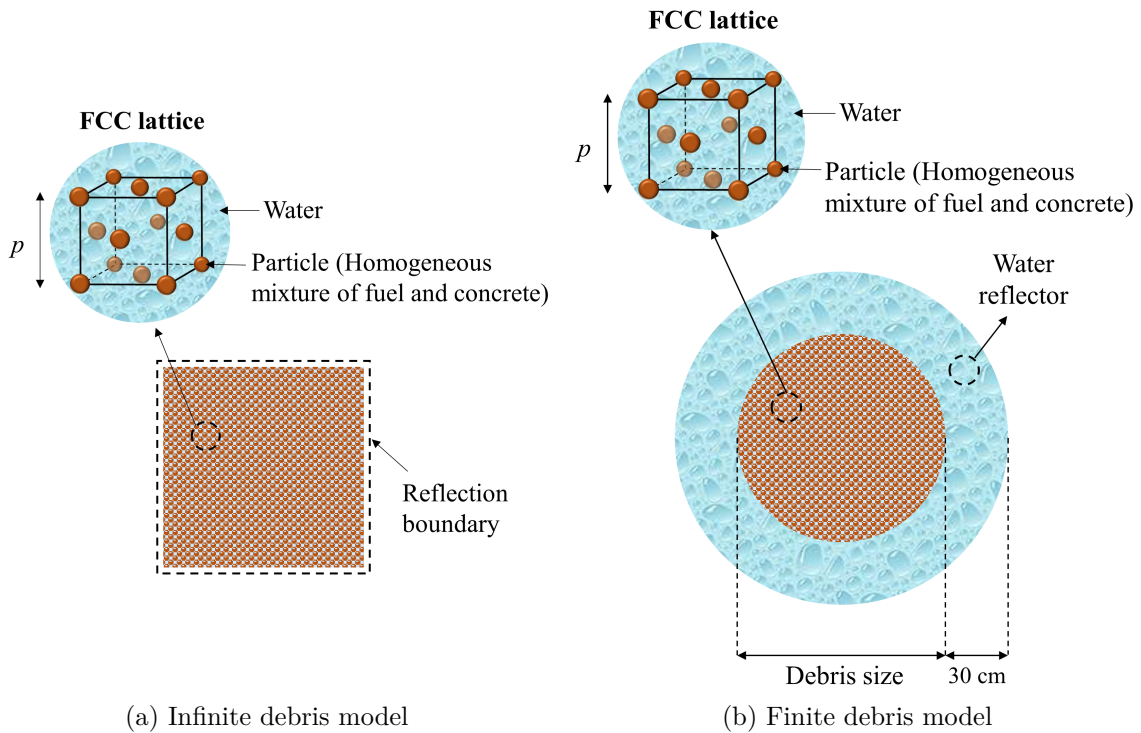
Figure 5.1: Debris bed models

The debris was modeled as a heterogeneous system of MCCI product particles submerged in water and spatially arranged in a FCC lattice. The particles are spheres with a 10.7 mm diameter, which is the equivalent size of a real fuel pellet. The pitch p of the FCC unit cell was used to vary the porosity of the debris. Porosities lower than 0.26 (highest density packing) were modeled by reducing the density of the water.

5.2.2   Debris bed composition

The MCCI product was modeled as a homogeneous mixture of fuel and concrete. For conservative reasons, no additional structural materials were considered.

Spent fuel with 12 GWd/t$_{HM}$ burnup was assumed (see isotopic composition in Appendix B). That is the burnup at which an intact "BWR STEP-3" assembly reaches the highest reactivity under normal operation.

The volume fraction of concrete inside the debris and the quantity of bound water remaining inside the concrete were widely varied. Table 5.1 shows the concrete composition used for the calculations in this study.

5.2.3   Coolant composition

Light water was used as coolant/moderator. Room temperature and standard atmospheric pressure were considered for all the calculations of this study. No void fraction was considered. Thus, the density of the pure water was set to 0.997 g/cm^3. Natural boron was added in every scenario in order to know the required concentration that guarantees the subcritical condition of the debris.

5.3   Criticality calculations

Parametric calculations were performed with the debris bed models described before to analyze the effects of concrete on the criticality. Five parameters were considered: concrete amount, bound water remaining in concrete, porosity, debris size, and water boration. They were varied widely in order to cover any possible scenario. The parameters, ranges of variation, and boundary values are summarized in Table 5.2.

Table 5.2: Parameter and ranges for the criticality calculations

Parameter	Range	Boundary value
Concrete amount	0 - 90 vol%	N/A
Bound water in concrete	0 - 100%	100%
Porosity	0.05 - 0.9	Optimal porosity
Debris size	10 - 300 cm	Infinite
Water boration	0 - 2600 ppm B	0

Table 5.3 sums up the parametric calculations performed for this study.

MCNP6.1 code [31] and ENDF/B-VII.1 [13] cross section libraries were used to perform the criticality calculations. The standard deviations of the estimated the neutron multiplication factors were always kept below the 0.1%. For that, a neutron source of

Table 5.3: Criticality calculations matrix

Calc. Set	Concrete		Porosity [-]	Debris size [cm]	Water boration [ppm B]
	Amount [vol%]	Bound water [%]			
1	0 - 90	0 - 100	0.05 - 0.9	Infinite	0
2	0 - 90	100	Optimal	10 - 300	0
3	0 - 90	100	0	Infinite	0 - 2600

4000 histories per cycle with a total of 300 cycles (100 skipped) was used for every single calculation.

5.4 Results

5.4.1 Criticality of UO$_2$-concrete systems without boron in water

In this section, the evolution of the k_∞ as a function of the debris porosity and concrete content is analyzed. Figure 5.2 plots the results in three different ways: a 3D criticality surface, a contour criticality plot, and a 2D graph with multiple curves.

The first thing to notice is that recriticality is achievable for a wide range of concrete-porosity possible combinations. Secondly, it stands out the displacement of the optimal porosity value as the concrete volume fraction changes. In a debris bed without concrete, the optimal porosity is around 0.75. As the quantity of concrete increases, this optimal porosity value gets smaller. That occurs because the concrete itself is also moderating neutrons. Thus, overall, the results confirm the good moderation capacities of concrete. Systems without concrete cannot become critical at low porosities due to the lack of sufficient moderator; however, the presence of concrete has a significant positive reactivity effect at very low porosities, which means that this structural material can thermalize the neutrons. The reactivity changes caused by the presence of concrete with respect to a system without any concrete are plotted in Figure 5.3. Indeed, the reactivity effect of concrete is remarkable. However, this capacity is largely due to the bound water content inside the concrete. For that reason, the effect of reducing the bound water inside the concrete is analyzed below.
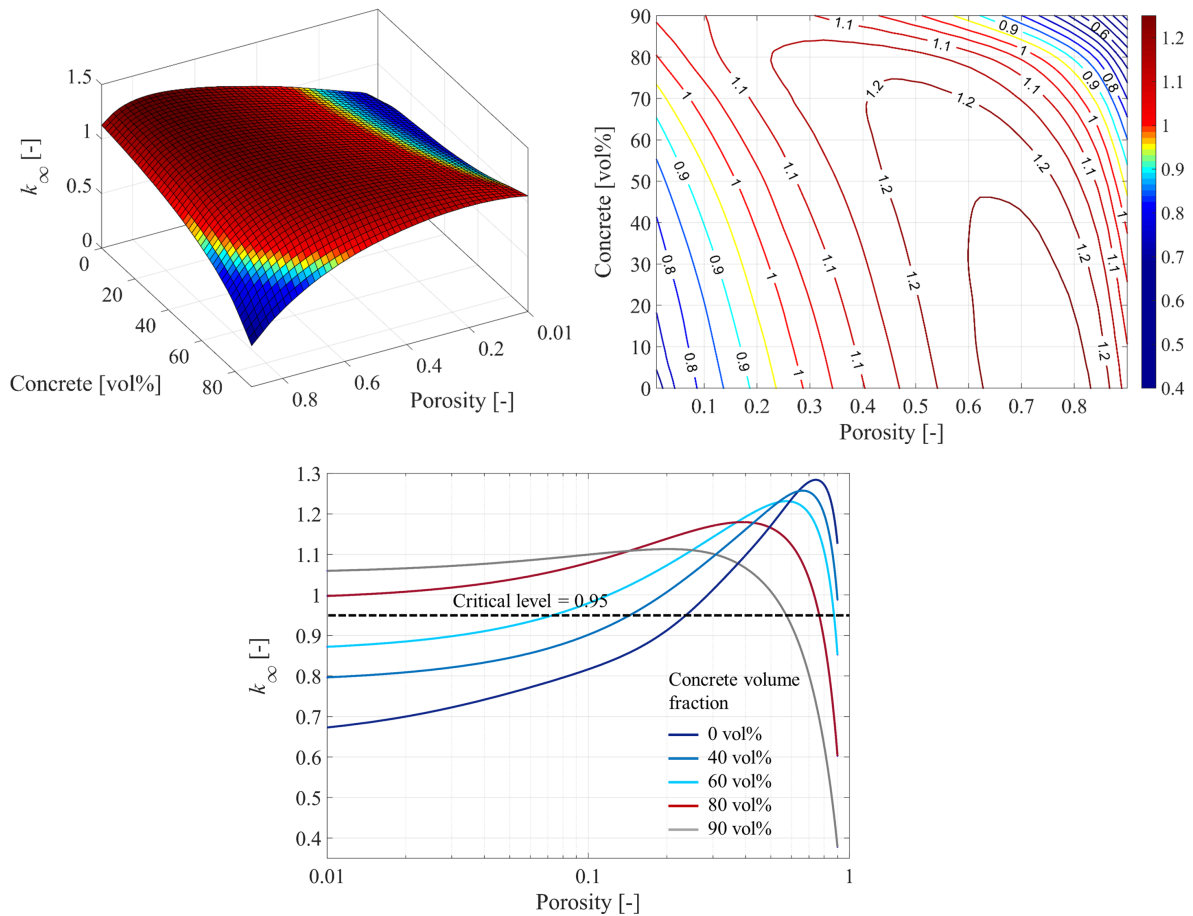
Figure 5.2: k_∞ of UO$_2$-concrete systems submerged in water (spent fuel: 12 GWd/t$_{\text{HM}}$)

5.4.1.1   Influence of bound water in concrete

In this section, the relevance of the bound water on the moderation capacities of concrete is analyzed. The percentage of water in concrete was reduced from 100% (standard concrete composition; no water evaporated during the MCCI process) to 0% (no water remaining inside the concrete; all water evaporated).

Figure 5.4 shows the effect of the bound water on the criticality. More specifically, the graph shows the reactivity changes caused by the bounding water (100% water remaining) in different UO$_2$-concrete systems with respect to those without any bound water inside ($\triangle\rho = \rho_{100\%\,bound\,water} - \rho_{no\,bound\,water}$). As suspected, the reactivity effect is very strong at low porosities but weakens considerably at high porosities, when the moderation is dominated by the coolant water surrounding the debris particles.

Figure 5.5 shows the evolution of the k_∞ as a function of the debris porosity and concrete content but assuming that all the bound water was released during the ablation
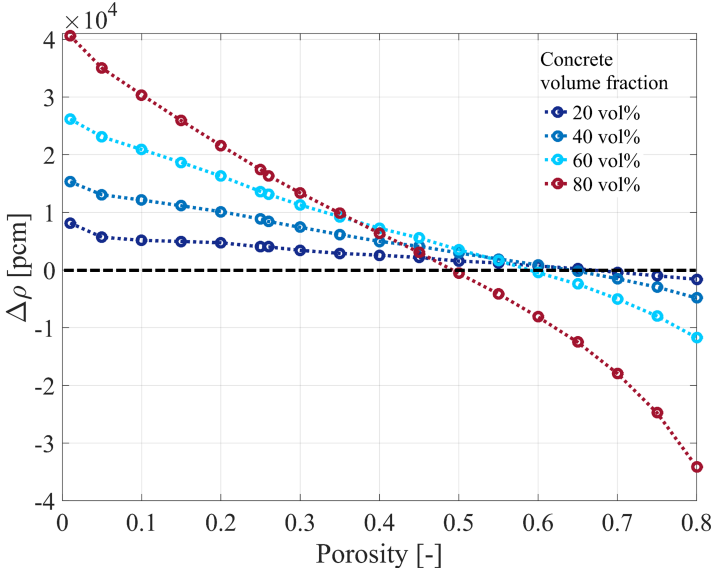
Figure 5.3: Reactivity changes due to the presence of concrete assuming all the bonding water inside (Reference: system without concrete)
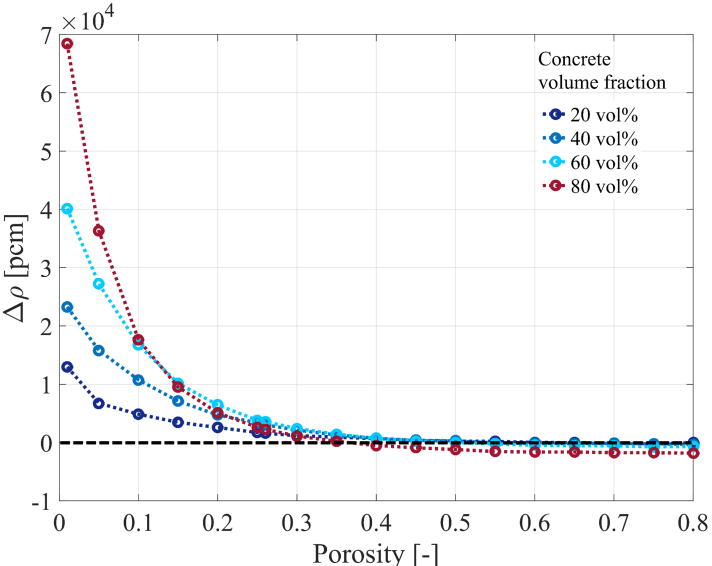
Figure 5.4: Reactivity changes due to the bounding water inside concrete (Reference: systems without water remaining in concrete)
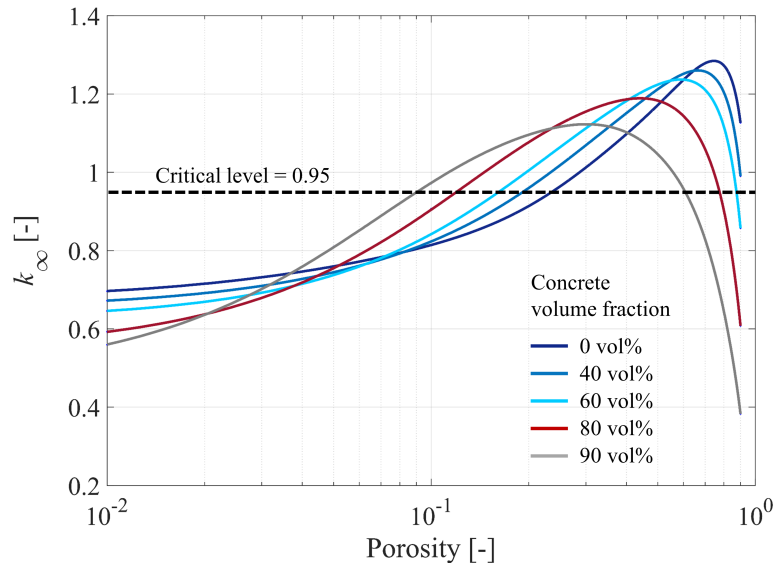
Figure 5.5: k_∞ of UO$_2$-concrete systems submerged in water without bound water inside concrete (spent fuel: 12 GWd/t$_{HM}$)

of concrete in the MCCI process. The absence of water can be clearly observed in the results if they are compared with those plotted in Figure 5.2. Additionally, it is noteworthy that all the systems with porosities between 0.1 and 0.4 and any amount of concrete have a neutron multiplication factor higher than the system containing only fuel. That means that any other concrete component besides water can moderate neutrons, very likely SiO$_2$, a major concrete component that might be a pretty good moderator. However, that supposition should be confirmed and supported by calculations in future works.

Finally, Figure 5.6 shows the reactivity effect caused by the presence of concrete but assuming no bound water remaining. Although considerable, the positive reactivity effect of concrete at low porosities is less pronounced than that shown in Figure 5.3, for which standard concrete was used.

5.4.2 Criticality of UO$_2$-concrete systems with boron in water

Given the high recriticality potential of the systems studied before, the concentration of boron in the cooling water that would ensure the subcriticality was calculated as a function of the concrete volume fraction. Only the worst-case scenarios were considered in these calculations, i.e., systems with optimal moderation conditions (optimal porosity) and concrete with all bound water inside. Figure 5.7 illustrates the results in two different representations: a 3D criticality surface and a contour criticality plot.
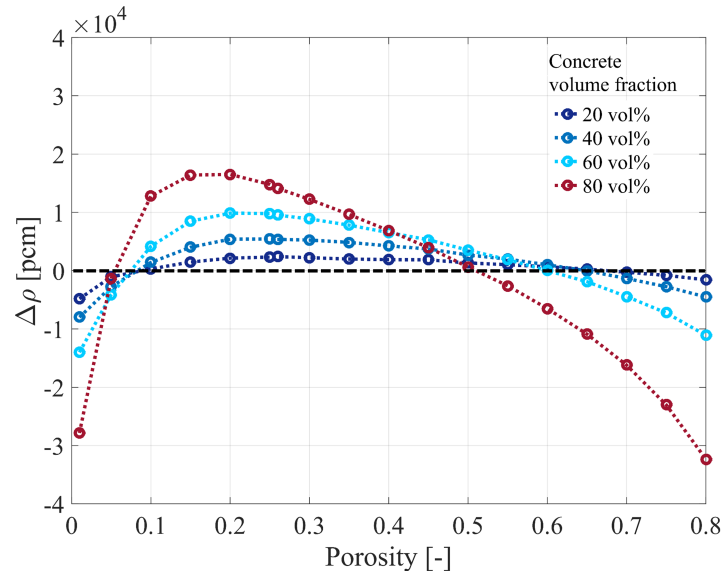
Figure 5.6: Reactivity changes due to the presence of concrete assuming no bonding water inside (Reference: system without concrete)
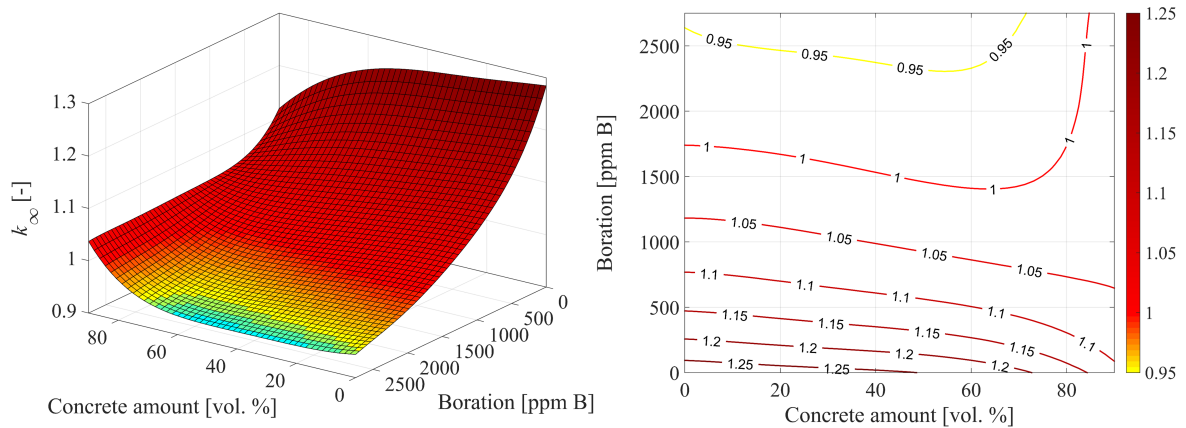
Figure 5.7: k_∞ of UO$_2$-concrete systems submerged in borated water (spent fuel: 12 GWd/t$_{HM}$)
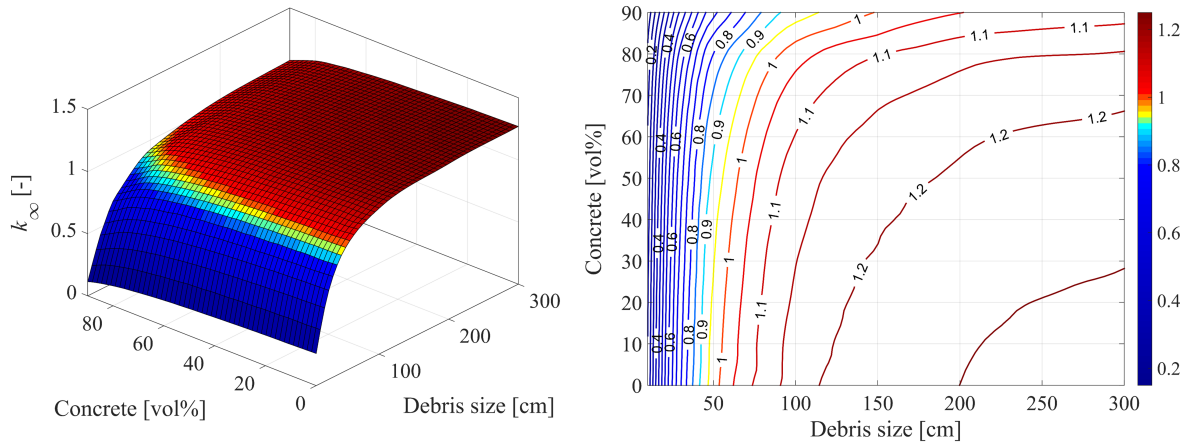
Figure 5.8: Evolution of k_∞ in UO_2-concrete systems depending on the debris size (spent fuel: 12 GWd/t_{HM})

The contour line $k_\infty = 0.95$ indicates the minimum boration required to prevent recriticality depending on the concrete amount. It is remarkable how the quantity of boron necessary to keep the debris subcritical raises drastically at high concrete volume fractions. That occurs in systems with very high concrete content since the maximum k_∞, as seen before, is reached for very low porosities. In such systems, the presence of water is minimal, and consequently, preventing the criticality with soluble boron becomes a very ineffective measure[1]. For these cases, alternative ways to prevent criticality, e.g., through insoluble neutron absorbers, need to be further investigated.

5.4.3 SFML of UO_2-concrete systems

The minimum debris size to reach criticality was calculated depending on the concrete content (see Figure 5.8). Once again, the optimal porosity and concrete with 100% bound water were always considered, i.e., optimal moderation conditions.

The critical size increases slightly as the concrete amount gets higher. This increase is very smooth for low concrete volume fractions and becomes more pronounced for debris beds with large concrete content. Such effect would be even more marked in case of dealing with masses instead of sizes. However, it was preferred to work with sizes, due to their relevance for the design of canisters, casks, or other debris transport devices that are employed during the debris removal and defueling activities. As an example, the safe fuel size limit for a debris without concrete is 45 cm, which corresponds to only 124

---

[1]The maximum solubility of boric acid in water is about 12000 ppm of B

kg. For a debris with 90% of concrete in volume, this value is 120 cm or an equivalent SFML of 658 kg of UO_2.

Recent measurements in the damaged reactors at Fukushima have confirmed that significant amount of debris bed were formed after the SA. The SFML would have been already exceeded, which highlights that the model assumptions are too conservative, because the debris are currently subcritical. A more realistic model was used for the sensitivity analysis performed in Chapter 6.

Chapter 6

Statistical criticality evaluation of debris beds

This chapter proposes a statistical method for the criticality evaluation of Fukushima debris beds. Although the debris characteristics are still uncertain, conservative assumptions may lead to excessive requirements for the criticality control system. The goal of this chapter is to provide a methodology to achieve a more realistic assessment based on the information available, obtained with in-core investigations, experiments, and SA codes. The methodology is based on sampling-based uncertainty and sensitivity analyses described in [42] and consists of six main steps:

1. Identification of uncertain parameters $\boldsymbol{X} = (x_1, x_2, .., x_{nX})$.

2. Definition of distributions $D_1, D_2, .., D_{nX}$ that characterize the epistemic uncertainty of the selected parameters.

3. Generation of parameter samples according with the previous distributions and possible correlations between the selected parameters: $\boldsymbol{x}_1$, $\boldsymbol{x}_2$, ..., $\boldsymbol{x}_{nS}$.

4. Propagation of samples through the numerical model to obtain $k_i(\boldsymbol{x}_i)$, $i = 1, 2, .., nS$

5. Presentation of uncertainty analysis results

6. Presentation of sensitivity analysis results

Figure 6.1 illustrates this methodology. Each step of the process will be explained more in detail throughout the chapter and will be applied to a practical case: the statistical evaluation of the debris bed at Fukushima Unit 1.
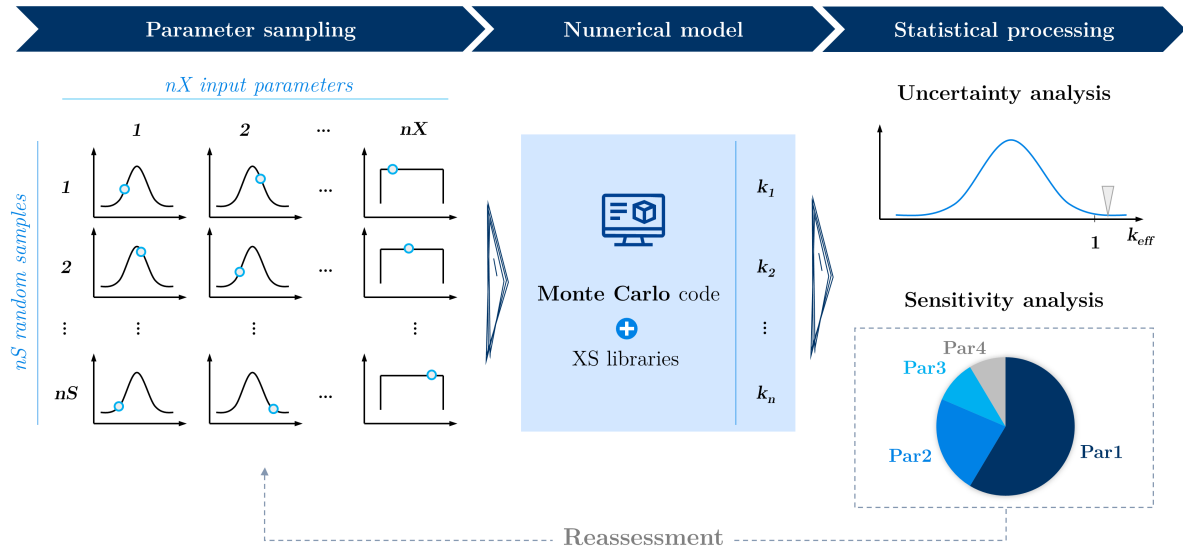
Figure 6.1: Scheme of the statistical evaluation method

The software tool SUSA (Software for Uncertainty and Sensitivity Analyses) [57] developed by the GRS was used to perform the statistical evaluation. This tool follows the propagation of input errors approach, also known as the GRS method [29], and it provides a choice of statistical tools to be applied during the uncertainty and sensitivity analysis.

Case study: "Criticality evaluation of Fukushima Unit 1 debris bed"

Ex-vessel debris bed model

Since the situation inside the damaged reactors is still very uncertain, a very general model of ex-vessel debris beds containing MCCI products was used to perform the statistical criticality evaluation (see Figure 6.2).

Geometry

The debris is represented as a two-layered cylindrical structure consisting of a particulate debris bed over an ingot debris bed submerged in water and surrounded by concrete. This configuration is based on the results of the COTELS project, where the structure of solidified debris in MCCI was investigated [127]. The ingot debris observed in the
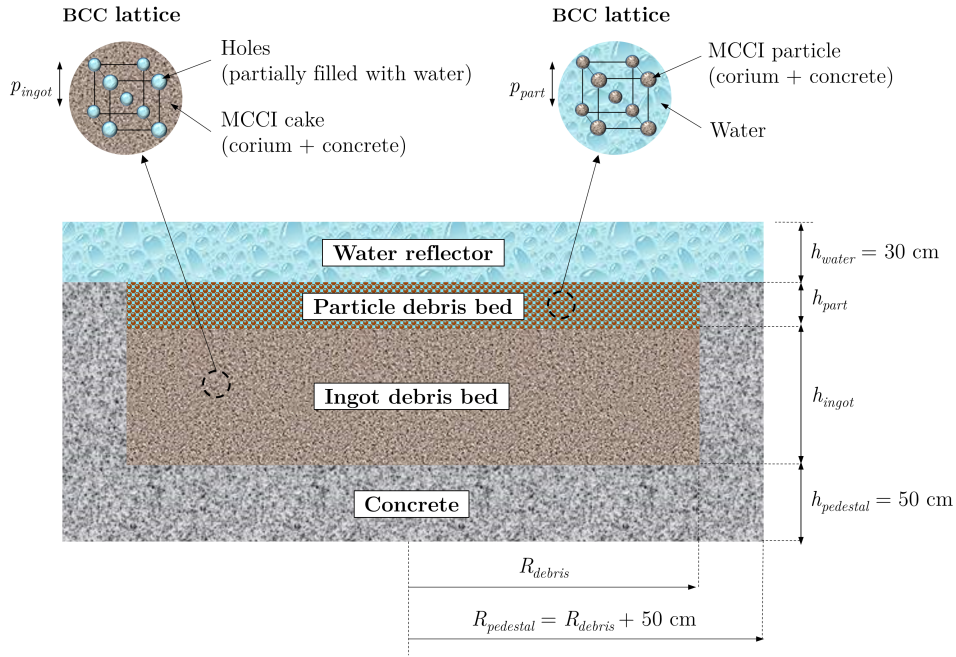
Figure 6.2: MCCI debris bed model

experiments was a highly cracked monolithic debris with many small cavities as well as crevices and channels penetrating from the bottom to the top surface, through which decomposition gases were released. The debris particles on top of the crust, which may be formed by melt eruptions, represented between 20-80% of the total debris mass with particle sizes from about 100 μm to 1 cm.

The main elements and geometric parameters of the ex-vessel debris bed model are described below:

- Lower ingot debris bed with radius R_{debris} and height h_{ingot}. The small holes inside the "cake" are represented as spheres of diameter d_{holes} regularly distributed in a BCC lattice of porosity ε_{ingot}. The holes are filled partially with water:

$$Fill = \frac{V_{filled\,holes}}{V_{holes}} \cdot 100 \qquad (6.1)$$

where $V_{,holes}$ is the total volume of holes in the ingot debris, and $V_{filled\,holes}$ is the volume of those filled with water.

- Upper particulate debris bed with radius R_{debris} and height h_{part}. The particles are spheres of diameter d_{part} regularly distributed in a BCC lattice of porosity ε_{part} and submerged in water.

- Water reflector of effectively infinite thickness $h_{water} = 30\,cm$ covering the debris.

- Concrete of thickness $h_{pedestal} = 50\,cm$ surrounding the debris.

The main component of the debris bed is the MCCI product, which is distributed between the particulate and ingot debris:

$$m_{MCCI} = m_{MCCI,part} + m_{MCCI,ingot} \qquad (6.2)$$

$$w_{part} = \frac{m_{MCCI,part}}{m_{MCCI}} \cdot 100 \qquad (6.3)$$

where w_{part} is the mass ratio of debris in particulate form, m_{MCCI} is the total mass of MCCI product, $m_{MCCI,part}$ is the mass of MCCI product in form of particulate debris, and $m_{MCCI,ingot}$ is the mass of MCCI product in form of ingot debris.

MCCI product composition

The MCCI product was modeled as a homogeneous mixture of corium and concrete:

$$m_{MCCI} = m_{corium} + m_{concrete} \qquad (6.4)$$

where m_{corium} is the total mass of corium released in the cavity and $m_{concrete}$ is the mass of ablated concrete that was incorporated into the melt.

The total mass of corium m_{corium} depends on the initial reactor core inventory m_{inv} and the meltdown grade *Melt*, i.e., the percentage of the core that melted down and was relocated in the reactor cavity:

$$Melt = \frac{m_{corium}}{m_{inv}} \cdot 100 \qquad (6.5)$$

The quantity of concrete in the mixture was managed through the erosion factor f_e, which was defined as the concrete volume fraction in the MCCI composite:

$$f_e = \frac{V_{concrete}}{V_{MCCI}} \cdot 100 = \frac{\rho_{MCCI} \cdot m_{concrete}}{\rho_{concrete} \cdot m_{MCCI}} \cdot 100 \qquad (6.6)$$

where $V_{concrete}$ and $\rho_{concrete}$ are the volume and density of ablated concrete respectively. Similarly, V_{MCCI} and ρ_{MCCI} are the volume and density of the MCCI product.

Corium composition During this analysis, "corium" refers only to the melted core material before MCCI, i.e., mainly fuel (UO_2) and structural materials (Zr, ZrO_2, steel,

and B$_4$C). Additionally, a small quantity of neutron poison (Gd) is also expected:

$$m_{corium} = m_{UO_2} + m_{Gd} + m_{struct} = m_{UO_2} + m_{Gd} + m_{Zr} + m_{SS} + m_{B_4C} \qquad (6.7)$$

where m_{UO_2} is the mass of fuel, m_{Gd} is the mass of gadolinium, and m_{struct} is the total mass of structural materials, which include Zircaloy from cladding in metallic and oxide form (m_{Zr}), steel from reactor structures and RPV (m_{SS}), and B$_4$C from control rods (m_{B_4C}). The relative quantities of each component can be expressed with the mass ratios:

$$w_{UO2-corium} = \frac{m_{UO_2}}{m_{corium}} \cdot 100 \qquad (6.8)$$

$$w_{Gd-corium} = \frac{m_{Gd}}{m_{corium}} \cdot 100 \qquad (6.9)$$

$$w_{struct-corium} = \frac{m_{struct}}{m_{corium}} \cdot 100 \qquad (6.10)$$

$$w_{Zr-struct} = \frac{m_{Zr}}{m_{struct}} \cdot 100 \qquad (6.11)$$

$$w_{SS-struct} = \frac{m_{SS}}{m_{struct}} \cdot 100 \qquad (6.12)$$

$$w_{B_4C-struct} = \frac{m_{B_4C}}{m_{struct}} \cdot 100 \qquad (6.13)$$

Concrete composition   The bound water remaining inside the concrete was defined as:

$$Bound = \frac{m'_{water}}{m_{water}} \cdot 100 \qquad (6.14)$$

where m_{water} is the mass of H$_2$O inside concrete before MCCI, and m'_{water} is the remaining quantity after the ablation process.

6.1   Identification of uncertain parameters

To achieve a realistic assessment of the criticality, all modeling assumptions, input parameters, and boundary conditions that are potentially important contributors to the

uncertainty of the neutron multiplication factor k_{eff} must be identified.

Based on the debris bed model described before, the uncertain parameters gathered in Table 6.1 were selected for the case study.

6.2 Characterization of uncertainty

The uncertainties under consideration in these analyses derive from a lack of knowledge or limited data regarding the debris characteristics. The definition of the distributions D_1, D_2, .., D_{nX} is the most important part of a sampling-based uncertainty and sensitivity analysis because these will determine both the uncertainty in the neutron multiplication factor k and its sensitivity to the parameters considered. The distributions are probability density functions typically determined by expert judgment and ideally defined by quantiles (e.g., 0.0, 0.1, 0.25, ..., 0.9, 1.0) [42].

In the case of Fukushima debris beds, the available data are so scarce that even experts find it very difficult to define the distributions of uncertain parameters. In cases like this, the strategy to follow is to perform an initial exploratory analysis with rather crude definitions and use the sensitivity analysis to identify the most important parameters, i.e., those parameters with the highest influence on the neutron multiplication factor. That will allow focusing future resources and research on accumulate knowledge of these inputs. Finally, the criticality will be reassessed with the improved distributions D'_1, D'_2, .., D'_{nX}, and more accurate results will be obtained.

For this first exploratory analysis, in the absence of more accurate data, the state of knowledge about the uncertain parameter was defined by uniform probability distributions, i.e., each value between minimum and maximum is equally likely. Table 6.1 collects the considered ranges, whose election is justified below.

Parameter 1: meltdown grade

Best estimate calculations made within the OECD/NEA BSAF project predicted large damage at the core region of Unit 1, failure of RPV, and large relocation of the corium in the pedestal floor [91]. Similarly, the accident progression analysis and sensitivity analysis conducted by IRID with MAAP and SAMSON codes concluded that most of the debris (~ 95% in Unit 1) is expected to be accumulated at the pedestal floor [47][79]. Muon tomographies have also estimated that almost no fuel remains in the core [113].

Based on the aforementioned results, a meltdown grade between 80 and 100% was assumed for the statistical analysis.

Table 6.1: Uncertain parameters

Id	Parameter	Description	Unit	Range	Reference
1	$\boldsymbol{Melt}$	Meltdown grade of the damaged reactor	%	80-100	BE calculations
2	$\boldsymbol{w_{UO_2-corium}}$	Mass ratio of UO_2 in corium	wt%	45-55	BE calculations
3	$\boldsymbol{w_{Gd-corium}}$	Mass ratio of Gd in corium	wt%	0-0.004	Conservative
4	$\boldsymbol{w_{SS-struct}}$	Mass ratio of SS in structural materials	wt%	35-60	BE calculations
5	$\boldsymbol{w_{B_4C-struct}}$	Mass ratio of B_4C in structural materials	wt%	0-0.5	Conservative
6	$\boldsymbol{R_{debris}}$	Debris bed radius	m	3-6	BE calculations
7	$\boldsymbol{f_e}$	Erosion factor	vol%	0-65	BE calculations
8	$\boldsymbol{Bound}$	Bound water remaining in concrete	%	0-5	Conservative
9	$\boldsymbol{\varepsilon_{ingot}}$	Porosity of ingot debris	-	0-0.3	Experiments
10	$\boldsymbol{d_{holes}}$	Size of holes in ingot debris	mm	1-15	Experiments
11	$\boldsymbol{Fill}$	Water fill ratio of holes	%	30-100	-
12	$\boldsymbol{\varepsilon_{part}}$	Porosity of particle debris	-	0.35-0.6	Experiments
13	$\boldsymbol{d_{part}}$	Size of particles in particle debris	mm	1-10	Experiments
14	$\boldsymbol{w_{part}}$	Percentage of debris bed in particle form	wt%	0-50	BE calculations

BE: Best Estimate

Parameters 2 to 5: corium composition

Many research teams estimated the composition of the corium in Fukushima Unit 1 after the accident. Table 6.2 collects the results from VTT's MELCOR calculations [104], OECD/NEA BSAF project [91], and the comprehensive assessment of reactor conditions made by IRID with SAMPSON/MAAP codes [47][79]. The last column contains the ranges of values selected for the exploratory sensitivity analysis.

Table 6.2: Estimations of corium composition in Fukushima Unit 1

Corium materials	MELCOR [104] (ton)	(%)	BSAF [91] (%)	SAMPSON/MAAP [47][79] (ton)	(%)	**Selection (%)**
UO$_2$	77.06	47.0	50-55	76	29-55 [51]	45-55
Struct. mat.	86.82	53.0	45-50	62-115 [73]	45-71 [49]	45-55
(Zr+ZrO$_2$)	(40.42)	(24.7)	(20-25)			(40-65)$^{\text{b}}$
(SS+SSO$_x$)	(45.74)$^{\text{a}}$	(27.9)	(15-30)			(35-60)$^{\text{b}}$
(B$_4$C)	(0.66)	(0.40)	(<1)			(0-0.5)$^{\text{b,c}}$
Total	163.87	100	100	138-191 [149]	100	100

$^{\text{a}}$ 20.5 ton from molten core shroud

$^{\text{b}}$ Percentage only over structural materials

$^{\text{c}}$ Conservative range

[ ]: most probable value

Given the uncertainty about the mixing grade between B$_4$C and fuel in debris beds, it was assumed conservatively that the maximum quantity of B$_4$C in the corium is about half of the initial inventory.

Additionally, the presence of gadolinium in corium was also parameterized. The remaining amount of Gd in Unit 1 at the moment of the accident was estimated to be about 0.004 wt% of the corium based on the initial inventory of a BWR-STEP 3 assembly and the burnup history (< 10 GWd/t exposure duration) [78]. Gd is expected to be closely mixed with fuel; nonetheless, quantities between 0 and the estimated value (0.004 wt%) were conservatively considered for the sensitivity analysis.

Parameter 6: debris radius

The debris radius is mainly determined by the debris bed spreading. Once the molten corium falls into the reactor containment, two scenarios can occur:

- There is no water accumulated on the pedestal floor. Consequently, the fluidity of the melt is high; it spreads easily up to the pedestal wall and then leaks out of the

pedestal to the drywell floor through the slit. The debris will become a flat mass with a large surface area.

- There is water accumulated on the pedestal floor. The corium is lumped together due to the cooling effects of the water, and the spreading is significantly reduced.

MAAP analysis made by TEPCO estimated that the corium spread outside the pedestal, although erosion did not occur outside the PCV [116]. Additionally, Fukushima Unit 1 has two drain sumps at the pedestal, where part of the debris is very likely accumulated in a more compacted form. Later on, enhanced ex-vessel analyses for Fukushima Unit 1 were performed by ORNL (Oak Ridge National Laboratory) and ANL (Argonne National Laboratory) with specialized codes containing more detailed modeling such as MELTSPREAD for melt spreading. Based on the pour conditions, the calculations predicted again that the melt has spread from the pedestal into the drywell and contacted the liner [97].

Taking into account that the pedestal interior wall face of Unit 1 has a 2.5 m radius and the drywell annular region has an external radius of 6.5 m radius, R_{debris} from 3 to 6 m was considered for the sensitivity analysis to cover any possible scenario.

Parameter 7: erosion factor

The ratio of corium and concrete in the MCCI product depends on the volume of ablated concrete. The extent of the MCCI was firstly estimated with MAAP calculations performed by TEPCO [116]. An erosion depth of about 65 cm was estimated in axial and radial directions in each sump pit, which is equivalent to 20-30 tons of concrete incorporated into the melt. Assuming 25 tons of ablated concrete ($\rho_{concrete} = 2300\,kg/m^3$) and 150 tons of corium released in the cavity with a composition 55:29:16 of UO_2:Zr:SS ($\rho_{corium} = 8500\,kg/m^3$) the erosion factor can be calculated as follow:

$$\rho_{MCCI} = \frac{1}{\frac{w_{corium}}{\rho_{corium}} + \frac{w_{concrete}}{\rho_{concrete}}} = \frac{1}{\frac{150\,t/175\,t}{8500\,kg/m^3} + \frac{25\,t/175\,t}{2300\,kg/m^3}} = 6137\,kg/m^3 \qquad (6.15)$$

$$f_e = \frac{V_{concrete}}{V_{MCCI}} \cdot 100 = \frac{\rho_{MCCI} \cdot m_{concrete}}{\rho_{concrete} \cdot m_{MCCI}} \cdot 100 = \frac{6137\,kg/m^3 \cdot 25\,t}{2300\,kg/m^3 \cdot 175\,t} \cdot 100 = 38\% \quad (6.16)$$

The simulations performed by IRID with SAMPSON/MAAP codes estimated a much larger concrete ablation, with up to 47 wt% of concrete in the final MCCI product

[47][79]. In this case, the erosion factor would be:

$$\rho_{MCCI} = \frac{1}{\frac{w_{corium}}{\rho_{corium}} + \frac{w_{concrete}}{\rho_{concrete}}} = \frac{1}{\frac{0.53}{8500\,kg/m^3} + \frac{0.47}{2300\,kg/m^3}} = 3750\,kg/m^3 \qquad (6.17)$$

$$f_e = \frac{V_{concrete}}{V_{MCCI}} \cdot 100 = \frac{\rho_{MCCI} \cdot m_{concrete}}{\rho_{concrete} \cdot m_{MCCI}} \cdot 100 = \frac{3750\,kg/m^3}{2300\,kg/m^3} \cdot 0.47 \cdot 100 = 77\% \quad (6.18)$$

The enhanced ex-vessel calculations performed by ORNL and ANL with CORQHENCH code predicted a maximal ablation depth of about 65 cm in the sump pits, up to 20 cm in the pedestal floor, and up to 10 cm in the drywell [97]. Furthermore, the possibility of damages in the containment building due to MCCI was excluded.

Based on the aforementioned estimations, f_e was considered to take values between 0 (no MCCI) and 65% (large MCCI).

Parameter 8: bound water in concrete

As explained in Chapter 5, the bound water is released as steam during the concrete erosion. Nonetheless, it was conservatively assumed a maximum of 5% of water remaining for the analysis.

Parameters 9 to 11: structure of ingot debris

The structure of the debris beds after MCCI was investigated in COTELS project [127]. Many small cavities with diameters between 1.5 and 15 mm were observed in the ingot debris. This range was used to define the uniform distribution of d_{ingot} for the statistical analysis.

Some of these cavities are connected through crevices and channels and may be filled with water; others are watertight compartments. In the absence of data from real debris or experiments, a water fill ratio from 30 to 100% was assumed.

The porosities were not measured in COTELS tests, but other experiments have observed that values up to 0.3 are representative of ingot debris. Consequently, ε_{ingot} was considered to vary from 0 to 0.3.

Parameters 12-13: structure of particulate debris bed

The structure of the particulate debris bed is characterized in this study by the porosity ε_{part} and particle size d_{part}. As explained in Section 3.1.6.1, based on the packing theory porosities of about 0.4 are expected; however, experiments have demonstrated

that greater porosities are more realistic. Thus, a distribution between 0.35 and 0.6 was considered to characterize ε_{part} in this study.

Particle sizes from some μm to 1-2 cm may be found in debris beds; however, sizes smaller than the standard particle size (10.7 mm) are more representative. Particles with a diameter from 1 to 10 mm were considered for the statistical analysis.

Parameter 14: percentage of debris in particulate form   Long-term MCCI and debris coolability calculations were performed with the specialized code CORQUENCH as part of the enhanced ex-vessel analysis for Fukushima Unit 1 made by ORNL and ANL [97]. Based on the phenomenology predicted by these analyses, the debris should be present as a highly cracked monolithic structure and not in particulate form. In particular, this is due to the very limited eruption activity expected (low-gas-content concrete). Based on this statement, the particulate debris was considered to represent from 0 to 50 wt% of the total debris for the statistical analysis.

6.3   Generation of samples

All uncertain parameters are varied simultaneously according to their distributions and dependencies to generate a number nS of samples.

There are several sampling strategies, e.g., random sampling or Latin hypercube sampling. The Latin hypercube sampling is very popular and recommended when computationally demanding models are being studied because its efficient stratification properties allow very good results with a relatively small sample size [40, 41].

Beyond that, the correlations between the uncertain parameters must be controlled and maintained in the samples generated.

SUSA tool facilitates enormously this step of the process. The user must only define the uncertain distributions and dependencies of the input parameters and SUSA generates the samples following the preferred sampling strategy. The software offers a wide range of possibilities to characterize the dependence information, e.g., association measure, full dependence, conditional distribution, function of parameters, or inequality (see the software manual for detailed information [57]).

For the exploratory analysis of Fukushima Unit 1 debris bed, no dependencies were imposed.

A significant advantage of the GRS method is that the number of calculations or samples needed is independent of the number of uncertain parameters. A prior expert review or screening calculations are not necessary to reduce the number of uncertain

Table 6.3: Minimum number of calculations nS for one-sided statistical tolerance limits.

α \ β	0.9	0.95	0.99
0.9	22	45	230
0.95	29	59	299
0.99	44	90	459
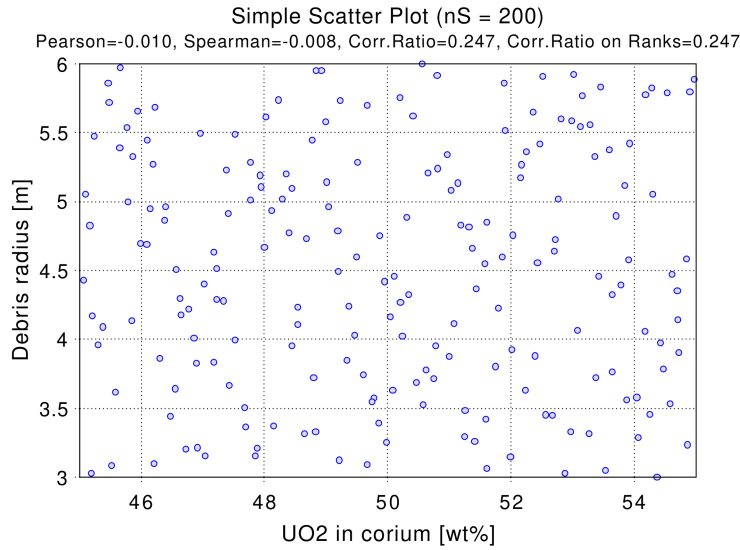
Figure 6.3: Example of Latin hypercube sampling to generate a sample of size $nS = 200$

parameters and computational cost. The required number of runs is given by Wilks' formula [123] and depends on the requested confidence levels of the tolerance limits of the code results, i.e., the neutron multiplication factor. For one-sided tolerance limits, Wilks' formula is:

$$1 - \alpha^{nS} \geq \beta \tag{6.19}$$

where $\beta \times 100$ is the confidence level (%) that the maximum code result will not be exceeded with a probability $\alpha \times 100$ (percentile) of the corresponding output distribution with nS calculations. The minimum number of runs can be found in Table 6.3.

For the exploratory analysis of Unit 1 debris bed a Latin hypercube sample of size $nS = 200$ was generated. Figure 6.3 shows one example.

6.4 Propagation of samples through the calculation model

The sample propagates through the numerical model to obtain the mapping between inputs and outputs: $[\boldsymbol{x}_{i,} k(\boldsymbol{x}_{i,})]$, $i = 1, 2, ..., nS$.

All the calculations were performed with MCNP6.1 [31] and ENDF/B-VII.1 [13, 31] cross section libraries so that the standard deviations of the computed neutron multiplication factors were always kept below 0.1%. For that, a neutron source of 4000 histories per cycle with a total of 300 cycles (100 skipped) was used for every single calculation.

The debris bed model was described in Section 6 (see Figure 6.2). Two sets of calculations were performed with two different fuels: spent fuel with 12 GWd/t$_{\mathrm{HM}}$ and 25.8 GWd/t$_{\mathrm{HM}}$ (averaged burnup of Unit 1 at the moment of the accident). Appendix B shows the corresponding isotopic compositions. Regular siliceous concrete was used for the calculations (see Table 5.1). Light water was used as moderator. Room temperature and standard atmospheric pressure were assumed. Thus, the density of the water was set to 0.997 g/cm^3. No boron was mixed with the coolant water for the sensitivity analysis.

A script was written to automatize the generation of MCNP input files from the samples produced by SUSA. Similarly, another script was committed to extracting the neutron multiplication factor $k(\boldsymbol{x}_{i,})$ from MCNP output files and transferring it to SUSA, where the information was statistically processed to produce the uncertainty and sensitivity results.

6.5 Uncertainty analysis results

Uncertainty analysis refers to the determination of the uncertainty in analysis results that derives from uncertainty in analysis inputs. The results are commonly presented as standard deviation values, density functions, or cumulative distribution functions. All the information necessary is contained in the mapping previously generated $[\boldsymbol{x}_{i,} k(\boldsymbol{x}_{i,})]$, $i = 1, 2, ..., nS$.

The results obtained for the neutron multiplication factor in Fukushima Unit 1 debris bed are shown in Figure 6.4. The probability of recriticality is practically zero. To be more precise, the upper 95% tolerance limit was calculated to be 0.71 for fuel with an averaged burnup of 25.8 GWd/t$_{\mathrm{HM}}$ and 0.77 for a more conservative scenario, in which a burnup of 12 GWd/t$_{\mathrm{HM}}$ is considered (in both cases with confidence level $\beta = 95\%$). The histograms show clearly that k_{eff} is slightly higher for the conservative fuel with most
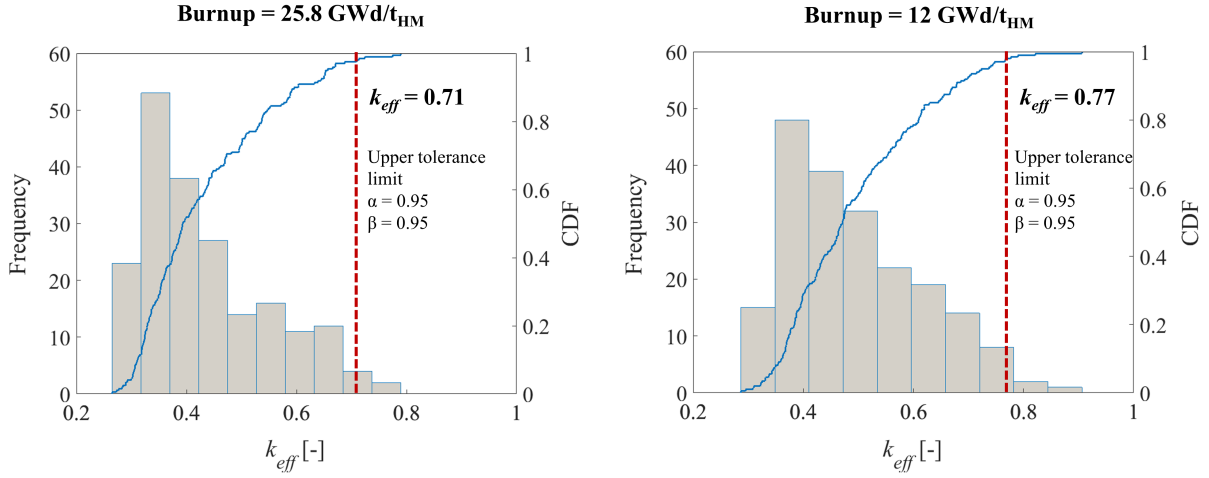
Figure 6.4: Uncertainty analysis results for Fukushima Unit 1 ex-vessel debris bed

of the values between 0.35 and 0.5. These results are aligned with the current situation of the ex-vessel debris bed, which until now have not shown any sign of criticality.

6.6   Sensitivity analysis results

The sensitivity analysis aims to quantify the influence of model input values on the model outcomes. Determining the sensitivity analysis results is not straight forward and the mapping $[\boldsymbol{x}_{i,}\, k(\boldsymbol{x}_{i,})]$, $i = 1, 2, ..., nS$ should be carefully explored to assess the effects of the parameters $\boldsymbol{x}$ on the neutron multiplication factor k [42].

There are many different correlation coefficients that can be calculated to characterize the linear and non-linear dependencies between inputs and output and quantify the sensitivity [42]. In this work, the following correlation coefficients were used:

- **Pearson's ordinary correlation** [90]: the correlation coefficient (CC) measures the strength of the linear relationship between x_j and k :

$$c(x_j, k) = \frac{cov(x_j, k)}{\sigma_{x_j}\sigma_k} = \frac{\frac{1}{nS}\sum\limits_{i=1}^{nS}(x_{ij} - \bar{x}_j)(k_i - \bar{k})}{\left[\frac{1}{nS}\sum\limits_{i=1}^{nS}(x_{ij} - \bar{x}_j)^2\right]^{1/2}\left[\frac{1}{nS}\sum\limits_{i=1}^{nS}(k_i - \bar{k})^2\right]} \qquad (6.20)$$

where the operator *cov* denotes the covarianze, σ is the standard deviation, and

$$\bar{x}_j = \sum_{i=1}^{nS} x_{ij}/nS \tag{6.21}$$

$$\bar{k} = \sum_{i=1}^{nS} k_i/nS \tag{6.22}$$

The CC $c(x_j, y)$ takes values between -1 (perfect negative linear correlation) and 1 (perfect positive linear correlation). The closer the coefficient gets to 1 (in absolute value), the stronger is the dependency. Thus, values close to 0 indicate very weak linear dependencies; however, the two variables may still be depending on each other in a non-linear way.

- **Spearman's rank correlation** [108]: a rank transformation can be used to convert a nonlinear but monotonic correlation into a linear one. The values of x_j and k are replaced by their corresponding ranks, i.e., the smallest value for a variable is assigned a rank 1, the second smallest value is assigned a rank 2, and so on up to the largest value, which is assigned a rank of nS. The rank correlation coefficient (RCC) measures the strength of a monotonic relationship between two variables and is equivalent to the Pearson CC between the rank values Rg_{x_j} and Rg_k of those variables:

$$\rho_S(x_j, k) = \frac{cov(Rg_{x_j}, Rg_k)}{\sigma_{Rg_{x_j}} \sigma_{R_k}} \tag{6.23}$$

where the operator *cov* denotes the covariance, and σ is the standard deviation. RCC will have an absolute value of 1 if the relationship between both parameters is perfectly monotone. A positive value indicates that x_j and k tend to increase or decrease together; a negative value indicates that both variables move in opposite directions.

- **Goodman and Kruskal's rank correlation** [30]: Goodman and Kruskal's gamma is an ordinal measure of association that can be interpreted as the proportion of ranked pairs in agreement:

$$\gamma = \frac{N_c - N_d}{N_c + N_d} \tag{6.24}$$

where N_c is the number of concordant pairs, and N_d is the number of discordant
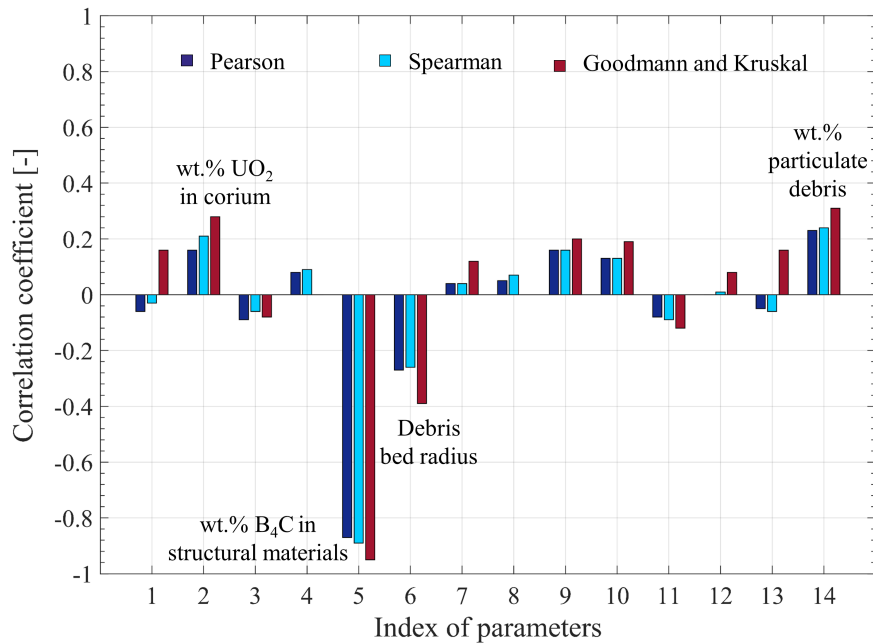
Figure 6.5: Sensitivity analysis results for Fukushima Unit 1 ex-vessel debris bed

pairs[1].

Once again, the coefficient γ varies from -1 (perfect inversion) to 1 (perfect agreement).

Figure 6.5 shows the correlation coefficients for the case study. The most relevant parameter, out of 14 potentially important parameters, is by far the mass ratio of B_4C from control rods in the structural materials. The sign of the correlation coefficient is negative, which means that the input parameter value and the result tend to move in opposite directions. The scatter plot gives a direct visual indication of the sensitivity of the B_4C mass ratio within the structural materials (see Figure 6.6). The great impact of B_4C on the criticality of the debris bed makes it necessary to investigate further the possible mixing of B_4C with fuel in the corium. To perform a realistic criticality assessment, samples of the debris should be taken to analyze the presence of B_4C. This will allow reducing the uncertainty of this parameter and, consequently, much more accurate results will be obtained. Additionally, for this study a homogeneous mixture of structural materials and corium was considered. Further modeling alternatives should be investigated in the future, e.g., heterogeneous mixtures or layered debris with separated metallic and oxide zones.

---

[1]In statistics, a concordant pair is a pair of observations, each on two variables, (X_1, Y_1) and (X_2, Y_2), having the property that $sgn(X_2 - X_1) = sgn(Y_2 - Y_1)$

Simple Scatter Plot (n = 200)
Pearson=-0.885, Spearman=-0.907, Corr.Ratio=0.904, Corr.Ratio on Ranks=0.914
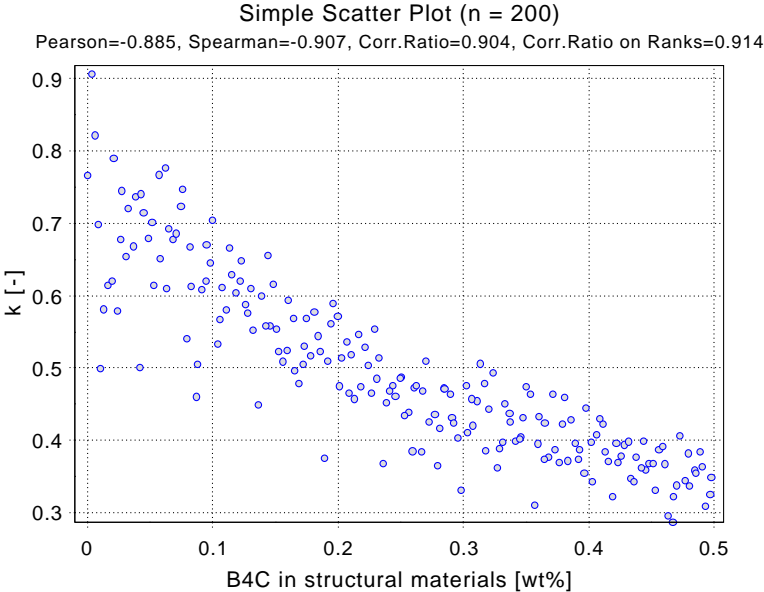
Figure 6.6: Scatter plot of k_{eff} against the amount of B$_4$C in structural materials (wt %)

In addition to the above, other relevant parameters are the mass ratio of UO$_2$ in the corium, the spread of the debris bed (or debris radius), and the percentage of debris in particulate form. Future resources and efforts should also focus on them. Surprisingly, the erosion factor does not appear as one of the most relevant parameters.

Chapter 7

Conclusions and future work

7.1 Summary and conclusions

Controlling debris bed subcriticality is one of the main SA management objectives. Debris beds are complex and unusual nuclear systems linked to high uncertainties. That makes traditional ways of assessing criticality in nuclear reactors inappropriate for them. New criticality safety strategies must be explored, and the current standards must be extended to broader conditions more typical of debris beds.

This thesis aimed to provide a methodology for the numerical assessment of criticality in debris beds that will facilitate future work. At the same time, it was intended to contribute to the international effort underway for developing a criticality map or database for debris beds. The first part of this work focused on finding an appropriate neutronic model for debris beds. Different ways of modeling the debris bed characteristics were proposed, from the most conservative simplifications to more realistic approaches. In the second part, a preliminary conservative evaluation of the criticality situation in Fukushima debris beds was performed, and safety parameter ranges were estimated. The third part was devoted to the effects of concrete on the criticality of ex-vessel debris beds formed after the MCCI. Finally, a statistical method was proposed as an alternative and more realistic way to evaluate the criticality in debris beds. A first exploratory analysis of the debris bed at Fukushima Unit 1 was performed, for which a rough estimation of the k_{eff} probability distribution was obtained. Additionally, the most relevant parameters were identified; based on them, future areas of research and improvement will be proposed in Section 7.2.

The main conclusions and achievements of this work are summarized below.

7.1.1 Debris bed modeling

The great uncertainty in the debris bed characteristics makes modeling one of the biggest challenges in the evaluation of criticality. Good modeling is characterized by a good compromise between the complexity of the model and the accuracy of the results; nonetheless, the lack of knowledge often leads inevitably to certain conservatism.

The first part of this work reviewed the debris bed characteristics with a potential influence on the neutron multiplication factor: debris bed mass, debris composition (fuel enrichment, fuel burnup, and presence of impurities), debris density, debris temperature, moderator/coolant conditions (temperature, void fraction and boration), and debris bed configuration (internal structure and external geometry). Different ways to model each of them were expounded, from the most simple and conservative simplifications to more complex and realistic approaches (see Figure 3.1).

7.1.1.1 Modeling of debris bed internal geometry

Concerning the debris bed internal geometry, the impact of possible simplifications was investigated at three different levels: particle shape, particle size, and particle arrangement. A suitability analysis was performed for three modeling alternatives: the homogeneous model, the regular lattice model, and the random model. Applicability ranges were discussed, and a methodology for calculating the equivalent diameter was presented. The major findings are:

- Debris particles can be conservatively modeled as spheres (negative correlation between k_∞ and the surface-to-volume ratio of the particles).

- The homogeneous model is not conservative, so it should be used carefully. For debris beds with low porosities and/or small particle sizes it can be used introducing a small error (see Figure 3.8).

- The regular lattice model provides very accurate results if an adequate particle size is chosen. Lattices such as SC, BCC, FCC, or similar can be used indistinctly but taking into account the limitations regarding the minimum porosities for each case.

- The random model provides results very similar to those obtained with the regular model for a given particle size.

- None of the mean diameters (i.e., volume mean diameter, surface mean diameter, etc.) can be generally used as equivalent diameter. Furthermore, the same size is

not always appropriate for the whole porosity spectrum.

The results proved that simplifications concerning the shape and arrangement of the particles are less significant than those concerning the size. Consequently, assuming spherical particles arranged regularly is recommended to save modeling and computing time. These models (i.e., regular lattices) can be easily built in Monte Carlo codes, achieving also a high efficiency in the neutron tracking routines.

Finding an adequate particle size (equivalent diameter) for a given debris bed is not easy; it depends on the particle size distribution, which in most of the practical cases will not be known, and may vary with the porosity. According to the sensitivity analysis performed in Chapter 6, the particle size is not among the most relevant parameters in the criticality evaluation of debris beds. Knowing this, and taking into account that FCI experiments have observed that particles sizes smaller than the standard fuel pellets are representative of debris beds, it might be concluded that a regular lattice model with spherical particles of about 10 mm diameter (10.7 mm is the equivalent size of a real pellet) will be suitable in most cases.

7.1.1.2   Modeling of debris bed thermohydraulic parameters

Realistic temperature and density profiles in debris beds were calculated with coupled MCNP-COCOMO calculations to find out the impact of possible simplifications. The power components (decay heat and fission power) determine the feedback of the neutronics into the thermohydraulics and were calculated for Fukushima debris beds at the present time. The following conclusions were extracted:

- Currently ($\approx$10 years after the accident), the decay heat P_d in Fukushima debris beds was calculated to be about 0.1 MW/core. The impact on the temperature and void fraction of water is so small that it is not worth considering.

- The power component P, which is mainly produced by fission reactions of the neutron source present in the debris bed, is negligible ($P << P_d$) for subcritical systems where k_{eff} is not very close to 1.

Consequently, it was concluded that assuming cool conditions and full water density is slightly conservative but adequate for assessing the criticality of Fukushima debris beds.

7.1.2   Criticality calculations

7.1.2.1   Criticality of UO$_2$-concrete systems

International efforts are underway to extend the current criticality standard, mostly based on UO$_2$-water systems, to broader conditions more typical of debris beds, e.g., UO$_2$-steel or UO$_2$-concrete composites. Recent studies warned about the good moderation capacities of concrete, which may pose a safety risk for ex-vessel debris beds formed after the MCCI. This work has expanded the knowledge gained so far, contributing more realistic calculations in which the concrete had lost the bound water during the ablation process.

It was found that systems without concrete cannot become critical at low porosities due to the lack of sufficient moderator; however, the presence of concrete has a significant positive reactivity effect at very low porosities. These effects decrease if no bound water is considered but they do not disappear. That means that not only the bound water is capable of thermalizing neutrons but also the SiO$_2$, a major component of concrete. Consequently, MCCI products should be treated carefully in the criticality analyses. In contrast to other structural materials (e.g., Zircaloy or steel), the presence of concrete cannot be conservatively neglected.

7.1.2.2   Criticality in Fukushima debris beds

Conservative calculations   A great number of calculations were performed using a conservative model and conservative boundary conditions to evaluate the criticality situation of Fukushima debris beds. Parameters such as the particle size, debris porosity, fuel composition (enrichment and burnup), debris size, water boration, and concrete amount were considered. The results are expected to be far from reality (very conservative); nonetheless, the objective of this assessment was to delimit safe parameter ranges and outline the criticality maps. The main conclusions are summarized below:

- Dry debris beds, i.e., debris beds not submerged in water, cannot become critical under any conditions.

- Debris beds submerged in water remain subcritical if the porosity is small enough. The porosity limit is 0.24 for debris beds without concrete and 0.1 for debris beds with an amount up to 90 vol% concrete.

- Small debris bed accumulations of less than 124 kg (sphere of 45 cm diameter) are always subcritical.

- 2600 ppm B would guarantee the subcriticality in Fukushima debris beds with up to 70 vol% of concrete under any conditions. Very compacted debris beds with more than 70 vol% concrete must be treated carefully; for such cases, the amount of boron necessary to control the criticality increases drastically and alternative control measures should be investigated.

The previous findings may be useful to define safety requirements and the criticality control strategy during the defueling process once validated.

Statistical calculations As an alternative to the conservative approach traditionally used in criticality safety, a statistical method was proposed to obtain more realistic results. The method consists of a sampling-based uncertainty and sensitivity analysis and uses the software tool SUSA, which follows the propagation of input errors approach (GRS method). A first exploratory assessment was performed for Fukushima Unit 1 debris bed. Given the high uncertainties regarding the debris bed conditions, very rough distributions were used to characterize the input parameters. The objective was to identify the most relevant parameters and, based on that, define lines of research for future work. The following conclusions were extracted from the evaluation:

- The probability of recriticality in the debris bed is extremely low. The upper tolerance limit of k_{eff} is 0.77 ($\alpha = 0.95$; $\beta = 0.95$) for a slightly conservative fuel (spent fuel with 12 GWd/t$_{HM}$ burnup).

- The amount of control rod material (B$_4$C) mixed with fuel is by far the most relevant parameter.

- Other parameters with a significant effect on the criticality are the percentage of fuel in corium, the percentage of debris in particulate form, and the debris bed spreading or debris radius.

The uncertainty analysis results should be treated carefully due to the crude definitions of the input parameters. Nonetheless, the lack of knowledge was overcome with certain conservatism so that it seems very unlikely that a recriticality event will occur in Fukushima, at least as long as the debris maintains its current status, i.e., before starting the defueling activities. The results of the sensitivity analysis will be used to target future resources and improve the current state of knowledge in the relevant areas (debris characterization research).

7.2   Recommendations for future work

The present thesis opens up avenues for future work regarding the debris bed modeling and criticality evaluations.

7.2.1   Debris bed modeling

7.2.1.1   Heterogeneous composition of debris

Recent studies have demonstrated that the mixing ratio of structural materials (e.g., stainless steel) with fuel in the debris bed has a strong negative reactivity effect [72]. Thus, assuming that fuel and structural materials are mixed homogeneously is not conservative and should be taken into account when modeling. On the other hand, if structural materials are not considered, there is a risk of falling into excessive conservatism. Consequently, debris bed models with heterogeneous compositions must be further investigated, e.g., with stochastic tessellations, where the medium is partitioned into a collection of random volumes (fissile and non-fissile) obeying a given mixing statistics [63].

Particular care must be taken when modeling control materials such as B_4C since the presence of a small amount of these neutron absorbers has a decisive influence on the criticality. Besides, experimental research claims that during the process of core meltdown, the oxides and metals would separate so that large portions of uranium would be in the oxide phase, where boron very rarely resides [4]. Such a statement should be confirmed with future analysis, and the criticality characteristics of two-layer (metallic and oxide) models should be investigated.

7.2.1.2   Thermohydraulic conditions soon after the accident

The impact of thermohydraulics on neutronics may be important soon after the accident, i.e., for decay heat values high enough so that the void fraction in the water is significant. Coupled neutronic-thermohydraulic calculations must be performed to assess the criticality in such debris beds and evaluate their behavior. It would be interesting to know until when after the accident the steam generated by the decay heat is high enough to ensure the subcriticality. Likewise, transient calculations would be interesting for the cases described above and for those where k_{eff} is very close to 1.

7.2.1.3   Random geometries

The stochastic capability of MCNP used to generate the random models in Section 3.2 is limited. That consists of random displacements of spheres within a cubical matrix cell; consequently, a completely chaotic arrangement is not achieved. Alternative random arrangements (e.g., stochastic tessellations) should be considered in future works to correctly analyze its impact on the criticality results.

7.2.1.4   Heterogeneous and low porosities

The regular lattice model proposed in Section 3.2 is limited to porosities higher than 0.26 (highest density packing). Although porosities below this value are not common in debris beds, they can exist and should be analyzed correctly. Throughout this work, very compacted debris was modeled by decreasing the density of the water, which has the same effect on k_{eff} as a reduction in the water volume. Alternative solutions should be investigated (e.g., the inverted model with spheres of water distributed in a debris matrix).

Additionally, debris beds may be more compact in the lower area due to the effect of gravity. Such heterogeneous layered porosity may have some impact on the criticality and is also an interesting point to consider in the future.

7.2.2   Criticality calculations

Concerning the criticality calculations in debris beds, two decisive points remain open:

- The development of a comprehensive criticality map or criticality database for debris beds. That is an arduous task with a high workload, which requires a high amount of calculations. It was initiated by JAEA but international collaboration is necessary to succeed.

- The performance of adequate criticality experiments for the validation of the criticality computations. Currently, STACY critical facility is in development in Japan and is expected to start producing results soon.

In the future, conservatism has to be gradually replaced by more realistic evaluations by using statistical methods like the one proposed in this work (see Chapter 6).

The characterization of the debris beds is one of the major research areas nowadays at Fukushima. The results of the preliminary sensitivity analysis performed within this thesis have brought to the fore some parameters whose state of knowledge should be

further investigated: B_4C amount in the corium, UO_2 amount, debris spreading, and percentage of debris bed in particulate form. The criticality in Fukushima debris beds should be reassessed with the improved distributions of these input parameters to obtain a more accurate estimation of the k_{eff}.

Complementary work aimed at investigating the impact of a hypothetical recriticality event and the behavior of the debris with non-stationary calculations is also necessary.

References

[1] Abedi, A., Vosoughi, N., and Ghofrani, M. (2011). An exact MCNP modeling of pebble bed reactors. *World Academy of Science, Engineering and Technology*, 59:959–963.

[2] Agency for Natural Resources and Energy, Ministry of Economy, Trade and Industry (METI) (2018). Important Stories on Decommisioning - Fukushima Daiichi Nuclear Power Station, now and in the future. Technical report, Japan.

[3] American Nuclear Society (2017). ANSI/ANS 8.24-Validation of Neutron Transport Methods for Nuclear Criticality Safety Calculations.

[4] An, S. M., Song, J. H., Kim, J.-Y., Kim, H., and Naitoh, M. (2016). Experimental investigation on molten pool representing corium composition at Fukushima Daiichi nuclear power plant. *Journal of Nuclear Materials*, 478:164–171. Publisher: Elsevier.

[5] Baek, W.-P., Yang, J.-E., Ball, J., Glowa, G., Bisconti, G., Peko, D., Bolshov, L., Burgazzi, L., De Rosa, F., and Conde, J. M. (2017). Safety Research Opportunities Post-Fukushima. Initial Report of the Senior Expert Group. Technical Report NEA-CSNI-R–2016-19, Organisation for Economic Co-Operation and Development.

[6] Bell, G. I. and Glasstone, S. (1970). Nuclear reactor theory. Technical Report TID-25606, US Atomic Energy Commission, Washington, DC (United States).

[7] Bonnet, J.-M., Cranga, M., Vola, D., Marchetto, C., Kissane, M., Robledo, F., Farmer, M. T., Spengler, C., Basu, S., and Atkhen, K. (2017). State-of-the-Art Report on Molten Corium Concrete Interaction and Ex-Vessel Molten Core Coolability. Technical Report NEA–7392, Organisation for Economic Co-Operation and Development.

[8] Bouyer, V., Journeau, C., Haquet, J. F., Piluso, P., Nakayoshi, A., Ikeuchi, H., Washiya, T., and Kitagaki, T. (2019). Large scale vulcano molten core concrete

interaction test considering fukushima daiichi condition. In *9th European Review Meeting on Severe Accident Research (ERMSAR2019)*, Prague, Czech Republic.

[9] Brown, D. A., Chadwick, M. B., Capote, R., Kahler, A. C., Trkov, A., Herman, M. W., Sonzogni, A. A., Danon, Y., Carlson, A. D., and Dunn, M. (2018). ENDF/B-VIII. 0: The 8th major release of the nuclear reaction data library with CIELO-project cross sections, new standards and thermal scattering data. *Nuclear Data Sheets*, 148:1–142. Publisher: Elsevier.

[10] Brown, F. B. (2009). A review of best practices for Monte Carlo criticality calculations. Technical Report LA-UR-09-03136; LA-UR-09-3136, Los Alamos National Lab.(LANL), Los Alamos, NM (United States).

[11] Buck, M. and Pohlner, G. (2016). Ex-vessel debris bed formation and coolability - challenges and chances for severe accident mitigation. volume 2, pages 1217–1226, San Franscisco, USA.

[12] Burwell, M. J., Lerchl, G., Miro, J., Teschendorff, V., and Wolfert, K. (1989). The thermalhydraulic code ATHLET for analysis of PWR and BWR systems. In *Fourth international topical meeting on nuclear reactor thermal-hydraulics (NURETH-4)*, volume 2.

[13] Chadwick, M. B., Herman, M., Obložinskỳ, P., Dunn, M. E., Danon, Y., Kahler, A. C., Smith, D. L., Pritychenko, B., Arbanas, G., and Arcilla, R. (2011). ENDF/B-VII. 1 nuclear data for science and technology: cross sections, covariances, fission product yields and decay data. *Nuclear data sheets*, 112(12):2887–2996. Publisher: Elsevier.

[14] Chatelard, P., Reinke, N., Arndt, S., Belon, S., Cantrel, L., Carenini, L., Chevalier-Jabet, K., Cousin, F., Eckel, J., and Jacq, F. (2014). ASTEC V2 severe accident integral code main features, current V2. 0 modelling status, perspectives. *Nuclear Engineering and Design*, 272:119–135. Publisher: Elsevier.

[15] Cheng, S., Yamano, H., Suzuki, T., Tobita, Y., Nakamura, Y., Zhang, B., Matsumoto, T., and Morita, K. (2013). Characteristics of self-leveling behavior of debris beds in a series of experiments. *Nuclear Engineering and Technology*, 45(3):323–334. Publisher: Elsevier.

[16] Christophe, J., Piluso, P., Correggio, P., Ferry, L., Fritz, G., Haquet, J. F., Monerris, J., Ruggieri, J.-M., Sanchez-Brusset, M., and Parga, C. (2012). Contributions

of the VULCANO experimental programme to the understanding of MCCI phenomena. *Nuclear Engineering and Technology*, 44(3):261–272. Publisher: Korean Nuclear Society.

[17] Clark, H. K. (1981). The American national standard for nuclear criticality safety in operations with fissionable materials outside reactors. *Transactions of the American Nuclear Society*, 39.

[18] Cross Sections Evaluation Working Group (2009). ENDF-6 Formats Manual Data Formats and Procedures for the Evaluated Nuclear Data File ENDF/B-VI and ENDF/B-VII. Technical Report BNL-90365-2009, Brookhaven National Laboratory (BNL) National Nuclear Data Center.

[19] Davison, B. and Sykes, J. B. (1958). *Neutron transport theory.* Clarendon Press, Oxford.

[20] Dean, J. C. and Tayloe, R. W. (2001). *Guide for Validation of Nuclear Criticality Safety Calculational Methodology.* Division of Fuel Cycle Safety and Safeguards, Office of Nuclear Material Safety and Safeguards, US Nuclear Regulatory Commission.

[21] Duderstadt, J. J. and Martin, W. R. (1979). *Transport theory.* John Wiley & Sons.

[22] EC, E. (2019). The European Green Deal. *Annex to the Communication from the Commission to the European Parliament, the European Council, the Council, the European Economic and Social Committee and the Committee of the Regions.*

[23] Electric Power and Research Institute (EPRI) (2013). Use of Modular Accident Analysis Program (MAAP) in Support of Post-Fukushima Applications. Technical Report 3002001785, Palo Alto, CA (United States).

[24] Energy, G. (2019). CO2 status Report. *IEA (International Energy Agency): Paris, France.*

[25] Farmer, M. T., Lomperski, S., Kilsdonk, D. J., and Aeschlimann, R. W. (2010). OECD MCCI-2 Project. Final Report. Technical Report OECD/MCCI-2010-TR07, Argonne National Lab.(ANL), Argonne, IL (United States).

[26] Foit, J. J., Fischer, M., Journeau, C., and Langrock, G. (2014). Experiments on MCCI with oxide and steel. *Annals of Nuclear Energy*, 74:100–109. Publisher: Elsevier.

[27] Frid, W., Höjerup, F., Lindholm, I., Miettinen, J., Nilsson, L., Puska, E. K., and Sjövall, H. (2001). Severe accident recriticality analyses (SARA). *Nuclear engineering and design*, 209(1-3):97–106. ISBN: 0029-5493 Publisher: Elsevier.

[28] Gauntt, R. O., Cole, R. K., Erickson, C. M., Gido, R. G., Gasser, R. D., Rodriguez, S. B., and Young, M. F. (2000). MELCOR computer code manuals. *Sandia National Laboratories, NUREG/CR*, 6119.

[29] Glaeser, H. (2008). GRS method for uncertainty and sensitivity evaluation of code results and applications. *Science and Technology of Nuclear Installations*, 2008.

[30] Goodman, L. A. and Kruskal, W. H. (1979). Measures of association for cross classifications. In *Measures of association for cross classifications*, pages 2–34. Springer, New York, NY.

[31] Goorley, John T., James, Michael R., Booth, Thomas E., Brown, Forrest B., Bull, Jeffrey S., Cox, Lawrence J., Durkee, Joe W. Jr., Elson, Jay S., Fensin, Michael Lorne, Forster, Robert A. III, Hendricks, John S., Hughes, H. Grady III, Johns, Russell C., Kiedrowski, Brian C., Martz, Roger L., Mashnik, Stepan G., McKinney, Gregg W., Pelowitz, Denise B., Prael, Richard E., Sweezy, Jeremy Ed, Waters, Laurie S., Wilcox,Trevor, and Zukaitis, Anthony J. (2013). *Initial MCNP6 Release Overview - MCNP6 version 1.0.* Los Alamos National Laboratory (LA-UR-13-22934).

[32] GPU Nuclear (1984). Reactor Coolant System Criticality Report.

[33] GPU Nuclear (1990). Three Mile Island Nuclear Station Unit II Defueling Completion Report. Technical report.

[34] Greenbaum, A. (1997). *Iterative methods for solving linear systems*, volume 17 of *Frontiers in Applied Mathematics*. Siam.

[35] Gunji, S., Tonoike, K., Izawa, K., and Sono, H. (2017). Study of experimental core configuration of the modified STACY for measurement of criticality characteristics of fuel debris. *Progress in Nuclear Energy*, 101:321–328. Publisher: Elsevier.

[36] Harada, Y., Nakano, M., Hayashi, Y., and Ishii, K. (2017). Criticality control system development for fuel debris removal in Fukushima Daiichi. In *Proceedings of 2017 international congress on advances in nuclear power plants (ICAPP2017)*, Japan.

[37] Harmon II, C. D. (1994). *Criticality calculations with MCNP: A Primer.* PhD thesis, University of New Mexico.

[38] Hassler, L. A., Pettus, W. G., Holman, P. L., Jones, H. M., and Worsham, J. R. (1986). TMI-2 defueling canister reactivity analysis. *Transactions of the American Nuclear Society*, 52.

[39] Hayashi, Y., Umano, T., Arakawa, A., Kimura, R., and Yamaoka, M. (2019). Criticality control technique for Fukushima Daiichi fuel debris - Statistical evaluation of criticality of 1F fuel debris assuming non-uniform positioning of UO2+Gd2O3. In *International Topical Workshop on Fukushima Decommissioning Research (FDR2019)*, volume FDR2019-1093, J-Village, Naraha, Fukushima, Japan.

[40] Helton, J. C. and Davis, F. J. (2002). Illustration of sampling-based methods for uncertainty and sensitivity analysis. *Risk analysis*, 22(3):591–622. Publisher: Wiley Online Library.

[41] Helton, J. C. and Davis, F. J. (2003). Latin hypercube sampling and the propagation of uncertainty in analyses of complex systems. *Reliability Engineering & System Safety*, 81(1):23–69. Publisher: Elsevier.

[42] Helton, J. C., Johnson, J. D., Sallaberry, C. J., and Storlie, C. B. (2006). Survey of sampling-based methods for uncertainty and sensitivity analysis. *Reliability Engineering & System Safety*, 91(10-11):1175–1209. Publisher: Elsevier.

[43] Hofmann, P. (1999). Current knowledge on core degradation phenomena, a review. *Journal of nuclear materials*, 270(1-2):194–211. Publisher: Elsevier.

[44] Hofmann, P., Hagen, S. J., Schanz, G., and Skokan, A. (1989). Reactor core materials interactions at very high temperatures. *Nuclear Technology*, 87(1):327–333. Publisher: Taylor & Francis.

[45] IAEA (2014). Criticality Safety in the Handling of Fissile Material. *IAEA Safety Standard Series*, No. SSG-27.

[46] International Research Institute for Nuclear Decommissioning (IRID) (2018). Annual Research Report 2017. Annual Research Report.

[47] IRID and IAE (2016). Improvement of recognition regarding the internal PCV condition using severe accident progression analysis and actual plant data. Completion report.

[48] Izawa, K., Tonoike, K., Sono, H., and Miyoshi, Y. (2014). Critical experiments for fuel debris using modified STACY. volume JAEA-Conf 2014-003, Kyoto, Japan.

[49] Izawa, K., Uchida, Y., Ohkubo, K., Totsuka, M., Sono, H., and Tonoike, K. (2012). Infinite multiplication factor of low-enriched UO2–concrete system. *Journal of Nuclear Science and Technology*, 49(11):1043–1047.

[50] Jacquemain, D., Cenerino, G., Corenwinder, F., Raimond, E. I., Bentaib, A., Bonneville, H., Clement, B., Cranga, M., Fichot, F., and Koundy, V. (2015). 5.3. Phenomena that could lead to delayed containment failure: Molten Core-Concrete Interaction (MCCI). In *Nuclear power reactor core melt accidents. Current State of Knowledge*, Science and Technology Series, pages 200–221. France.

[51] JAEA (2015). Study on criticality control of fuel debris by Japan Atomic Energy Agency to support Nuclear Regulation Authority of Japan. In *International Cooperation in Nuclear Criticality Safety*, Charlotte, NC, USA.

[52] Jamali, K. (2015). Achieving reasonable conservatism in nuclear safety analyses. *Reliability Engineering & System Safety*, 137:112–119. Publisher: Elsevier.

[53] Karbojian, A., Ma, W., Kudinov, P., and Dinh, T. (2009). A scoping study of debris bed formation in the DEFOR test facility. *Nuclear Engineering and Design*, 239:1653–1659.

[54] Kasada, R., Ha, Y., Higuchi, T., and Sakamoto, K. (2016). Chemical State Mapping of Degraded B 4 C Control Rod Investigated with Soft X-ray Emission Spectrometer in Electron Probe Micro-analysis. *Scientific reports*, 6:25700. Publisher: Nature Publishing Group.

[55] Kim, E., Jung, W. H., Park, J. H., Park, H. S., and Moriyama, K. (2016). Experiments on sedimentation of particles in a water pool with gas inflow. *Nuclear Engineering and Technology*, 48(2):457–469. Publisher: Elsevier.

[56] Kitagaki, T., Ikeuchi, H., Yano, K., Ogino, H., Washiya, T., Haquet, J.-F., Brissonneau, L., Tormos, B., and Piluso, P. (2018). Characterization of the VULCANO test products for fuel debris removal from the Fukushima Daiichi Nuclear Power Plant. *Prog. Nucl. Sci. Technol.,(To be published)*.

[57] Kloos, M. (2015). SUSA -Software for uncertainty and sensitivity analyses, Version 4.0. User's Guide and Tutorial GRS-P-5, Garching, Germany.

[58] Kloos, M. and Cester, F. (2015). Weiterentwicklung des Analysewerkzeugs SUSA für Unsicherheits- und Sensitivitätsanalysen im Rahmen einer fortschrittlichen PSA. Technical Report GRS - 371.

[59] Knief, R. A. (1985). *Nuclear Criticality Safety: Theory and Practice.* American Nuclear Society.

[60] Konovalenko, A., Basso, S., Kudinov, P., and Yakush, S. E. (2016). Experimental investigation of particulate debris spreading in a pool. *Nuclear Engineering and Design*, 297:208–219. Publisher: Elsevier.

[61] Kudinov, P., Karbojian, A., Tran, C.-T., and Villanueva, W. (2013a). Agglomeration and size distribution of debris in DEFOR-A experiments with Bi2O3–WO3 corium simulant melt. *Nuclear Engineering and Design*, 263(Supplement C):284 – 295.

[62] Kudinov, P., Konovalenko, A., Grishchenko, D., Yakush, S., Basso, S., Lubchenko, N., and Karbojian, A. (2013b). Investigation of debris bed formation, spreading and coolability. Technical report, Nordisk Kernesikkerhedsforskning, Denmark.

[63] Larmier, C., Zoia, A., Malvagi, F., Dumonteil, E., and Mazzolo, A. (2018). Neutron multiplication in random media: Reactivity and kinetics parameters. *Annals of Nuclear Energy*, 111:391–406. Publisher: Elsevier.

[64] Leppänen, J. (2015). Serpent a continuous-energy Monte Carlo reactor physics burnup calculation code. *VTT Technical Research Centre of Finland*, 4.

[65] Lewis, E. and Miller, W. (1984). *Computational methods of neutron transport.* John Wiley and Sons, Inc, United States.

[66] Libby, R. A., Tokarz, R. D., Scott, W. B., Wooton, R. O., Denning, R. S., and Tayloe Jr, R. W. (1990). Recriticality in a BWR following a core damage accident. Technical Report NUREG/CR-5653.

[67] Magallon, D. (2006). Characteristics of corium debris bed generated in large-scale fuel-coolant interaction experiments. *Nuclear Engineering and Design*, 236:1998–2009.

[68] Marchuk, G. L. and Lebedev, V. I. (1986). Numerical methods in the theory of neutron transport.

[69] McConn Jr, R. J., Gesh, C. J., Pagh, R. T., Rucker, R. A., and Williams III, R. G. (2011). Compendium of material composition data for radiation transport modeling. Technical Report PNNL-15870 Rev. 1, Pacific Northwest National Lab. (PNNL), Richland, WA (United States), United States.

[70] Miyoshi, Y., Izawa, K., Sono, H., Kida, T., Murazaki, M., Sakon, A., and Tonoike, K. (2015). Present Status of STACY Modification Program and Fundamental Nuclear Properties of Experimental Cores Related to Fuel Debris Criticality. In *Proceedings of International Conference on Nuclear Criticality Safety (ICNC 2015)*, pages 1308–1319, Charlotte, NC.

[71] Mori, T., Nagaya, Y., Ando, H., and Sasaki, M. (2000). Development of statistical geometry model of coated fuel particles for continuous energy Monte Carlo code MVP. Technical Report JAERI-REVIEW–99-031.

[72] Morimoto, Y., Akaike, M., Takeo, S., and Maruyama, H. (2019). Proposal of a statistical evaluation method for the criticality of the Fukushima Daiichi nuclear power plants. *Nuclear Technology*, 205(12):1652–1660. Publisher: Taylor & Francis.

[73] Mosteller, R. D., Brown, F. B., and Kiedrowski, B. C. (2011). An expanded criticality validation suite for MCNP. LA-UR-11-04170; LA-UR-11-4170, Los Alamos National Lab.(LANL), Los Alamos, NM (United States).

[74] Murray, R. L., Williams, D. S., and Rommel, J. C. (1986). Benchmarking TMI-2 core and canister calculations. *Transactions of the American Nuclear Society*, 52.

[75] Nagasaka, H., Kato, M., Sakaki, I., Cherepnin, Y., Vasilyev, Y., Kolodeshnikov, A., Zhdanov, V., and Zuev, V. (1999). COtelS Project (1): Overview of Project to study FCI and MCCI during a Severe Accident. In *OECD Workshop on Ex-Vessel Debris Coolability*, pages 15–18.

[76] Nagaya, Y., Okumura, K., Mori, T., and Nakagawa, M. (2005). MVP/GMVP 2: general purpose Monte Carlo codes for neutron and photon transport calculations based on continuous energy and multigroup methods. Technical Report JAERI-1348, Japan Atomic Energy Research Inst., Tokyo (Japan).

[77] NEA (Nuclear Energy Agency) (2016). Burn-up Credit Criticality Safety Benchmark Phase III-C. Nuclide Composition and Neutron Multiplication Factor of a Boiling Water Reactor Spent Fuel Assembly for Burn-up Credit and Criticality Control

of Damaged Nuclear Fuel. Technical Report NEA/NSC/R/(2015)6, OECD (Organization for Economic Cooperation and Development).

[78] Nishihara, K., Iwamoto, H., and Suyama, K. (2012). Estimation of fuel compositions in Fukushima-Daiichi nuclear power plant. JAEA-DATA/CODE–2012-018, Japan Atomic Energy Agency, Tokai, Ibaraki (Japan).

[79] Nuclear Damage Compensation and Decommissioning Facilitation Corporation (2016). Technical Strategic Plan 2016 for Decommissioning of the Fukushima Daiichi Nuclear Power Station of Tokyo Electric Power Company Holdings, Inc. Technical report.

[80] Nuclear Safety Standards Commission (Kerntechnischer Ausschuss, K. (2003). Storage and Handling of Fuel Assemblies and Associated Items in Nuclear Power Plants with Light Water Reactors. Technical Report KTA 3602.

[81] OECD Nuclear Energy Agency (2011). *International handbook of evaluated criticality safety benchmark experiments*. 7038. París.

[82] Okumura, K., Kugo, T., Kaneko, K., and Tsuchihashi, K. (2007). SRAC2006: a comprehensive neutronics calculation code system. Technical Report JAEA-DATA/CODE–2007-004, Japan Atomic Energy Agency.

[83] Okuno, H., Naito, Y., and Okuda, Y. (1994). Computation on Fuel Particle Size Capable of Being Regarded as Homogeneous in Nuclear Criticality Safety Analysis. *Journal of Nuclear Science and Technology*, 31(9):986–995.

[84] Okuno, H., Suyama, K., and Ryufuku, S. (2017). A guide to introducing burnup credit, preliminary version (English translation). Technical Report JAEA-REVIEW–2017-010, Japan Atomic Energy Agency.

[85] Okuno, H., Suyama, K., Tonoike, K., Yamane, Y., Uchiyama, G., Yamamoto, T., and Miyoshi, Y. (2009). Second version of data collection part of nuclear criticality safety handbook (Contract Research). Technical report, Japan Atomic Energy Agency.

[86] Ozawa, M., Yabuki, K., Shimada, A., and Ueno, T. (2014). Chemical component analysis of core boring samples at reactor building in Fukushima-1 nuclear power plant. In *Proc. 2014 Annual Meeting of AESJ*, Tokyo, Japan.

[87] Parlett, B. N. (1998). *The symmetric eigenvalue problem*, volume 20 of *Classics in applied mathematics*. siam.

[88] Pavel Kudinov, A. Karbojian, Weimin Ma, and Nam Truc Dinh (2008). An experimental study on debris formation with corium simulant materials. In *International Conference on Advances in Nuclear Power Plants*, volume 170, pages 1191–1199.

[89] Pazukhin, E. M. (1994). Fuel-containing lavas of the Chernobyl NPP fourth block: topography, physicochemical properties, and formation scenario. *Radiochemistry*, 36(2).

[90] Pearson, K. (1895). VII. Note on regression and inheritance in the case of two parents. *Proceedings of the royal society of London*, 58(347-352):240–242. Publisher: The Royal Society London.

[91] Pellegrini, M., Dolganov, K., Herranz, L. E., Bonneville, H., Luxat, D., Sonnenkalb, M., Ishikawa, J., Song, J. H., Gauntt, R. O., and Moguel, L. F. (2016). Benchmark study of the accident at the Fukushima Daiichi NPS: best-estimate case comparison. *Nuclear Technology*, 196(2):198–210.

[92] Petrie, L. M. and Landers, N. F. (1984). KENO Va: an improved Monte Carlo criticality program with supergrouping. Technical Report NUREG/CR–0200-VOL. 2.

[93] Prinja, A. K. and Larsen, E. W. (2010). General principles of neutron transport. In *Handbook of nuclear engineering*.

[94] Pruvost, N. L. and Paxton, H. C. (1996). Nuclear criticality safety guide. Technical Report LA-12808 UC-714, Los Alamos National Laboratory.

[95] Rearden, B. T. and Jessee, M. A. (2016). SCALE code system. Technical Report ORNL/TM–2005/39-V-6.2, Oak Ridge National Laboratory (ORNL).

[96] Rintala, V., Suikkanen, H., Leppänen, J., and Kyrki-Rajamäki, R. (2015). Modeling of realistic pebble bed reactor geometries using the Serpent Monte Carlo code. *Annals of Nuclear Energy*, 77:223 – 230.

[97] Robb, K. R., Francis, M. W., and Farmer, M. T. (2013). Enhanced Ex-Vessel Analysis for Fukushima Daiichi Unit 1: Melt Spreading and Core-Concrete Interaction. Technical Report ORNL/TM-2012/455.

[98] Saad, Y. (1992). *Numerical methods for large eigenvalue problems.* Manchester University Press.

[99] Sakon, A., Izawa, K., Sono, H., Tonoike, K., and Miyoshi, Y. (2015). Representability Evaluation of Fuel Debris Nuclear Characteristics by Heterogeneous Core of STACY. In *International Conference on Nuclear Criticality Safety (ICNC 2015)*, pages 1320–1330, Charlotte, USA.

[100] Santamarina, A., Bernard, D., Blaise, P., Coste, M., Courcelle, A., Huynh, T. D., Jouanne, C., Leconte, P., Litaize, O., and Mengelle, S. (2009). The JEFF-3.1. 1 nuclear data library. *JEFF report*, 22(10.2):2. Publisher: Organisation for Economic Co-operation and Development.

[101] Schmidt, W. (2004). Influence of multidimensionality and interfacial friction on the coolability of fragmented corium. PhD Thesis IKE 2 - 149.

[102] Sehgal, B. R. (2011). *Nuclear safety in light water reactors: Severe accident phenomenology.* Academic Press.

[103] Sevón, T. (2005). Molten core-concrete interactions in nuclear accidents. *Theory and Design of an Experimental Facility. VTT Technical Research Centre of Finland.*

[104] Sevón, T. (2015). A MELCOR model of Fukushima Daiichi Unit 1 accident. *Annals of Nuclear Energy*, 85:1–11. Publisher: Elsevier.

[105] Shibata, K., Iwamoto, O., Nakagawa, T., Iwamoto, N., Ichihara, A., Kunieda, S., Chiba, S., Furutaka, K., Otuka, N., and Ohsawa, T. (2011). JENDL-4.0: a new library for nuclear science and engineering. *Journal of Nuclear Science and Technology*, 48(1):1–30. Publisher: Taylor & Francis.

[106] Sono, H., Kobayashi, F., Ogawa, K., Tonoike, K., Sumiya, M., Miyoshi, Y., Izawa, K., Fukaya, H., Kida, T., and Umeda, M. (2015a). Modification of the STACY Critical Facility for Experimental Study on Fuel Debris Criticality Control. In *Nuclear Back-end and Transmutation Technology for Waste Disposal*, pages 261–270. Springer Open.

[107] Sono, H., Kobayashi, F., Ogawa, K., Tonoike, K., Sumiya, M., Miyoshi, Y., Izawa, K., Fukaya, H., Kida, T., and Umeda, M. (2015b). Modification of the STACY Critical Facility for Experimental Study on Fuel Debris Criticality Control. In *Nuclear Back-end and Transmutation Technology for Waste Disposal*, pages 261–270. Springer Open.

[108] Spearman, C. (1906). Footrule for measuring correlation. *British Journal of Psychology*, 2(1):89. Publisher: Cambridge University Press.

[109] Spencer, B. W., Wang, K., Blomquist, C. A., McUmber, L. M., and Schneider, J. P. (1994). Fragmentation and quench behavior of corium melt streams in water. Technical Report NUREG/CR-6133; ANL-93/32, Nuclear Regulatory Commission, Washington, DC (United States).

[110] Stacey, W. M. (2018). *Nuclear reactor physics.* John Wiley & Sons.

[111] Stratton, W. R. (1987). Review of the State of Criticality of the Three Mile Island Unit 2 Core and Reactor Vessel. Technical Report DOE/NCT-01, TMI-2 Safety Advisory Board GPU-Nuclear, Middletown, PA 17057.

[112] Suyama, K., Mochizuki, H., Takada, T., Ryufuku, S., Okuno, H., Murazaki, M., and Ohkubo, K. (2009). SWAT3. 1-the integrated burnup code system driving continuous energy Monte Carlo codes MVP and MCNP. Technical Report JAEA-Data/Code-2009-002, Japan Atomic Energy Agency, Tokai, Ibaraki (Japan).

[113] TEPCO and IRID (2015). Reactor imaging technology for fuel debris detection by cosmic ray muon: measurement status report in unit 1. Technical report, Tokyo.

[114] TEPCO Holdings (2013). *Evaluation of the Situation of Cores and Containment Vessels of Fukushima Daiichi Nuclear Power Station Units-1 to 3 and Examination into Unsolved Issues in the Accident Progression—Progress Report No. 4.* December.

[115] Thomas, J. T. (1984). Effect of boron and gadolinium concentration on the calculated neutron multiplication factor of U(3)O2 fuel pins in optimum geometries. Technical Report ORNL/CSD/TM–218, Oak Ridge National Lab.

[116] Tokyo Electric Power Company (2011). The Evaluation Status of Reactor Core Damage at Fukushima Daiichi Nuclear Power Station Units 1 to 3.

[117] Tonoike, K. (2015). Criticality Characteristics of MCCI Products Possibly Produced in Reactors of Fukushima Daiichi Nuclear Power Station. In *Proceedings of International Conference on Nuclear Criticality Safety (ICNC 2015)*, pages p.292 – 300, Charlotte, NC, USA.

[118] Tonoike, K. and Yamane, Y. (2015). Development of criticality risk evaluation method for fuel debris in Fukushima-Daiichi NPS. In *Proceedings of International*

Conference on Nuclear Criticality Safety (ICNC 2015), pages 1517–1528, Charlotte, NC, USA.

[119] Tonoike, K., Yamane, Y., Umeda, M., Izawa, K., and Sono, H. (2015). Study on Criticality Control of Fuel Debris by Japan Atomic Energy Agency to Support Nuclear Regulation Authority of Japan. In *Proceedings of International Conference on Nuclear Criticality Safety (ICNC 2015)*, pages 20–27, Charlotte, NC, USA.

[120] Trellue, H. R. (2006). Safety and neutronics: A comparison of MOX vs UO2 fuel. *Progress in Nuclear Energy*, 48(2):135–145. Publisher: Elsevier.

[121] Way, K. and Wigner, E. P. (1948). The rate of decay of fission products. *Physical Review*, 73(11):1318. Publisher: APS.

[122] Westfall, R. M., West, J. T., Whitesides, G. E., and Thomas, J. T. (1979). Criticality analyses of disrupted core models of Three Mile Island Unit 2. Technical Report ORNL/CSD/TM–106, Union Carbide Corp., Oak Ridge, TN (USA). Nuclear Division.

[123] Wilks, S. S. (1941). Determination of sample sizes for setting tolerance limits. *The Annals of Mathematical Statistics*, 12(1):91–96.

[124] Williams, D. S., Rommel, J. C., and Murray, R. L. (1989). An overview of nuclear criticality safety analyses performed to support Three Mile Island unit 2 defueling. *Nuclear Technology*, 87(4):1134–1144. Publisher: Taylor & Francis.

[125] Wilson, W. B., Perry, R. T., Charlton, W. S., Parish, T. A., and Shores, E. F. (2005). Sources: a code for calculating (α, n), spontaneous fission, and delayed neutron sources and spectra. *Radiation protection dosimetry*, 115(1-4):117–121.

[126] Yamada, K., Amri, A., Bevington, L., and Vincze, P. (2016). Post-Fukushima Research and Development Strategies and Priorities for Water Cooled Reactor Technology Development. In *2016 24th International Conference on Nuclear Engineering*. American Society of Mechanical Engineers Digital Collection.

[127] Zhdanov, V., Vasilyev, Y., Kolodeshnikov, A., and Cherepnin, Y. (1999). COtelS Project (4) : Structural Investigation of Solidified Debris in MCCI. In *OECD Workshop on Ex-Vessel Debris Coolability*, Karlsruhe, Germany.

Appendix A

Definition of neutron transport quantities

A.1 Neutron density and flux

Definition A.1. *The population of neutrons is described by the **angular neutron density***

$$N(\boldsymbol{r}, \boldsymbol{\Omega}, E, t)$$

which represents the number of neutrons at position $\boldsymbol{r}$, traveling in direction $\boldsymbol{\Omega}$ with energy E at time t per unit volume per unit energy and per unit solid angle $[n \cdot cm^{-3} \cdot sr^{-1} \cdot MeV^{-1}]$. Thus,

$$N(\boldsymbol{r}, \boldsymbol{\Omega}, E, t) d\boldsymbol{V} d\boldsymbol{\Omega} dE$$

is the number of neutrons in the volume dV around the point $\boldsymbol{r}$ traveling within the cone $d\boldsymbol{\Omega}$ in direction $\boldsymbol{\Omega}$ with energies in (E, E + dE) at time t.

Figure A.1 represents a neutron $_0^1n$ in the volume dV around the point $\boldsymbol{r}$ traveling within the cone $d\boldsymbol{\Omega}$ in direction $\boldsymbol{\Omega}$ with energy $E = \frac{1}{2}mv^2$, where $\boldsymbol{v} = v\boldsymbol{\Omega}$ is the neutron velocity and m is the neutron mass.

Definition A.2. *The integral of the angular neutron density over all directions is the **standard neutron density***

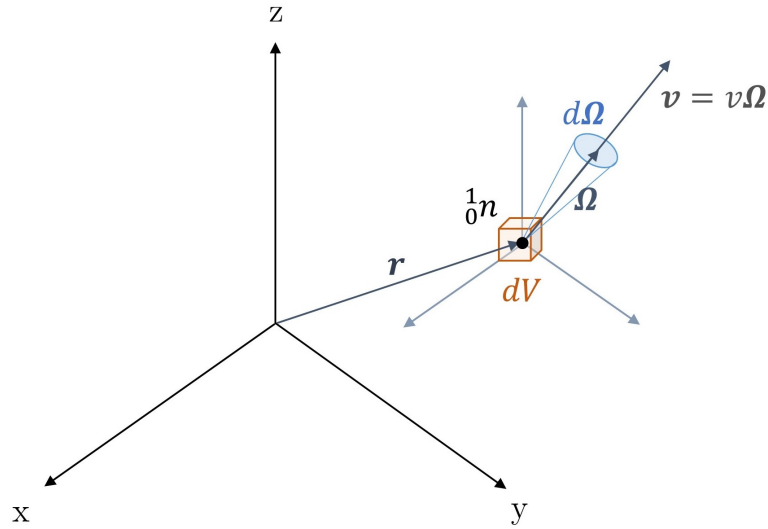$$n(\boldsymbol{r}, E, t) = \int_{4\pi} N(\boldsymbol{r}, \boldsymbol{\Omega}, E, t) d\boldsymbol{\Omega}$$

Figure A.1: The volume element dV and angular element $d\boldsymbol{\Omega}$

which accounts for the number of neutrons at $\boldsymbol{r}$ with energy E at time t per unit volume and per unit energy $[n \cdot cm^{-3} \cdot MeV^{-1}]$.

Definition A.3. *The product of the velocity module v and the angular neutron density is called the* ***angular neutron flux***

$$\psi(\boldsymbol{r}, \boldsymbol{\Omega}, E, t) = v(E) \cdot N(\boldsymbol{r}, \boldsymbol{\Omega}, E, t) = \sqrt{\frac{2E}{m}} \cdot N(\boldsymbol{r}, \boldsymbol{\Omega}, E, t)$$

and represents the number of neutrons per unit area, per unit energy, per unit solid angle per unit time at time t $[n \cdot cm^{-2} \cdot sr^{-1} \cdot MeV^{-1} \cdot s^{-1}]$.

Definition A.4. *The integral over all directions of the angular neutron flux is the* ***scalar neutron flux***

$$\phi(\boldsymbol{r}, E, t) = \int_{4\pi} \psi(\boldsymbol{r}, \boldsymbol{\Omega}, E, t) d\boldsymbol{\Omega} = v(E) \cdot n(\boldsymbol{r}, E, t)$$

which can be interpreted as the number of neutrons with energy E crossing a sphere of unitary radius centered at $\boldsymbol{r}$ per second $[n \cdot cm^{-2} \cdot MeV^{-1} \cdot s^{-1}]$.

A.2   Neutron current

Definition A.5. *The **neutron current** is defined as*

$$\boldsymbol{J}(\boldsymbol{r}, E, t) = \int_{4\pi} \boldsymbol{v}(E) \cdot N(\boldsymbol{r}, \boldsymbol{\Omega}, E, t) d\boldsymbol{\Omega} = v \int_{4\pi} \boldsymbol{\Omega} \cdot N(\boldsymbol{r}, \boldsymbol{\Omega}, E, t) d\boldsymbol{\Omega} = \psi(\boldsymbol{r}, \boldsymbol{\Omega}, E, t) \cdot \boldsymbol{\Omega}$$

and represents the net number of neutrons at position $\boldsymbol{r}$, with energy E and direction $\boldsymbol{\Omega}$ at time t crossing unit area per unit energy and time $[n \cdot cm^{-2} \cdot MeV^{-1} \cdot s^{-1}]$.

A.3   Cross sections

The nuclear cross sections quantify the neutron interaction probability in a material.

Definition A.6. *The **microscopic cross section** is a characteristic area proportional to the probability of interaction between a neutron and a nucleus: the larger the area the more probable the event. These microscopic cross sections depend on the target nucleus properties, the energy of the incident neutron and the temperature of the medium:*

$$\sigma_{i,k}(E, T)$$

where i represents the target nucleus (e.g. ^{235}U, ^{238}U) and k is the type of interaction:

- *$k = t$ (total). Any type of neutron-nucleus interaction.*

- *$k = a$ (absorption). The neutron is absorbed by the nucleus, independently of the outcome. Absorption includes capture and fission.*

- *$k = c$ (radioactive capture). The neutron is absorbed into the nucleus creating a heavier isotope.*

- *$k = f$ (fission). The neutron triggers a fission reaction.*

- *$k = s$ (scattering). The neutron is scattered into another direction and/or energy. The scattering can be elastic or inelastic.*

*Thus, the **total microscopic cross section** can be defined as*

$$\sigma_t = \sigma_a + \sigma_s = \sigma_c + \sigma_f + \sigma_s$$

The units of the microscopic cross section are $[cm^{-2}]$, although usually it is expressed in barns: $1b = 10^{-28}m^2 = 10^{-24}cm^2$.

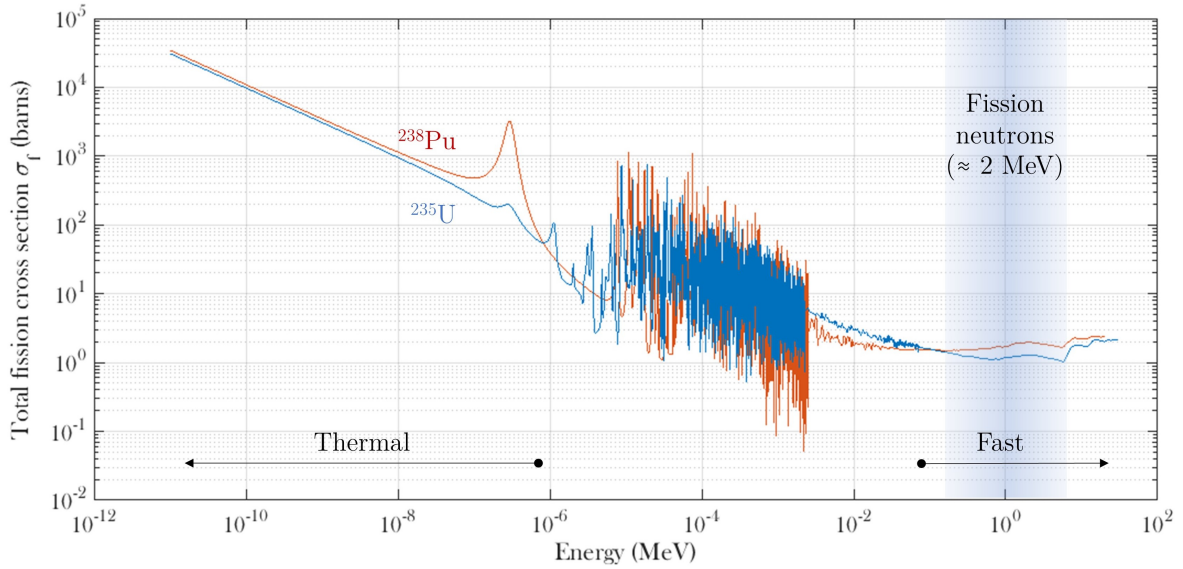Figure A.2: Total fission cross section data of ^{235}U and ^{239}Pu [9]

Definition A.7. *The **macroscopic cross section***

$$\Sigma_{i,k}(\boldsymbol{r}, E) = ND_i(\boldsymbol{r}) \cdot \sigma_{i,k}(E)$$

is the probability of interaction at energy E, per unit length of neutron travel $[cm^{-1}]$. $ND_i = \frac{\rho_i N_A}{A_i}$ is the number density, i.e., the number of nuclei i per unit volume. ρ_i represents the density, A_i is the atomic number and N_A is the Avogadro's number.

The numerical values of the different cross sections are obtained from a combination of experimental measures and predictions of nuclear model calculations. The values are finally tabulated to produce evaluated data sets or cross section libraries. These include the Evaluated Nuclear Data File (ENDF) libraries [13], the Joint Evaluated Fission and Fusion File (JEFF) [100] and the Japanese Evaluated Nuclear Data Libraries (JENDL) [105]. As it is stated in reference [18], the libraries are *"a collection of documented data evaluations stored in a defined computer-readable format that can be used as the main input to nuclear data processing programs"*. As an example, the neutron cross sections for fission of ^{235}U and ^{239}Pu are plotted in Figure A.2 with data from ENDF/B-VIII.0 [9], released in 2018.

Appendix B

Fuel isotopic compositions

This appendix collects the fuel isotopic compositions used for the calculations performed through this thesis.

B.1 Fresh fuel

Table B.1: Isotopic compositions in [atoms/barn/cm] of UO_2 fresh fuel for different enrichments ($\rho_{UO_2} = 10.412 \, g/cm^3$)

Isotope/ Element	Enrichment [wt% ^{235}U]				
	2	3	3.7	4	5
^{235}U	$4.703 \cdot 10^{-4}$	$7.054 \cdot 10^{-4}$	$8.700 \cdot 10^{-4}$	$9.405 \cdot 10^{-4}$	$1.176 \cdot 10^{-3}$
^{238}U	$2.275 \cdot 10^{-2}$	$2.252 \cdot 10^{-2}$	$2.236 \cdot 10^{-2}$	$2.228 \cdot 10^{-2}$	$2.206 \cdot 10^{-2}$
O	$4.645 \cdot 10^{-2}$	$4.645 \cdot 10^{-2}$	$4.646 \cdot 10^{-2}$	$4.646 \cdot 10^{-2}$	$4.646 \cdot 10^{-2}$

B.2 Spent fuel

The nuclides considered for the criticality safety calculations with spent fuel were selected based on the recommendations of "A guide introducing Burnup Credit" by JAEA [84]. For a more realistic evaluation, both actinides and fission products (FPs) were considered:

- **Actinide nuclides**: ^{234}U, ^{235}U, ^{238}U, ^{238}Pu, ^{239}Pu, ^{240}Pu, ^{241}Pu, ^{242}Pu, and ^{241}Am.

- **FP nuclides**: ^{95}Mo, ^{99}Tc, ^{103}Rh, ^{133}Cs, ^{143}Nd, ^{145}Nd, ^{147}Sm, ^{149}Sm, ^{150}Sm, ^{152}Sm, ^{153}Eu, and ^{155}Gd

The following FP were excluded: nuclides with small neutron absorption, nuclides with short half-lives, gaseous or volatile nuclides (Kr, Xe, Br, and I), and semi-volatile nuclides (Rb, Te, Se, Cd, Sb, and Ag).

Considering the importance of the criticality control of damaged fuel at Fukushima Daiichi NPP, the NEA Expert Group on Burnup Credit Criticality (EGBUC) organized in 2012 a international burnup calculation benchmark for 9x9 STEP-3 BWR fuel assemblies [77]. The average isotopic composition of spent nuclear fuel as a fuction of burnup was calculated by 16 different institutes in 9 countries. The objective was to provide necessary data for an adequate criticality safety analysis of the Fukushima damaged reactors.

A constant specific power of 25.3 MW/t_{HM} was assumed. Three cases were evaluated with different cooling times after the burnup: 0, 5, and 15 years. A constant void fraction of 0, 40, or 70% during the burnup was considered. Data for burnups of 12, 20, 30, and 50 GWd/t_{HM} were provided by the participants.

In Table B.2 the averaged isotopic compositions used for the calculations in this thesis are collected. Results corresponding to 40% void fraction and 5 year of cooling were used.

JAEA also estimated the fuel composition in the damaged reactors for different times after the accident (immediately after, 1 hour, 3 hours, ..., up to 20 years) taking into account the burnup history of each unit [78].

The composition in Unit 1 five years after the accident was used for the calculations in this thesis (see Table B.3).

Table B.2: Isotopic compositions of spent fuel for 9x9 STEP-3 BWR fuel assemblies (atoms/barn/cm) [77]

Isotope/ Element	Burnup [GWd/t$_{HM}$]			
	12	20	30	50
^{234}U	$5.85 \cdot 10^{-6}$	$5.30 \cdot 10^{-6}$	$4.66 \cdot 10^{-6}$	$3.55 \cdot 10^{-6}$
^{235}U	$6.19 \cdot 10^{-4}$	$4.74 \cdot 10^{-4}$	$3.18 \cdot 10^{-4}$	$1.15 \cdot 10^{-4}$
^{238}U	$2.13 \cdot 10^{-2}$	$2.12 \cdot 10^{-2}$	$2.11 \cdot 10^{-2}$	$2.07 \cdot 10^{-2}$
^{238}Pu	$2.06 \cdot 10^{-7}$	$7.06 \cdot 10^{-7}$	$1.93 \cdot 10^{-6}$	$6.29 \cdot 10^{-6}$
^{239}Pu	$7.92 \cdot 10^{-5}$	$9.49 \cdot 10^{-5}$	$1.02 \cdot 10^{-4}$	$9.78 \cdot 10^{-5}$
^{240}Pu	$1.39 \cdot 10^{-5}$	$2.65 \cdot 10^{-5}$	$4.11 \cdot 10^{-5}$	$6.24 \cdot 10^{-5}$
^{241}Pu	$4.24 \cdot 10^{-6}$	$9.47 \cdot 10^{-6}$	$1.56 \cdot 10^{-5}$	$2.24 \cdot 10^{-5}$
^{242}Pu	$5.37 \cdot 10^{-7}$	$2.24 \cdot 10^{-6}$	$6.33 \cdot 10^{-6}$	$2.04 \cdot 10^{-5}$
^{241}Am	$1.25 \cdot 10^{-6}$	$2.91 \cdot 10^{-6}$	$4.97 \cdot 10^{-6}$	$7.33 \cdot 10^{-6}$
^{95}Mo	$1.72 \cdot 10^{-5}$	$2.79 \cdot 10^{-5}$	$4.04 \cdot 10^{-5}$	$6.19 \cdot 10^{-5}$
^{99}Tc	$1.69 \cdot 10^{-5}$	$2.76 \cdot 10^{-5}$	$4.01 \cdot 10^{-5}$	$4.01 \cdot 10^{-5}$
^{103}Rh	$9.59 \cdot 10^{-6}$	$9.59 \cdot 10^{-6}$	$2.24 \cdot 10^{-5}$	$3.23 \cdot 10^{-5}$
^{133}Cs	$1.82 \cdot 10^{-5}$	$1.57 \cdot 10^{-5}$	$4.28 \cdot 10^{-5}$	$6.49 \cdot 10^{-5}$
^{143}Nd	$1.46 \cdot 10^{-5}$	$2.23 \cdot 10^{-5}$	$2.96 \cdot 10^{-5}$	$3.59 \cdot 10^{-5}$
^{145}Nd	$1.03 \cdot 10^{-5}$	$1.66 \cdot 10^{-5}$	$2.36 \cdot 10^{-5}$	$3.51 \cdot 10^{-5}$
^{147}Sm	$4.03 \cdot 10^{-6}$	$6.20 \cdot 10^{-6}$	$8.33 \cdot 10^{-6}$	$1.07 \cdot 10^{-5}$
^{149}Sm	$1.05 \cdot 10^{-7}$	$1.03 \cdot 10^{-7}$	$9.86 \cdot 10^{-8}$	$8.83 \cdot 10^{-8}$
^{150}Sm	$3.28 \cdot 10^{-6}$	$5.67 \cdot 10^{-6}$	$8.71 \cdot 10^{-6}$	$1.44 \cdot 10^{-5}$
^{152}Sm	$1.63 \cdot 10^{-6}$	$2.70 \cdot 10^{-6}$	$3.80 \cdot 10^{-6}$	$5.41 \cdot 10^{-6}$
^{153}Eu	$8.87 \cdot 10^{-7}$	$1.84 \cdot 10^{-6}$	$3.24 \cdot 10^{-6}$	$6.09 \cdot 10^{-6}$
^{155}Gd	$1.17 \cdot 10^{-6}$	$8.04 \cdot 10^{-8}$	$1.22 \cdot 10^{-7}$	$2.26 \cdot 10^{-7}$
O	$4.68 \cdot 10^{-2}$	$4.68 \cdot 10^{-2}$	$4.68 \cdot 10^{-2}$	$4.68 \cdot 10^{-2}$

Table B.3: Isotopic compositions of spent fuel in Fukushima damaged reactors (g/core) [78]

Isotope/ Element	25.8 GWd/t$_{\text{HM}}$* Unit 1
^{234}U	$5.11 \cdot 10^2$
^{235}U	$1.11 \cdot 10^6$
^{238}U	$6.53 \cdot 10^7$
^{238}Pu	$7.74 \cdot 10^3$
^{239}Pu	$3.08 \cdot 10^5$
^{240}Pu	$1.05 \cdot 10^5$
^{241}Pu	$4.60 \cdot 10^4$
^{242}Pu	$2.02 \cdot 10^4$
^{241}Am	$1.69 \cdot 10^4$
^{95}Mo	$1.18 \cdot 10^4$
^{99}Tc	$4.28 \cdot 10^4$
^{103}Rh	$2.46 \cdot 10^4$
^{133}Cs	$6.29 \cdot 10^4$
^{143}Nd	$4.58 \cdot 10^4$
^{145}Nd	$3.76 \cdot 10^4$
^{147}Sm	$1.04 \cdot 10^4$
^{149}Sm	$1.68 \cdot 10^2$
^{150}Sm	$1.44 \cdot 10^4$
^{152}Sm	$6.01 \cdot 10^3$
^{153}Eu	$5.87 \cdot 10^3$
^{155}Gd	-
O	$9.28 \cdot 10^6$

* Averaged burnup

Appendix C

Effect of debris bed parameters on the optimal porosity

The optimal porosity is the porosity value at which the moderation conditions of a nuclear system are optimal and, consequently, the neutron multiplication factor reaches a maximum. Assuming optimal porosity is one of the most common boundary conditions in conservative criticality analysis.

The porosity is an especially important parameter for the criticality safety in debris beds because it may change significantly during the defueling activities. The worst-case scenario should be considered to implement appropriate control measures.

The optimal porosity varies depending on the physical conditions of the system. This Appendix collects some calculation results, which show the effect of some parameters (particle size, fuel enrichment, water boration or concrete amount) on the optimal porosity value. These results complement to those presented in Chapter 4 and Chapter 5. The debris bed model and boundary conditions are exactly the same (see Figures 4.1 and 5.1).

C.1   Particle size

Figure C.1 shows the results of the calculation set 1 (see Table 5.3). A slightly negative effect of the particle size on the optimal porosity is appreciated.
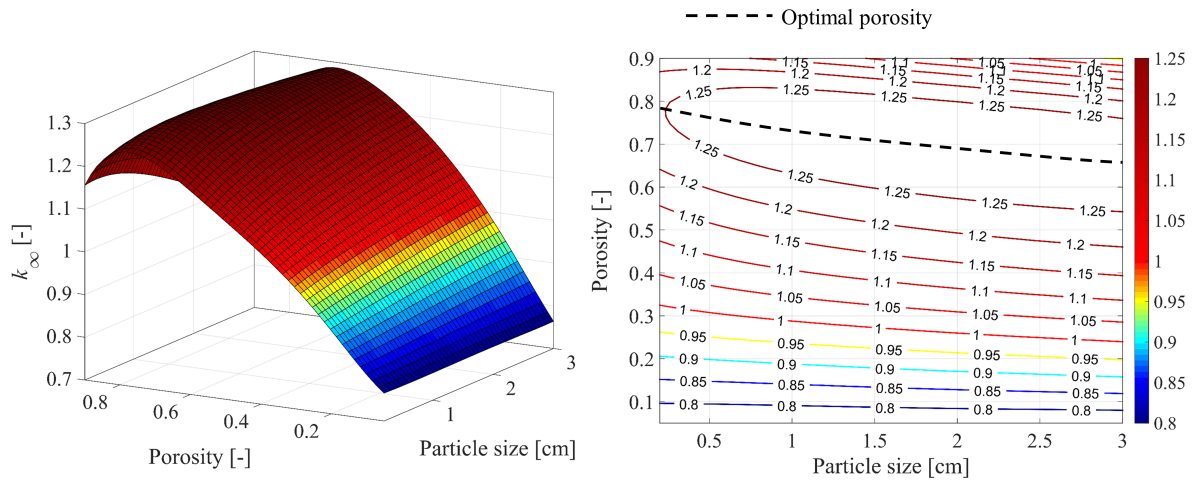
Figure C.1: Effect of particle size on the optimal porosity

C.2   Fuel enrichment

The results of the calculation set 6 (see Table 5.3) are plotted in Figure C.2. As the enrichment increases the porosity necessary to reach optimal moderation gets higher.
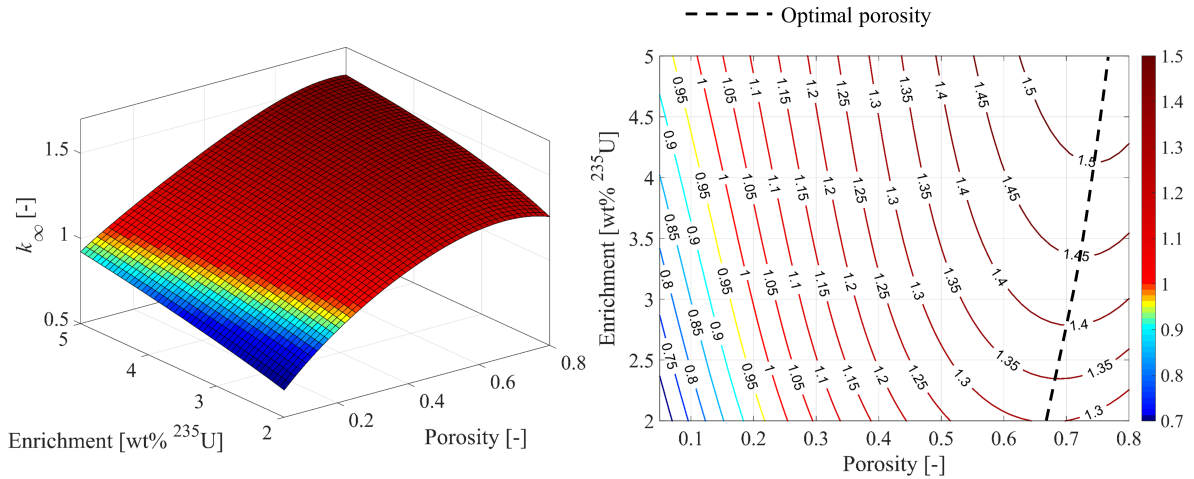

Figure C.2: Effect of fuel enrichment on the optimal porosity

C.3   Water boration

Figure C.3 shows the effect of the water boration on the optimal porosity (calculation set 7, see Table 5.3). The optimal porosity decreases significantly as the boration increases.

This is because a lower porosity in this case not only means less hydrogen atoms to thermalize neutrons but also less B^{10} to absorb them.
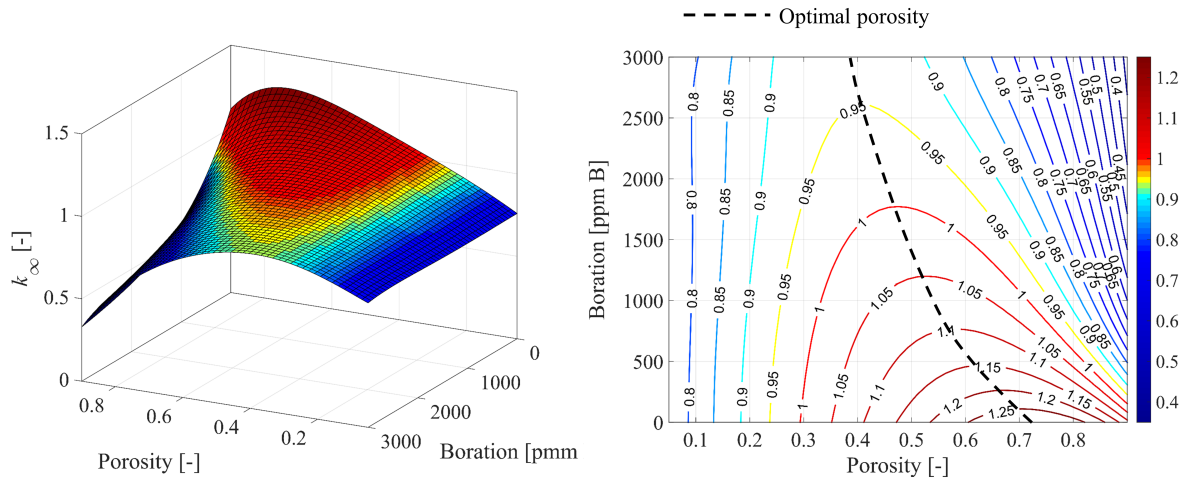

Figure C.3: Effect of water boration on the optimal porosity

C.4 Concrete amount

The presence of concrete in the debris bed (MCCI product) reduces significantly the optimal porosity value. This is due to the combined effect of a reduction of the density of fissile material and the moderation capabilities provided by the concrete itself.
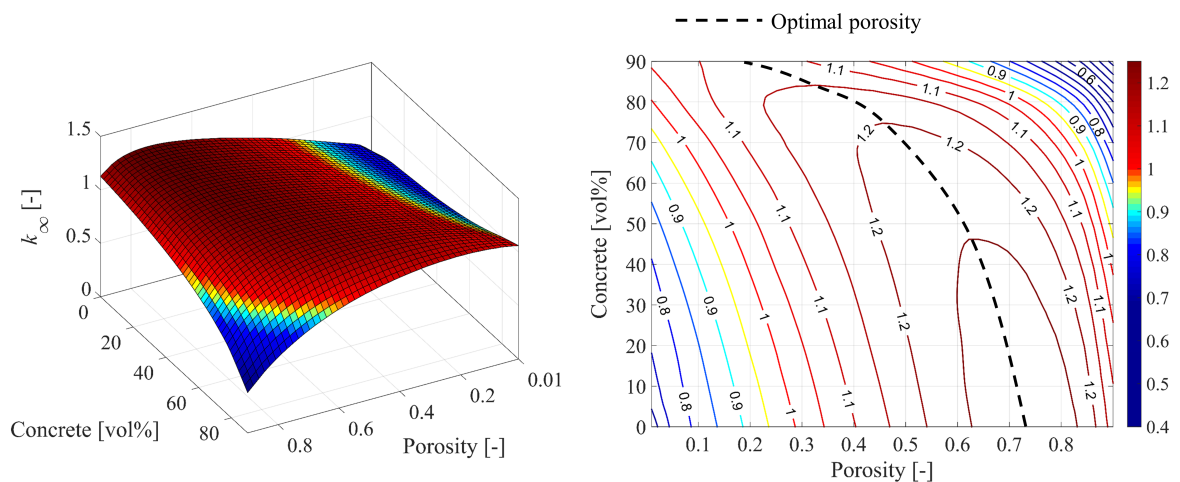

Figure C.4: Effect of concrete amount on the optimal porosity

Institut für Kernenergetik und
Energiesysteme

Universität Stuttgart
Pfaffenwaldring 31

D- 70569 Stuttgart